NORTHWESTERN UNIVERSITY

Investigating *MTCH2* as a genetic modifier of cardiomyopathy

A DISSERTATION

SUBMITTED TO THE GRADUATE SCHOOL
IN PARTIAL FULFILLMENT OF THE REQUIREMENTS

for the degree

DOCTOR OF PHILOSOPHY

Walter S. and Lucienne Driskill Graduate Program in Life Sciences

By

Julie A. Fischer

EVANSTON, ILLINOIS

December 2022

ABSTRACT

Genetic variation in genes regulating metabolism may be advantageous in some settings but not others. The non-failing adult heart relies heavily on fatty acids as a fuel substrate and source of ATP. In contrast, the failing heart favors glucose as a fuel source. A bootstrap analysis for genes with deviant allele frequencies in cardiomyopathy cases versus controls identified the *MTCH2* gene as having unusual variation. *MTCH2* encodes an outer mitochondrial membrane protein, and prior genome-wide studies associated *MTCH2* variants with body mass index, consistent with its role in metabolism. We identified the referent allele of rs1064608 (p.Pro290) as being overrepresented in cardiomyopathy cases compared to controls, and linkage disequilibrium analysis associated this variant with the *MTCH2 cis* eQTL rs10838738 and lower *MTCH2* expression. To evaluate *MTCH2*, we knocked down *Mtch* in Drosophila heart tubes which produced a dilated and poorly functioning heart tube, reduced adiposity and shortened life span. Cardiac *Mtch* mutants generated more lactate at baseline, and they displayed impaired oxygen consumption in the presence of glucose but not palmitate. Treatment of cardiac *Mtch* mutants with dichloroacetate, a pyruvate dehydrogenase kinase inhibitor, reduced lactate and rescued lifespan. Deletion of *MTCH2* in human cells similarly impaired oxygen consumption in the presence of glucose but not fatty acids. These data support a model in which *MTCH2* reduction may be favorable when fatty acids are the major fuel source, favoring lean body mass. However, in settings like heart failure, where the heart shifts toward using more glucose, reduction of *MTCH2* is maladaptive.

ACKNOWLEDGEMENTS

Completing this dissertation has been a whirlwind in the best way possible. I simply could not have done it without the support of those around me. I would like to express my gratitude toward my advisor, Elizabeth McNally, MD PhD, who has been a pleasure to learn from over the last five years. She taught me how to think about science in a way that I don't believe I would have learned elsewhere. Dr. McNally graciously gave me a chance to work in her lab and allowed me to continue to study what I knew best: flies! I will forever be grateful for the opportunity to join her lab and work with high-caliber scientists that have been further supportive to me. Much of the brainstorming during my thesis work was done in the office of Megan Puckelwartz, PhD, who always made time to speak with me whenever I knocked on her door. She guided me through the many questions I had about human genetics and gave me ideas whenever I felt my project had come to a standstill. I would also like to thank Lorenzo Pesce, PhD, who was the computational powerhouse behind this project. He was always patient whenever I asked him to run another statistical analysis and was always happy to talk me through it. I would also like to thank Tanner Monroe, PhD, Mattia Quattrocelli, PhD, Konrad Sawicki, MD PhD, Isabella Salamone, PhD, and Anthony Gacita, MD PhD, for their expert mentorship and allowing me to bounce ideas off them whenever I felt my project was stuck. This work could not be concluded without the help of Rosemary Bauer and Samuel Kearns, who aided in data collection and analysis, and were the extra hands I needed to complete these studies. I am also grateful for our collaborator, Matthew J Wolf, MD PhD, who imaged endless fly heart tubes, and to my thesis committee members, Joseph Bass MD PhD, Gemma Carvill, PhD, and Gregory Beitel, PhD. Their expert and gracious advice guided me through some of the toughest aspects of my projects. Special thanks to the those that have provided me great project ideas and let me borrow equipment and reagents whenever I was in need, such as The Bass Lab, The Chandel Lab, and the Metabolomics core facility.

I of course would like to thank the rest of the McNally Lab, who have made Northwestern and lab life feel like home. I will miss our Friday Beer Hours, Annual Christmas Party, Lab Outings, Baseball Socials, Tuesday Treats, and the genuine happy demeanor and kindness of those in the lab. I have never felt more welcome and comfortable in a workplace thanks to those around me. This includes, but is not limited to Alexis Demonbreun, PhD, Dave Barefield, PhD, Eugene Wyatt, PhD, Dominic Fullenkamp, MD PhD, Marissa Stachowski, PhD, Elena Bogdanovic, PhD, Gregory Aubert, MD PhD, Frank Li, PhD, Brian Leverson, PhD, Ashlee Long, PhD, Lisa Castillo, MS, Ellis Kim, MD PhD, Andy Vo, PhD, Tess Pottinger, PhD, Chi-Chi Ohiri, Joe O'Brien, Alex Telenson, Daniel Selgrade, Alex Willis, Michelle Lee, Garima Tomar, Avery Robinson, Kiara Meza, Michelle Mohney, Patrick Page, Kate Fallon, Lauren Vaught, Nina Reiser, Michele Hadhazy, Jodi Curtin, Eoin Code, Jason Kwon, Gabby Cowen, Clare Oosterbaan, Ivana Chychula, Nora Ibrahim, Ibrahim Tahtah, MD, Matt Velez, Ryan Hsieh, Cory Holgren, Felix Karthik, Sloane Harris, and Taurean Egan-Henderson.

Lastly, I would like to thank my friends, family, and fiancé, who have supported me through all the ups and downs of the graduate school process. They were the encouragement I needed and the sound advice to guide me through the last 5 years. Of course, it would not be in "Julie-fashion" to neglect thanking my two little Boston Terriers, Oskar and Milo, who have been the unmatched comedic relief throughout this whole journey.

Thank you to the Driskill Graduate Program, Northwestern University, and the McNally Lab for giving me the opportunity to learn and grow at a world-class institution. I will forever be grateful.

LIST OF COMMON ABBREVIATIONS

ATP: adenosine triphosphate

BMI: body mass index

BOA: bis(benzylthio)octanoic acid

CoA: coenzyme A

DCA: dichloroacetic acid

DCM: dilated cardiomyopathy

eQTL: expression quantitative trait loci

HCM: hypertrophic cardiomyopathy

GWAS: genome wide association study

LD: linkage disequilibrium

OCR: oxygen consumption rate

OXPHOS: oxidative phosphorylation

PDH: pyruvate dehydrogenase

PDK: pyruvate dehydrogenase kinase

PPR: proton production rate

PPP: pentose phosphate pathway

ROS: reactive oxygen species

SNP: single nucleotide polymorphism

nsSNV: non-synonymous single nucleotide variant

TCA: tricarboxylic acid cycle

TMRM, tetramethylrhodamine, methyl ester

WGS: whole genome sequencing

TABLE OF CONTENTS

LIST OF TABLES, FIGURES, ILLUSTRATIONS, AND GRAPHS

FIGURES

TABLES

CHAPTER 1

Metabolic homeostasis is imperative to cardiac function

1.1 Overview

Heart failure is a leading cause of death worldwide, and heart failure is often associated with cardiomyopathy. Cardiomyopathy is a disease of the cardiac muscle, where contraction and/or relaxation of the heart are impaired. There are many underlying causes of cardiomyopathy, and genetic variation contributes significantly to the risk for developing cardiomyopathy, through primary pathogenic variants as well as polygenic contributions. Onset and severity of cardiomyopathy is highly variable, even with the same primary gene variants, and this variation is, in part, driven by additional genetic variants, referred to as genetic modifiers. However, many potential modifiers of cardiomyopathy have yet to be identified.

Under normal conditions, the healthy adult heart relies heavily on fatty acids and oxidative phosphorylation as its major source of ATP. In contrast, the failing heart shifts to glucose and glycolysis as a primary source of ATP, and this fuel shift is a shared feature across all forms of heart failure. The failing heart's increased reliance on glycolysis is not matched by an increase in mitochondrial oxidation or pyruvate derived from glycolysis, resulting in lactate accumulation and reduced oxygen consumption. Genes encoding proteins important for cardiac metabolism are well positioned to serve as modified of heart failure and cardiomyopathy.

In this introduction, I will review cardiac metabolism and the ways in which the heart responds to environmental nutrient availability and stress. Due to the high energy demand of the heart, it is critical that metabolic pathways be tightly regulated and adaptive. I will also detail the metabolic changes during the progression to heart failure and the impact this has on meeting the energy demand of the heart. This chapter will also discuss the complexity of cardiomyopathy and the role of metabolism and genetic modifiers. While many genetically mediated cardiomyopathies are inherited in an autosomal dominant manner, there is considerable

variable expression and penetrance, highlighting that there are many other factors that influence the onset and severity of disease. This includes other variation within the genome as well as physiological parameters such as diet and exercise.

This chapter contains excerpts from the Oxford University Press' Human Molecular Genetics article published in 2022, "Opposing effects of genetic variation in *MTCH2* for obesity versus heart failure," authored by Julie Fischer, Tanner Monroe, PhD, Lorenzo Pesce, PhD, Konrad Sawicki, MD PhD, Rosemary Bauer, Samuel Kearns, Matthew Wolf, MD PhD, Megan Puckelwartz, PhD, and Elizabeth McNally, MD PhD. Components of the introduction from this manuscript are incorporated into this chapter, which was written by Julie Fischer in collaboration with Megan Puckelwartz, PhD, and Elizabeth McNally, MD PhD.

1.2 Introduction

1.2.1 The Heart, Energy Consumption, and Mitochondria

The heart is a small but mighty organ, responsible for oxygenating tissues throughout the body to maintain essential life processes. Because the heart is under a constant state of contractile work, cardiac energy consumption is much higher than that of other vital organs (Hamilton 2013). Energy demand of the heart is high, consuming nearly 1mM of adenosine triphosphate (ATP) every second, accounting for nearly 20% of whole body energy expenditure (Ventura-Clapier 2011). Most cardiac ATP consumption occurs in the myocardium, the specialized tissue containing the contractile cells, the cardiomyocytes. Unlike other cardiac cell types like fibroblasts, the cytosol of a cardiomyocyte is mostly occupied by sarcomeres. Each contraction of the sarcomere hydrolyzes an ATP molecule. Considering the heart is always active, this means ATP hydrolysis within the heart is constant. To account for this energy requirement, contractile cells are rich in mitochondria, which account for nearly 30% of the cellular volume (Piquereau 2013). These mitochondria generate ATP to satisfy the high-energy need of the contractile cardiomyocytes.

Because of its high energetic requirement, the heart requires ample nutrient availability to survive. The healthy adult heart is metabolically flexible in its ability to metabolize multiple substrates in response to nutrient availability. Under normal physiological conditions, the adult left ventricle derives 60-90% of its ATP from oxidative phosphorylation (Lopaschuk 2010). In contrast, a failing heart shifts to relying on glucose and other sources for ATP production, with all known varieties of heart failure converging on this late-stage phenotype (Bertero 2018; Ritterhoff 2017; Selvaraj 2020). The increase in glycolysis in the failing heart is not matched by an increase in the mitochondrial oxidation of pyruvate derived from glycolysis, resulting in lactate accumulation, reduced oxygen consumption, and impaired ATP production.

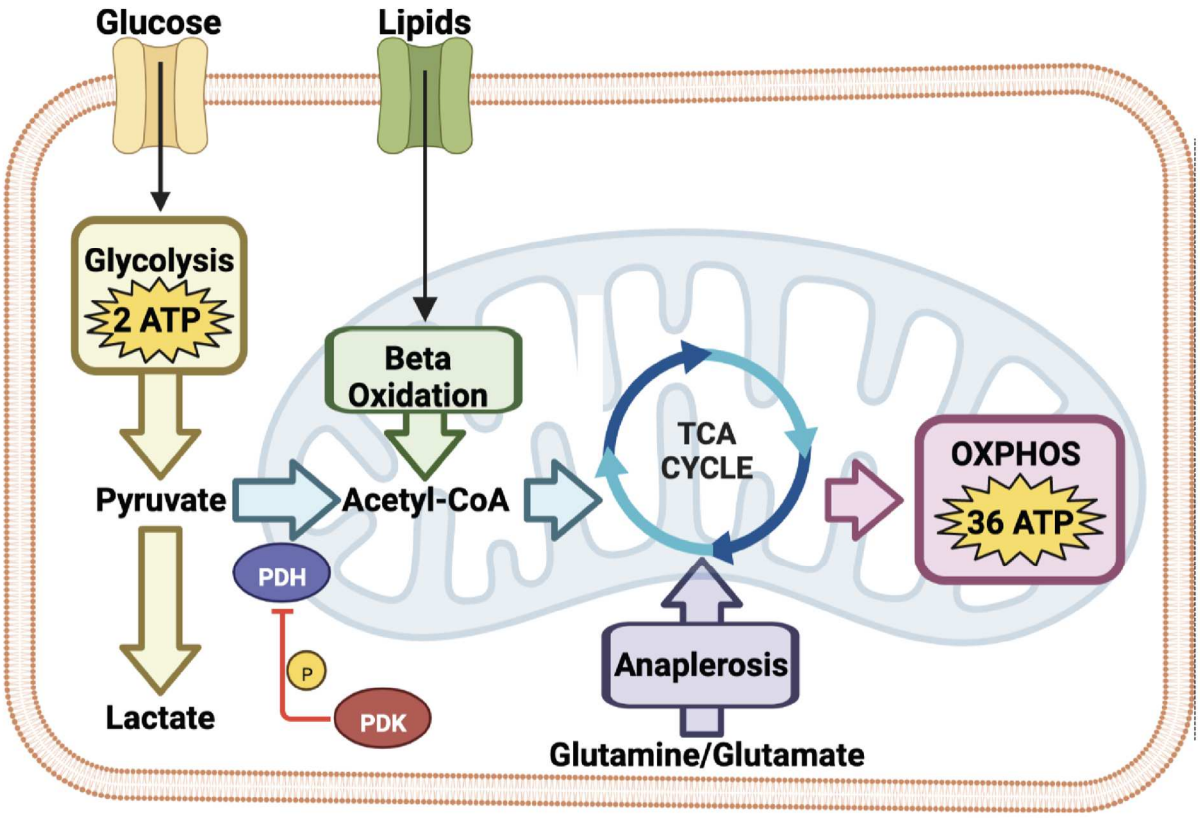

Figure 1.1: Substrate utilization in the healthy cell. A functional cardiomyocyte can utilize many substrates, including glucose and lipids. Glycolysis is rapid, but only generates 2 ATP molecules for every glucose molecule consumed, whereas OXPHOS is more enzymatically complex but generates 36 ATP molecules. The pyruvate dehydrogenase kinase-pyruvate dehydrogenase (PDK-PDH) axis is a central regulator of substrate preference and oxidative metabolism, where PDH is a promoter of glucose oxidation, and PDK inhibits PDH in situations such as hypoxia or high fatty acid availability.

Heart failure is accompanied by a metabolic switch, which are reflected by changes in mitochondrial activity. Mitochondria are responsible for most of the energy generation in the cell since the are the major site for oxidative phosphorylation (OXPHOS). While cytosolic glycolysis can produce ATP, only 2 ATP molecules are produced per glucose molecule consumed in contrast to the 36 molecules of ATP that are produced per glucose molecule by OXPHOS. Furthermore, OXPHOS can derive ATP from substrates other than glucose **(Figure 1.1)**.

Glucose, fatty acid, protein, and ketone sources can all contribute to the generation of acetyl coenzyme A (CoA), which fuels the tricarboxylic acid cycle (TCA). Many amino acids, including glutamate, glutamine, valine, and aspartate, can also be converted to TCA cycle intermediates that can enter the cycle at specific stages to be used for ATP production. These substrate derivatives become available to TCA cycle usage through mitochondrial substrate importers, known as solute carriers.

1.2.2 The SLC25 family and MTCH2

The solute carrier 25 (SLC25) family of proteins include more than 50 mitochondrial solute carriers, that permit the passage of metabolites across the mitochondrial membrane)(Ruprecht 2020). The mitochondrion is a double-membraned organelle, possessing both an outer mitochondrial membrane (OMM) and an inner mitochondrial membrane (IMM). While most solute carriers are localized to the IMM, a few are known to function at the OMM, transporting substrate and ions. SLC25 members contain 6 transmembrane domains and include family members implicated in the transport of inorganic ions, nucleotides, amino acids, fatty acids and other moieties (Ogunbona 2019; Palmieri 2013; Ruprecht 2020). Many members of the SLC25 family are orphan carriers, including MTCH1 and MTCH2, whose solutes have not been defined (Ruprecht 2020). Disruption in carrier function of any of the SLC25 members can affect the import and export of cargo and therefore cellular metabolism. However, about one-third of the mitochondrial SLC25 proteins are considered orphan carriers, where the solute transported has not been identified for the given carrier, therefore exact consequences of their dysfunction are not defined.

The discovery of another SLC25 member, the mitochondrial ATP/ADP carrier, revolutionized understanding of cellular energetics. The Vignais and Klinenberg laboratories demonstrated in the 1960s using isotope-labeled ADP and ATP metabolites that the exchange between cellular ADP and ATP levels is permitted by permeability properties of the

mitochondria, which is now known to be the mitochondrial ADP/ATP carrier (Heldt 1965; Pfaff 1965; Duee 1965). It was also shown that the exchange of ADP for ATP is regulated by an electrochemical gradient, where there is dynamic movement of charged metabolites across the mitochondrial membranes, rather than ATP synthesis being limited to substrates permanently contained within the mitochondria (Heldt 1965). Prior to this finding, it was believed that energy synthesis was limited to utilizing substrates endogenous to the mitochondria and that energy synthesis was rather static in nature, where there was no intermembrane movement of metabolites and no gradient properties to the mitochondrial membranes. The mitochondrial ADP/ATP carrier complex is encoded by four different SLC25 genes (Clémençon 2013). This carrier transports cytosolic ADP into the mitochondrial matrix to undergo OXPHOS-mediated phosphorylation, forming ATP. ATP synthesized from OXPHOS undergoes ADP/ATP carrier mediated export from the mitochondria and into the cytosol for usage in energy-consuming processes. ATP is hydrolyzed when consumed for energy, once again forming ADP, which can then be recycled back to the mitochondria via the ATP/ADP transporter to promote ATP synthesis. This is an energy-efficient mechanism that reuses the adenine nucleotides available to the cell, rather than synthesizing new nucleotides for energetic processes.

1.2.3 MTCH2 is a mediator of metabolic homeostasis

In 2005, the Gross Lab discovered a novel SLC25 protein, MTCH2, as a major regulator of apoptosis (Zaltsman 2010; Grinberg 2005). Truncated BH3-interacting domain death agonist (tBID) is a member of the B-cell lymphoma 2 (Bcl-2) protein family, which regulates apoptosis where tBID is a pro-apoptosis ligand. Bcl-2 proteins can be both promote and prevent apoptosis, depending on cellular context (Wang 2013).

While MTCH2 has mainly been studied in an apoptotic context, it is becoming more appreciated that MTCH2 has a role of a metabolic regulator in oxidative phosphorylation. In 2015, the Gross Lab deleted *Mtch2* in murine hematopoietic stem and progenitor cells. They

found that deletion of *Mtch2* enhanced proliferation with an accompanying increase in oxygen consumption rate and increase in transcriptional expression of electron transport chain machinery, suggesting MTCH2 may serve a more complex metabolic role outside of mitochondrial-mediated apoptosis (Maryanovich 2015). These findings led the Gross lab to focus on MTCH2 as a potential metabolic regulator. In 2016, mice were generated in which *Mtch2* was deleted in cardiac and skeletal muscle using a Cre driver under the control of the muscle creatine kinase (MCK) promoter and resulting in increased muscle metabolism and energy expenditure (Buzaglo-Azriel 2016). These mice displayed increased left ventricular ejection fraction (LVEF), a hallmark of hypertrophic cardiomyopathy (HCM), suggesting a role for *MTCH2* in cardiac function (Green 2016; Ho 2017; O'Gara 1987). Additionally, these striated muscle *Mtch2*-deleted mice displayed major metabolic changes, such as resistance to weight gain with high fat diet, increased lactate output, and increased mitochondrial DNA (mtDNA) and area, suggesting deletion of *Mtch2* leads to major changes in mitochondrial phenotypes. *MTCH2* was also recently shown to be a regulator of other mitochondrial processes. Specifically, *MTCH2* deletion in the colon cancer cell line HCT 116 and *Mtch2* deletion in murine embryonic stem cells both displayed failed mitochondrial elongation with accompanying mitochondrial fragmentation (Bahat 2018; Labbé 2021). These data demonstrate a role for MTCH2 in regulating mitochondrial morphology, specifically fission and fusion capabilities, an essential component in cellular response to stress and maintaining metabolic homeostasis which will be discussed more in depth later in this chapter.

Myotubes isolated from mice generated by the Gross Lab with *Mtch2* deletion in cardiac and skeletal muscle demonstrated a preference for carbohydrates as an energy source, although the heart normally utilizes fatty acids for fuel (Buzaglo-Azriel 2016). Under non-pathogenic conditions, the heart will primarily use fatty acids as a fuel substrate (Doenst 2013). However, this source does not generate ATP as rapidly compared to glycolysis. Furthermore, in

heart failure, by reducing fatty acid usage, the heart is less efficient in its capacity to produce ATP. This has been demonstrated in previous studies, where proteomic profiles are altered during heart failure, such that enzymes involved in fatty acid metabolism are downregulated, and those involved in glucose metabolism may be upregulated (Nagoshi 2011). ATP-producing pathways such as OXPHOS and glycolysis are upregulated in cases of heart failure to respond to increased energy demands (Doenst 2013). Depletion of *MTCH2* is shown to alter OXHPOS in multiple cell models, and *Mtch2* deficiency in both cardiac and skeletal muscle of mice increases glucose uptake in primary myotubes, which suggests increase in glycolytic pathways (Maryanovich 2015; Khan, Mullokandov, 2017; Buzaglo-Azriel 2016). Furthermore, evidence of increased glucose uptake and disrupted glucose homeostasis has been seen in cases of human heart failure, suggesting the critical role of metabolic regulation in cardiac function (Trico 2016; Vakrou 2014).

1.2.4 MTCH2 plays a role in apoptosis

The Gross Lab originally discovered that MTCH2 plays a role in tBID recruitment by the cross-linking and biochemical purification of the mitochondrial complex that forms with tBID in hematopoietic FL5.12 cells (Grinberg 2005). When analyzed, it was discovered that MTCH2 is a part of this complex, providing evidence that MTCH2 is an outer mitochondrial membrane (OMM) protein. Because of this, MTCH2 is considered an unusual member of the SLC25 family in that it encodes an outer, rather than inner, mitochondrial membrane protein. However, although it has been demonstrated through protease sensitivity assays that MTCH2 localizes to the OMM, it is unknown if MTCH2 has the ability to dissociate from the OMM or localize elsewhere in the cell in a tissue-specific manner or under other cellular conditions.

It has also been shown that cardiolipin serves a similar role as MTCH2 in tBID recruitment and Bcl-2-mediated apoptotic signaling. Cardiolipin is a mitochondrial-specific phospholipid that is a critical component of the mitochondrial membrane and makes up a

significant amount of the mitochondrial membrane mass (Zaltsman 2010; Ahmadpour 2020). It has been demonstrated that cardiolipin plays a role in the specificity of tBID targeting to the mitochondria (Ahmadpour 2020; Lutter 2000). While it has been shown that MTCH2 plays a similar role as cardiolipin in apoptosis, it has only been recently discovered that the main receptor of tBID recruitment, MTCH2 or cardiolipin, is determined by cellular context. Furthermore, cells lacking both cardiolipin and MTCH2 are still able to undergo apoptosis, suggesting that neither MTCH2 nor cardiolipin are essential to apoptosis (Raemy 2016). However, global deletion of *Mtch2* results in embryonic lethality in mice at day 7.5, suggesting a role for MTCH2 beyond mediating apoptosis (Zaltsman 2010; Bahat 2018).

1.2.5 MTCH2 is implicated in obesity

Through the previous findings, *MTCH2* has been shown to have a role in metabolism, mainly as a regulator of lipid storage and oxidative phosphorylation. However, the mechanism by which this occurs has yet to be delineated. In *C. elegans,* global shRNA-mediated knockdown of the worm ortholog, *mtch-1*, reduces whole body lipid accumulation and increases expression of β-oxidation genes, suggesting a greater metabolic turnover and usage of fats when *MTCH2* is reduced (Rottiers 2017). This mirrors the finding in mice with *Mtch2* deleted under the skeletal muscle MCK promoter results in resistance to diet-induced obesity and overall reduction in fat mass and increase in lean mass in mice (Buzaglo-Azriel 2016). Additionally, overexpression of *Mtch2* in 3T3-L1 mouse embryonic fibroblasts displays increased lipid accumulation, where greater *Mtch2* expression leads to greater fat accumulation. In pigs, it has also been demonstrated that *N*^{6}-methyladenosine (m^{6}A) of *MTCH2* promotes adipogenesis, further suggesting that *MTCH2* plays a role in lipid metabolism where *MTCH2* serves as a pro-adipogenesis factor.

MTCH2 has also been implicated with fat metabolism in humans. Genome-wide association studies (GWAS) have implicated several *MTCH2* variants in obesity in both children

and adults, specifically rs1064608, rs10838738, and rs3817334, which are in the *MTCH2* coding region, and rs59360790, and rs78339356 which are near the *MTCH2* coding sequence, but fall in a noncoding region (Willer 2009; Heid 2010; Mei 2012; Ng 2010; Bauer 2009; Cornelis 2014). Furthermore, mRNA levels of the *MTCH2* transcript have been shown to be elevated in the white adipose tissue in obese subjects (Kulyté 2011).

1.2.6 Paralogs of MTCH2

MTCH2 is a paralog of *MTCH1*, another mitochondrial protein involved in proapoptotic (Li 2013). *MTCH2* and *MTCH1* are homologous in their central mitochondrial carrier domains and overall have 49% identity, but they significantly deviate at the N-terminus, where MTCH1 has an extended N-terminus that is essential for proapoptotic signaling (Mao 2008; Lamarca 2007). This critical amino acid sequence in MTCH1 is absent in MTCH2. Although MTCH2 and MTCH1 are both implicated in similar processes, they assert their function through separate pathways and are not known to directly interact with each other (Robinson 2012; Willer). MTCH1 has been shown to induce apoptosis through a mechanism independent of MTCH2 (Lamarca 2008; Lamarca 2007). Specifically, expression of MTCH1 N-terminal proapoptotic peptide sequences in HeLa and HEK293T cells were sufficient to induce apoptosis without tBID-mediated apoptosis that is observed under MTCH2-mediated apoptosis.

Furthermore, genetic variations at each of these loci differ in their disease contexts, where *MTCH2* is typically linked to obesity and cardiovascular-associated risk factors, while *MTCH1* is strongly associated with Alzheimer's Disease (Kulyté 2011; Broce 2019; Xu 2002). Because of these differences, we hypothesize that the roles of these genes do not overlap, and *MTCH2* can be studied independently of *MTCH1* in cardiovascular disease.

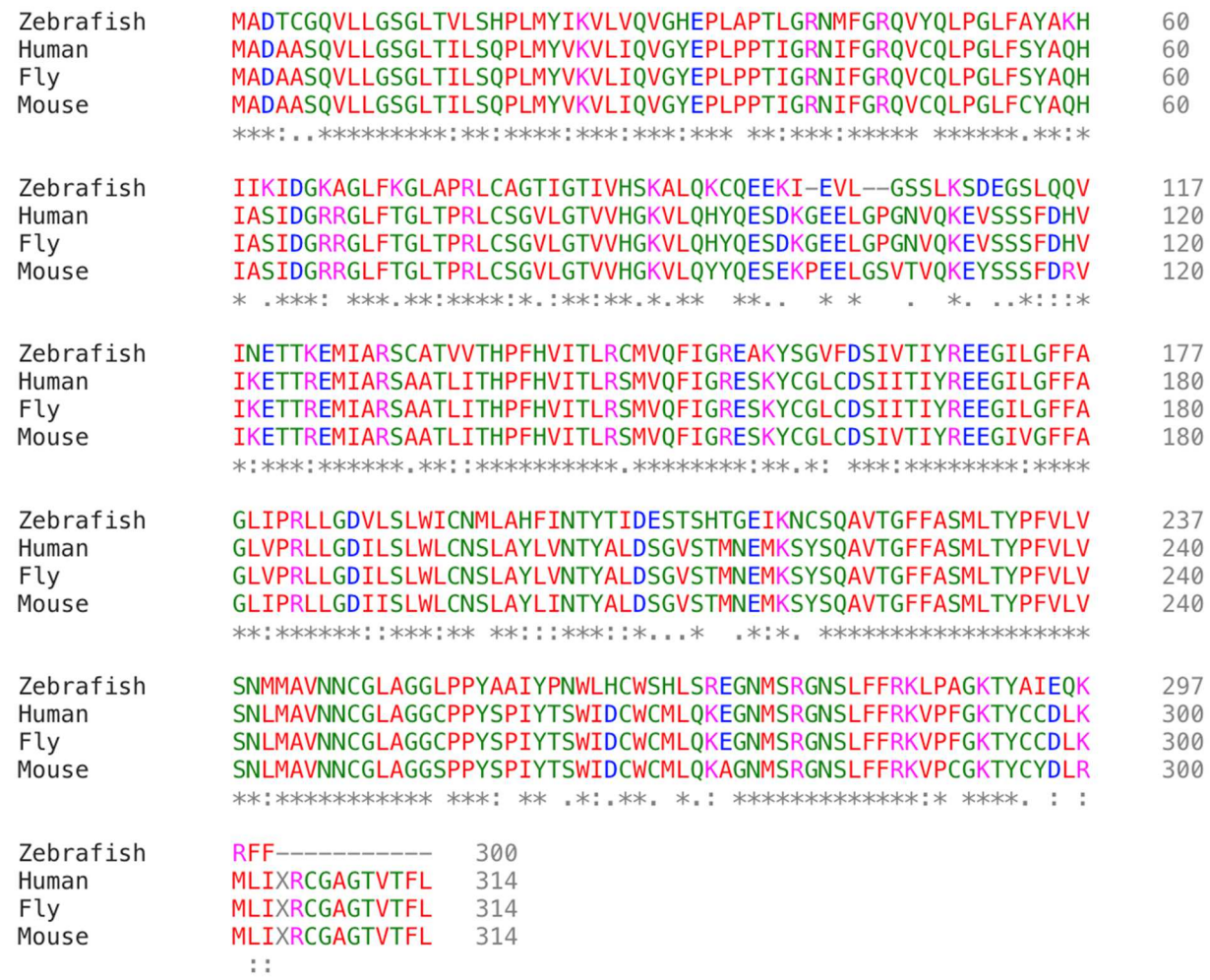

Figure 1.2: The MTCH2 protein is highly conserved across species, suggesting a crucial function and evolutionary importance for this mitochondrial protein.

Depletion of *MTCH2* was shown to alter OXHPOS in multiple cell models, and *Mtch2* deficiency in both cardiac and skeletal muscle of mice increases glucose uptake in primary myotubes, which suggests increase in glycolytic pathways (Maryanovich 2015; Khan, Mullokandov, 2017; Buzaglo-Azriel 2016). Furthermore, evidence of increased glucose uptake and disrupted glucose homeostasis has been seen in humans with both hypertrophic and dilated cardiomyopathy, suggesting the critical role of metabolic regulation in these specific

cardiomyopathies (Trico 2016; Vakrou 2014; Tadamura 1996). MTCH2 is a known regulator of energy production and has been implicated in metabolic dysfunction, where deletion of *MTCH2* in both worms and mice has shown to reduce tissue adiposity, and *MTCH2* gene expression in increased in the adipose tissue of obese subjects (Bar-Lev 2016; Kulyté 2011; Rottiers 2017). Additionally, we found that MTCH2 is highly conserved across species, suggesting an evolutionary importance for this mitochondrial protein (**Figure 1.2).**

1.2.7. Altered mitochondrial dynamics in response to metabolic stress

Metabolic reprogramming during development and heart failure is complex in that some of these changes are adaptative whereas others are maladaptive. Because mitochondria are central hubs of metabolic apoptotic signaling, there has been an emerging focus on mitochondrial networks and dynamics in controlling myocardial cell fate (Kassab 2021; Shanmughapriya 2020; Tian 2019). Mitochondria are dynamic organelles that are multifaceted in their response to outside perturbations such as stress and metabolic demand. One of these ways is through fission and fusion to mitigate stress or adjust to the cellular energetic state. Broadly speaking, mitochondrial fission aids in generating more mitochondria to increase metabolic robustness, whereas mitochondrial fusion is a way to consume damaged mitochondria such that they are not wasting energy and new healthier mitochondria can be generated (Youle 2012). Because mitochondria carry their own mitochondrial genome that is different from nuclear DNA, mitochondrial DNA (mtDNA) can be measured to assess mitochondrial status and health. Increased mitochondrial copy number may be indicative phenomena like greater respiratory capacity or changes in fusion and fission activity.

Another indicator of mitochondrial function and health is the morphology of the cristae. Cristae are the folding of the inner mitochondrial membrane, which is the site of OXPHOS and ATP synthesis. To increase inner mitochondrial surface area such that more OXPHOS and ATP synthase machinery can be expressed within the mitochondria, the inner mitochondrial

membranes are finely folded to pack more of these enzymes into the organelle. Generally, the greater the cristae folds, the greater the aerobic capacity of the mitochondria. In diseases such as heart failure, loss of cristae is often observed, accompanied by a reduction in oxygen consumption and energetic output (Chen 2009; Liu 2014). Mice with pathological cardiac hypertrophy that was induced through transverse aortic constriction have disorganization and loss of mitochondrial cristae, which likely leads to a reduction in ATP synthesis and oxygen consumption due to the inability of electron transport chain machinery to properly localize (Gao 2021; Bugger 2010).

Cristae integrity can be compromised through oxidative stress (Plecitá-Hlavatá 2016). Oxidative stress occurs from the overproduction of reactive oxygen species (ROS), which triggers inflammatory pathways and damages macromolecules like DNA and lipids as well as organelles. ROS is an all-encompassing term to classify oxygen derivatives that have the capacity to be malignant to the cell. This includes but is not limited to peroxide, superoxide anions, hydrogen peroxide, hydroxyl ions, and hydroxyl radicals, each of which have different levels of reactivity and damage capacities (Zandi 2022; Hasanuzzaman 2021). Toxic levels of ROS accumulation is also associated with altered mitochondrial morphology where cristae structure becomes disorganized (Eramo 2020). Levels of ROS and other disease markers are known to cause disarray of the cristae, limiting ATP synthesis and respiratory efficiency. Increased ROS is often correlated with poor cardiac outcomes, where oxidative stress is a hallmark of heart failure (Tsutsui 2011; D'Oria 2020; Misra 2009)

1.2.8 Mechanisms of Energy Sensing & Metabolic Flexibility

The mitochondrial pyruvate carrier (MPC) is another essential carrier protein implicated in mitochondrial function and metabolism and is not an SLC25 member. The MPC is comprised of two subunits: MPC1 and MPC2 (*SLC54A1* and *SLC54A2)*. These subunits function as

heterodimers and are part of the solute carrier 54 (SLC54) family (Herzig 2012). The SLC54 family is made up exclusively of pyruvate carriers, all which localize to the IMM. The only other member of the SLC54 family other than the MPC1 and MPC2 is the paralog MPC1L (SLC54A3), which is thought to be a tissue-specific pyruvate transporter that does not alter transport efficiency (Vanderperre 2016).

Together, the MPC carriers play pivotal roles in mechanisms of metabolic flexibility, the ability to sense energetic conditions and utilize and store available nutrients accordingly. As mentioned previously, the ability to nutrient sense and respond to different metabolic conditions is imperative to cardiac health and function (Karwi 2018; Gibb 2018), and most recently the cardiac importance of mitochondrial pyruvate carriers was shown in the enhanced heart failure phenotypes in the absence of these carriers (Cluntun 2021; McCommis 2020; Zhang 2020; Fernandez-Caggiano 2020). While it is known that metabolic preference shifts during heart failure, the mechanism by which this occurs is unknown. A common observation during this shift is the alteration of glucose utilization, where there is a shuttling of pyruvate toward cytosolic lactate accumulation via the lactate dehydrogenase enzyme, which generates significantly less energy than pyruvate oxidation (Dai 2020; Ardehali 2012; Nagoshi 2011). This fuel change is a shared feature across all forms of heart failure (Bertero 2018; Ritterhoff 2017).

The more energy-efficient route of pyruvate metabolism is conversion of pyruvate to acetyl-CoA by pyruvate dehydrogenase (PDH) for usage in the citric acid cycle TCA for maximum downstream ATP generation through glucose oxidation (Ardehali 2012; Fillmore 2018). PDH is a critical player in cardiac glucose metabolism, which converts pyruvate to acetyl CoA in the mitochondria, and its activity is tightly regulated by its phosphorylation status and is inhibited by phosphorylation via pyruvate dehydrogenase kinase **(Figure 1.2)** (Zhang, Hulver, 2014; Tovar-Méndez 2005)**.** PDH is reversibly phosphorylated through the E1 subunit by one of the four PDK isoforms that have been identified in mammalian tissue (Peters 2003; Connaughton 2010). The PDK isoforms 1-4 are ubiquitously expressed, but PDK4 is expressed

most highly in the skeletal and cardiac muscle (Lawlor 2002; Pilegaard 2004). PDH activity is reduced in heart failure, where examination of left ventricular tissue of failed versus non failed donor hearts revealed reduced *PDH* expression in those with heart failure (Seymour 1997). Similarly, rats with surgically induced myocardial infarction show reduction in PDH activity paired with a reduction in TCA activity (Dodd 2014). Because reduction in PDH activity has been regularly reported with heart failure, others have sought to determine whether the PDH inhibitor, PDK, demonstrates increased activity. Cardiac-specific overexpression of *PDK4* has been shown to exacerbate heart failure in mice, as seen by reduced overall survival and onset of ventricular thrombus (Zhao 2008). Genetic variation that disrupts splice sites in *PDK4* have been described in Doberman Pinschers who develop cardiomyopathy and heart failure; these variants reduce *PDK4* expression (Bolfer 2020; Taggart 2017).

These findings demonstrate that PDH and PDK function in a tightly regulated relationship. Proper regulation of the PDK-PDH axis is crucial to the functionality of metabolic flexibility, and the cellular ability to sense and adapt to substrate availability (Zhang, Hulver, 2014). Phosphorylation of PDH by PDK has been shown to limit acetyl CoA production in both human cells and in mice (Holness 2003; Sellers 2015). Although the healthy adult heart is primarily dependent on fatty acids as an energetic substrate, the heart is still a metabolic omnivore, where many substrates can be efficiently consumed and converted to energy. Dysregulation of this axis can lead to metabolic inflexibility, and ultimately disrupt energy homeostasis (Cluntun 2021; Zhao 2008).

Metabolic flexibility is essential for adaptation to nutrient conditions and maintain the balance between anabolic and catabolic processes. Here, I will discuss cellular mechanisms for energy sensing, and how substrate utilization is critical to survival.

The Randle Cycle

PDK regulation is often discussed in the context of the Randle Cycle, otherwise known as the glucose-fatty acid cycle (Hue 2009). The Randle Cycle is a phenomenon first described in 1963, which discusses the competition for glucose and fatty acid substrates occurring between skeletal muscle and adipose tissue, where glucose oxidation is inhibited by an abundance of fatty acid availability (Hue 2009). When fatty acids are in excess or the only available substrate, PDK inhibits PDH via phosphorylation, preventing glucose oxidation form occurring, which promotes fatty acid utilization instead (Hue 2009; Guo 2015). This marks a change in nutrient utilization mediated in the absence of hormonal signaling (i.e., insulin signaling). Although the Randle Cycle is most often discussed in conjunction with skeletal muscle, it has become increasingly described in cardiac muscle as well (Lopaschuk 2016). It has been argued that the Randle Cycle was evolutionarily beneficial during times of nutrient deprivation, however Randle Cycle outcomes of glucose oxidation inhibition become counter beneficial in some cases since the inception of the Western Diet, which is characterized by high fat content(Griffin 2016). In some cases, this excess fatty acid availability inhibits glucose utilization, even in the presence of insulin signaling, resulting in fatty acid-induced insulin resistance(Martins 2012; Hirabara 2010).

Similarly, extreme forms of Randle Cycle outcomes are observed during heart failure, where glucose oxidation is maladaptively inhibited, since the cell becomes metabolically inflexible, and this is characterized by reduced PDH activity and enhanced PDK activity. This shift forces glucose to be shunted towards lactate generation, an inefficient method of ATP production. A chemical inhibitor of PDK, Dichloroacetate (DCA), has been shown to reactivate PDH, prompting glucose oxidation to resume(Archer 2013). This provides a potential therapeutic route of reverting some of the metabolic inflexibility that occurs with extreme Randle Cycle outcomes, where inhibition of PDK may promote metabolic rebalance in situations of metabolic inflexibility such as obesity, insulin resistance, and heart failure.

The Warburg Effect

Nearly a century ago, it was first observed that cancer cells display a preference for anerobic metabolism, even in the presence of oxygen, called the Warburg Effect (Hue 2009; Warburg 1956; Warburg 1926). Although the purpose of the Warburg Effect remains undefined, there have been extensive novel observations and hypotheses generated regarding the mechanism of this so-called “aerobic glycolysis.” Most hypotheses assume this shift occurs in cancer cells because rapidly dividing cells outcompete healthy cells by quickly consuming nutrients and generating ATP via rapid anerobic glycolysis rather than through slower oxidative phosphorylation. Furthermore, glucose consumption also fuels the Pentose Phosphate Pathway (PPP), which is upregulated in cancer cells to accommodate cellular growth (Ghanem 2021). This is also accompanied by an activation of HIF-1α, which is normally induced during hypoxia and is associated with increased glycolysis and inflammation. However, this does not entirely explain the more recent acknowledgement that the Warburg Effect is seen in the failing heart, where glycolysis is upregulated in the presence of oxygen (Chen 2018). Like cancer cells, the PPP is often upregulated during heart failure (specifically in pathological cardiac hypertrophy), and HIF-1α is also activated (Tran 2019; Sousa Fialho 2019). These shifts reflect the reprogramming of metabolism during heart failure, which will be described in greater detail below, where a shift towards glucose metabolism occurs. In pigs with balloon catheter-induced myocardial infarction, metabolic signatures of Warburg effect occur in the cardiac tissue, where glycolysis is upregulated even in the presence of oxygen (Baz-Lopez 2021). Similarly, in canine models of tachycardia-mediated heart failure, there is an upregulation of Warburg Effect and cardiac fibrosis, and inhibition of Warburg Effect glycolysis with DCA improves glucose utilization and reverses some fibrosis (Hu 2019).

As discussed above in conjunction with, but independent of, the Randle Cycle, DCA has also been shown to ameliorate aerobic glycolysis that is observed in the Warburg Effect

(Sanchez 2013). It is assumed that the inhibition of PDK alleviates PDH from PDK-mediated inhibition, allowing PDH to promote pyruvate conversion to Acetyl-CoA for TCA cycle usage and downstream oxidative phosphorylation.

Anaplerosis

While it is well known that TCA cycle activity and oxidative metabolic pathways are reduced during heart failure, it has been demonstrated that the heart is capable of upregulating secondary pathways in a possible attempt to revitalize ATP generation (Fransson 2006; Gibala 2000). Anaplerosis describes secondary reactions that occur in order to replenish important intermediary metabolites, such as those in the TCA cycle **(Figure 1.2).** TCA cycle intermediates can be replenished through anaplerotic reactions, where glutamine is ultimately converted to α-ketoglutarate through a series of reactions for TCA cycle usage (Des Rosiers 2011). Amino acids can contribute to anaplerosis replenishment, as it has been demonstrated through isotope tracing that amino acids can enter an oxidative pathway via the TCA cycle (Zhang, Ahn, 2014). The rate of anaplerosis increases during heart failure, potentially as a consequence of compensatory reactions to promote oxidative metabolism (Des Rosiers 2011). However, our understanding of the role of anaplerosis during heart failure remains limited.

Ketosis and Ketone Bodies

While the healthy adult heart is predominantly reliant on fatty acids for energy production, the heart is equipped with ways to adapt when fats are not readily available. Under normal conditions, both fats and carbohydrates are readily metabolized through β-oxidation and glycolysis to generate Acetyl-CoA which is then utilized by the TCA cycle for maximal ATP production through OXPHOS. When carbohydrates are persistently limited, such as through low carbohydrate diets or starvation, metabolism is shifted to mostly fatty acid metabolism (Nasser

2020). However, only consuming fats is not enough to nourish the heart, and cells will consume all fats that are available and then will still need a nutritional source. To keep contributing to metabolism, fat reserves will be broken down to generate ketone bodies in which some can be utilized through ketosis for fueling the TCA cycle and increasing OXPHOS once again (Ludwig 2020; Nasser 2020). However, systemically, persistent ketosis has been linked to negative effects such as increased low density lipoprotein cholesterol (LDL) from elevated saturated fat consumption as well as ketoacidosis from the buildup of ketone bodies (Salas Noain 2020; Dhatariya 2020)

Lactate Metabolism

As discussed previously, the healthy adult heart is primarily reliant on fatty acids for ATP synthesis, whereas the failing heart shifts to greater carbohydrate usage and metabolism through glycolysis (Bertero 2018; Ritterhoff 2017). Lactate is generated cytosolically from glycolysis through lactate dehydrogenase. This is a reversible reaction and lactate can be reconverted to pyruvate through lactate dehydrogenase, which can then be used to generate acetyl-CoA through PDH (Schumann 2002). However, during heart failure, there is a broad decline in PDH activity that is consequential of the reduction in metabolic flexibility in the failing heart (Karwi 2018; Lopaschuk 2021). This coincides with a reduction in pyruvate-derived acetyl-CoA, and pyruvate is instead forced towards lactate production(Fillmore 2018). Furthermore, lactate dehydrogenase levels have been shown to elevate in mouse models of heart failure (Dai 2020). The greater reliance on glycolysis by the failing heart and increase in lactate output is a common to all forms of human heart failure, and increased blood lactate levels are a marker of poor prognosis in heart failure (Le Guen 2011; Zymliński 2018). However, lactate is more than just a waste product of anerobic respiration and can be recycled as fuel in the heart to generate pyruvate or be used in gluconeogenesis (Brooks 2021). Isolated mitochondria from rat hearts and circulatory fluid samples from coronary sinus and arterial catheters in humans have shown

that circulating lactate is consumed as a result of exercise-induced cardiac stress (Hütter 1984; Gertz 1988). Lactate is exported and imported into cells through the monocarboxylate transporters, which also import and export pyruvate (Bosshart 2019; Rabinowitz 2020). *MCT1,* a lactate transporter, is shown to be upregulated in cardiomyocytes in a rat model of heart failure (Jóhannsson 2001). This further suggests that lactate catabolism is likely important during cardiac stress, although it is unknown whether this is adaptive or maladaptive in different settings.

Collectively, metabolism of both the healthy and the failing heart has features that may be beneficial in the short term but chronically deleterious. The healthy adult heart can metabolize many substrates and can adapt to different conditions and substrate availability. Cardiac substrate preferences change throughout the course of development, and that this is controlled by gradual metabolic reprogramming during heart development. The fetal heart is normally characterized by high levels of anaerobic metabolism, where anaerobic glycolysis accounts for the majority of energy production and glucose and fatty acid oxidation is only attributed to about 15% of ATP synthesis, as glycolysis is more efficient under the lower oxygen conditions compared to the high oxygen environment of the healthy adult heart (Piquereau 2018; Tran 2019) **(Figure 1.3)**. Consequentially, basal lactate levels in the fetal heart are high, which can be converted back to pyruvate for fuel through the reversible reaction driven by lactate dehydrogenase. The metabolism of the fetal heart is likely influenced by the comparatively lower oxygen environment.

After birth and as the heart matures, the energetic state transitions to a greater reliance on fatty acids as the main energy-driving substrate, where fatty acid oxidation accounts for nearly 90% of total energy generation (Gertz 1988; Wisneski 1985). This is also accompanied by an increase in mitochondrial biogenesis to account for the upregulation of aerobic metabolism and oxygen consumption. After birth, upregulation of peroxisome proliferator-

activated receptor alpha (*PPAR-α)* and its coactivator *PGC-1α* is quickly observed to aid in the cardiac adjustment to an oxygen-rich environment (Buroker 2008). Activation of these genes increases the size and number of mitochondria, better equipping the cell for aerobic respiration. The adult heart is also marked by an upregulation of carnitine palmitoyltransferase 1 (CPT1), which localizes to the outer mitochondrial membrane and is essential for efficient import of free fatty acids into the mitochondrial matrix (Wisneski 1985; Schreurs 2010). Fatty acids react cytosolically with CoA, forming acyl-CoA. Acyl-CoA then reacts with carnitine, a metabolite derivative of amino acids, to generate acylcarnitine, which then can be transported into the mitochondria by CPT1. Once in the mitochondrial matrix, acyl-CoA can be manipulated in a series of reactions to undergo β-oxidation to generate acetyl-CoA, which can then fuel the TCA cycle (Bartlett 2004; Talley 2022).

During stress and heart failure, the heart undergoes metabolic reprogramming marked by an upregulation of glycolysis, even in the presence of normoxia. The metabolic profile during heart failure reverts to a more fetal-like state, where it is known that not only are substrate dependencies similar, but also the metabolic gene expression possesses a signature highly analogous to that in fetal heart tissue (Razeghi 2001) **(Figure 1.3)**. The reason for this upregulation of anerobic metabolism during heart failure is suggested to be an attempt by the heart to revert to the fetal state, perhaps to promote regeneration, whereas other theories suggest that upregulating glycolysis is a compensatory way to quickly generate energy (Taegtmeyer 2010; Schurr 2022; Fillmore 2018). Although glycolysis rapidly produces ATP, this is a much more inefficient route to energy production when compared to oxidative metabolism of fats and carbohydrates. As the heart progresses towards heart failure, this reduction in oxidative metabolism and reliance on glycolysis is marked by nearly a 70% decrease in myocardial ATP output (Fillmore 2013). Thus, shifting to glycolysis cannot meet the ongoing energy demand of

the heart, leading to heart failure. Better understanding these metabolic shifts will aid in the understanding of heart failure, and hopefully identify additional early warning signs of cardiac disorders and increase the likelihood of developing therapeutics that can intervene in deleterious pathways.

Disruptions in any of these critical metabolic pathways in the heart can affect the overall health of the myocardium. When normal metabolism is disrupted, this can cause a lack of

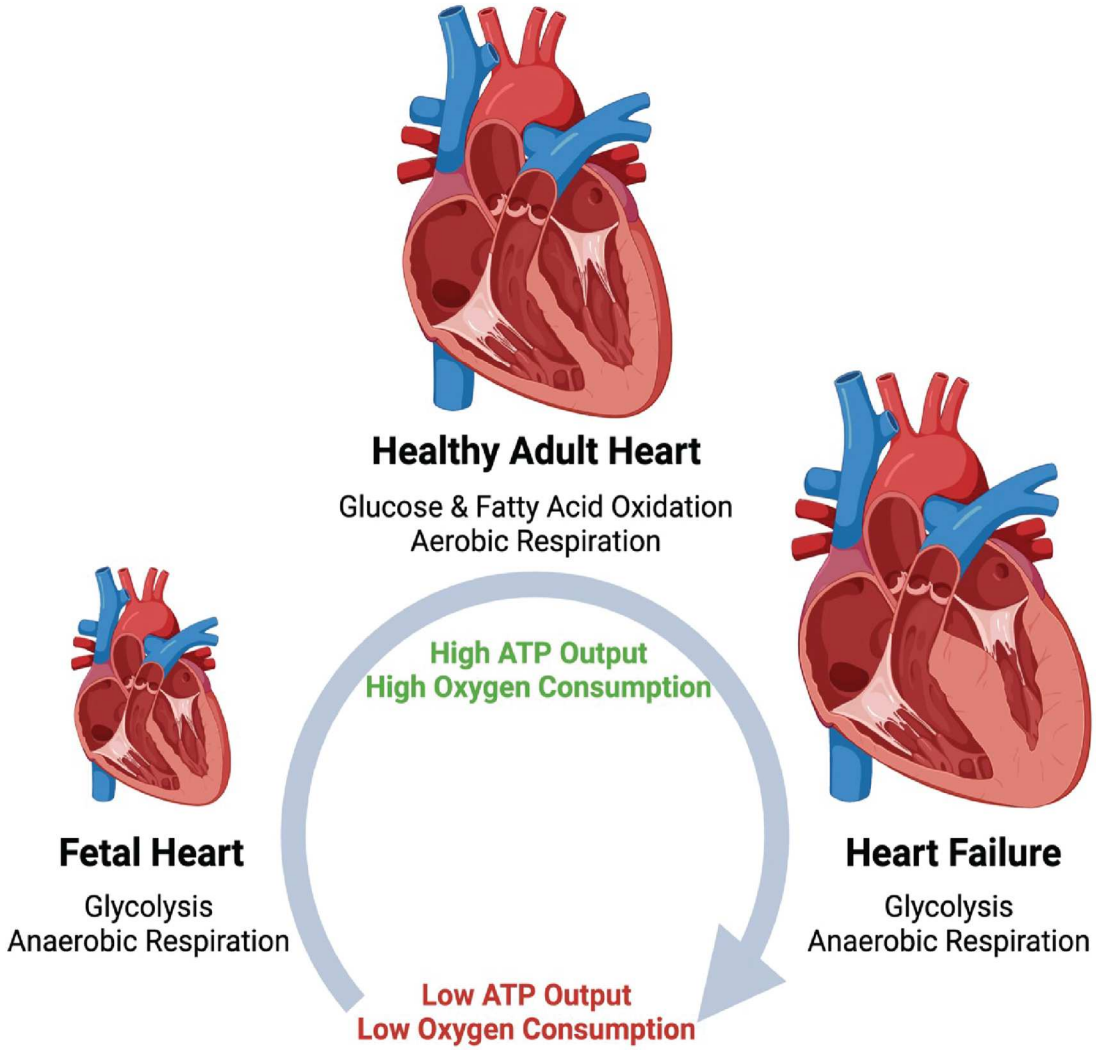

Figure 1.3: Cardiac substrate preference changes throughout the course of development and heart failure.

energy production, leading to heart failure. However, metabolic responses can also differ based on genetic landscape.

1.2.9 Cardiomyopathy is under genetic influence with variable expression

Cardiomyopathy affects about 1 in 250-500 adults and is characterized by morphological abnormalities of the heart associated with impaired cardiac function (Maron 2012; Hershberger 2013). Cardiomyopathy is often inherited, usually in an autosomal dominant manner, and this includes both hypertrophic cardiomyopathy (HCM), in which the left ventricle has thickened walls with impaired filling, and dilated cardiomyopathy (DCM), in which the left ventricle is enlarged and poorly contractile **(Figure 1.4)**

. HCM and DCM both arise from mutations in genes that affect the structure and contraction of cardiac muscle (Marian 2017; McNally 2017). HCM is characterized as having

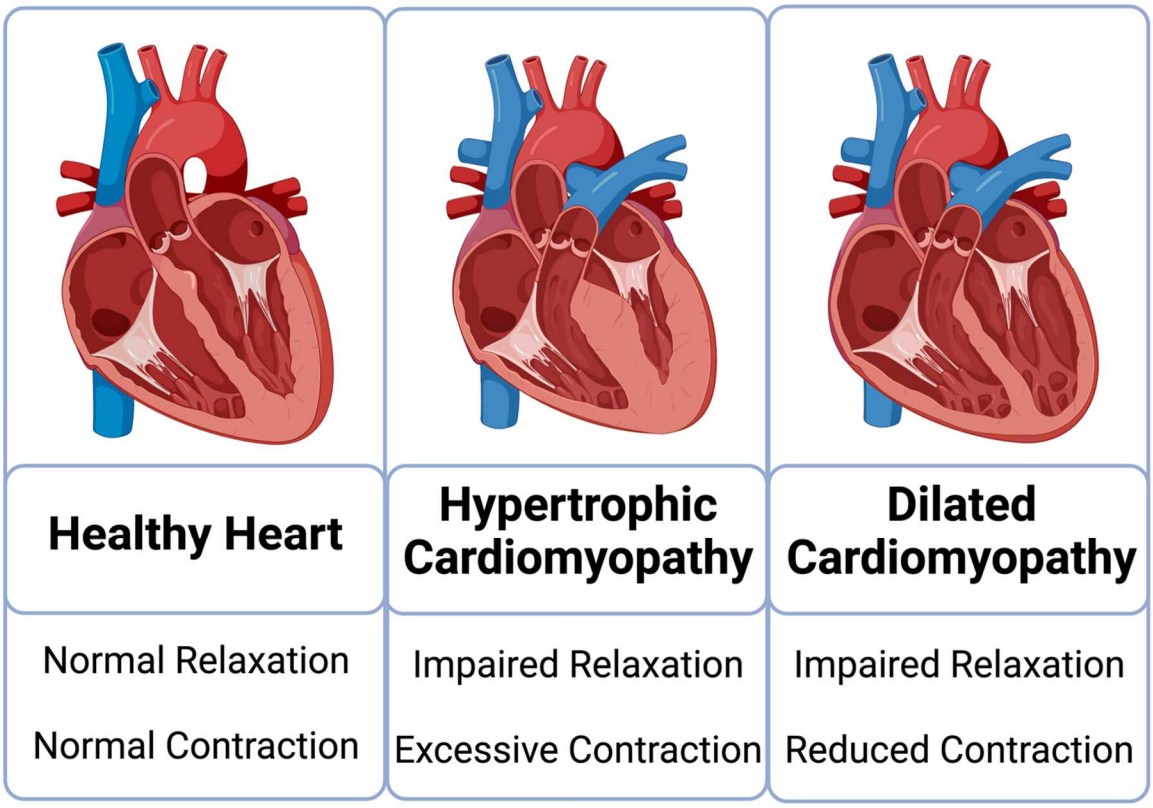

Figure 1.4: Comparison of cardiomyopathy subtypes with the healthy adult heart

hyperdynamic function especially early in the course of disease Ho (2017); (O'Gara 1987). For both HCM and DCM, the primary genetic mutations causing cardiomyopathy are variable in their clinical presentations. Over 100 genes have been linked to heritable cardiomyopathy, and this number continues to grow (McNally 2015). The expression of these mutations is modified by environmental and additional genetic factors, which are referred to as genetic modifiers.

Genetic modifiers are a common phenomenon in determination of disease phenotypes, such as those observed during heart failure. Although genetic modifiers may not be pathogenic on their own, in the setting of a primary pathogenic disease-driving variant, these modifiers can exacerbate or alleviate the expected phenotype (Rahit 2020; Dipple 2000; Dipple 2001; Nadeau 2001). Identifying genetic modifiers is crucial to understanding heart failure progression, since these pathways also represent potential targets for developing new approaches to treat heart failure.

Limb-Girdle Muscular Dystrophy Type 2C (LGMD 2C) arises from loss of function mutations in the gene encoding the dystrophin-associated protein, γ-sarcoglycan. In this disorder, many patients harbor the same primary founder mutation, but this identical mutation results in different clinical phenotypes, even within families (McNally 1996). Similarly, for many primary cardiomyopathy mutations including those in *MYH7*, *MYBPC3*, *TTN* and many others, the same primary mutation can result in the full clinical range from severe heart failure to a normal heart (Gacita 2021; Barp 2015; Verdonschot 2020). A study in a large DCM cohort demonstrated that over a third of patients were shown to have rare mutations in cardiomyopathy genes other than the known disease-causing pathogenetic variants (Haas 2015). Furthermore, increased non-synonymous single nucleotide variants (nsSNVs) within cardiomyopathy genes correlates with an increased risk and severity of DCM compared to HCM suggesting that this increased variation may be especially important in DCM (Puckelwartz 2021). This suggests that genetic background and modifier variants significantly contribute to disease. Identifying and

better understanding these variants will aid in defining the etiology and progression of cardiomyopathy.

1.2.10 Models of cardiomyopathy

While other genetic models of cardiomyopathy exist, here we present data using *Drosophila melanogaster* as our model of choice. This is partially because *Drosophila* are easily genetically manipulated with tissue specificity, and they have rapid reproduction that permits collection of large numbers of replicates for experimentation. Furthermore, *Drosophila* have shorter lifecycles such that genetic consequences on lifespan and survival can be quickly recorded.

Gene expression in *Drosophila* can be easily regulated using the Gal4/UAS system, which is a powerful genetic toolkit for knocking down or activating gene expression with precise tissue specificity. This is a transgenic model where Gal4, a yeast-specific protein, is engineered to be expressed under a tissue-specific promoter of choice. Gal4 is then translated in whichever tissue the promoter of choice is active (Duffy 2002). Gal4 will bind the UAS (upstream activating site) sequence which has also been engineered into the fly genome. Binding of Gal4 to the UAS sequence will activate the transcription of a gene or RNAi sequence of choice that is directly downstream of UAS and will only be transcribed upon UAS activation by Gal4 binding. This common technique in fly genetics permits targeted expression with tissue specificity such that a wide variety of genes can be functionally validated. This system can be manipulated to examine the effects of cardiac-specific genes, by inducing knockdowns under cardiac specific promoters. The tinC driver is a cardiac-specific promoter commonly used in the Gal4/UAS system to induce knockdown or expression of genes in the fly myocardium and has been used to perturb cardiac gene expression to model cardiomyopathy (Wolf 2006; Zarndt 2017; Novak 2015; Lin 2011).

Much of cardiac research in *Drosophila* has been focused on early development. However, with new technologies emerging, modeling adult cardiovascular disease in flies has become more feasible. Among these technologies is optical coherence tomography (OCT), which permits high-resolution, *in vivo* live imaging of individual flies, which provides a unique advantage of using flies as a model of cardiomyopathy (Men 2016; Wolf 2006; Choma 2006; Lee 2019). OCT imaging of fly hearts was first documented in 2006, by the Izatt lab to record heartbeat (Choma 2006). Since then, OCT imaging technology has progressed with greater speed and resolution, allowing the capture of 1-2μm images of the heart tube. (Lee 2019).

Although *Drosophila* possess obvious biological differences from vertebrate models, they have proven to be an excellent model for cardiac disease. *Drosophila* do not have chambered hearts and a closed circulatory system, rather, they have a segmented contractile heart tube and an open circulatory system, where oxygenated and deoxygenated circulatory fluids are free to diffuse across membranes (Das 2008; Hartley 2016; Rotstein 2016). However, the similarities in these cardiac networks outweigh the differences when it comes to modeling disease. For example, developmental patterns and cardiac cell types are highly analogous between fly and human hearts, and the fly and human heart demonstrate similar aging traits (Vogler 2009). Furthermore, myocardial cells in flies possess similar sarcomere structure and proteome signatures as do those in humans (Cammarato 2011). However, flies traditionally were mainly used to investigate developmental cardiac disorders rather than adult cardiovascular disease. With the ability to now conduct *in vivo* phenotyping of fly hearts, flies are more commonly used for a model of adult cardiac disease than ever before (Wolf 2006). Additionally, over 75% of recorded human disease-driving genes have a known fly ortholog, making flies a suitable model of genetic disease, such as cardiomyopathy (Lee 2019). *Drosophila* models of genetic cardiomyopathy have recapitulated phenotypes observed in humans **(Table 1.1)** (Wolf 2012).

Human Ortholog (McNally 2015)	**Associated Cardiomyopathy Subtype**	**Fly Ortholog**	**Associated Fly Phenotype**
MYL2	HCM	*Mlc2*	Abnormal heart tube contraction(Manivannan 2020)
RYR2	HCM	*RyR*	Fibrillating heart tube(Sullivan 2000)
ABCC9	DCM	*Sur*	Pacing-induced heart failure(Ocorr 2007)
CRYAB	DCM	*l(2)efl*	Arrhythmia and an increase in systolic heart diameter(Xie 2013)
LAMA4	DCM	*LanA*	Age-associated heart tube restriction and increased contractility(Sessions 2017)
LMNA	DCM	*LamC*	Arrythmia, conduction defects(Bhide 2018)
SGCD	DCM	*Scgdelta*	Enlarged heart tube with reduced contractility(Allikian 2007)
TAZ	DCM	*yki*	Cardiac hypertrophy without hyperplasia(Yu 2015)
CSRP3	HCM & DCM	*Mlp84B*	Diastolic interval prolongation, heart rhythm abnormalities(Mery 2008)
MYH6	HCM & DCM	*Mhc*	Reduced heart rate, morphological defects(Dahl-Halvarsson 2018)
TNNI3	HCM & DCM	*wupA*	Enlarged heart tube diameter and impaired systolic function(Wolf 2006)
TNNT2	HCM & DCM	*up*	Reduced fractional shortening(Viswanathan 2014)

TNNI3	HCM & DCM	*wupA*	Enlarged heart tube diameter and impaired systolic function(Wolf 2006)
TPM1	HCM & DCM	*Tm2*	Arrythmia(Ma 2010)
VCL	HCM & DCM	*Vinc*	Alteration of cardiac metabolism and contractility(Ma 2010)

Table 1.1: Known Drosophila models of genetic cardiomyopathy and their human orthologs.

1.3 Hypothesis and Research Design

In a search for genetic modifiers of heart failure, we identified *MTCH2* as having decreased nonsynonymous variation in humans with cardiomyopathy when compared to a population without heart failure (Puckelwartz 2021). The missense variant, rs1064608 (MTCH2 p.Pro290Ala), was the primary driver variant underlying this observation, and this variant was also previously associated with increased BMI in a genome-wide association study (GWAS) (Turcot 2018). An additional GWAS identified a separate variant, rs10838738 within a noncoding region in *MTCH2* as a major SNP for increased BMI. The index SNP (rs10838738) is in near complete linkage disequilibrium (LD) with rs1064608 (MTCH2 p.Pro290Ala). Importantly, rs10838738 has also been identified as a *cis* eQTL for increased *MTCH2* expression, suggesting that the referent haplotype has relatively lower expression. We found this haplotype underrepresented in a cardiomyopathy cohort. *MTCH2* also appears highly resistant to loss of function, with very few such alleles identified in consortium level databases. Therefore, we hypothesized that expression level is driving the signal in the cardiomyopathy cohort.

To evaluate cardiac reduction of MTCH2 *in vivo*, we generated a *Drosophila* model with cardiac-specific knockdown of the *MTCH2* ortholog *Mtch*. Additionally, we engineered a homozygous *MTCH2* deletion in a human cell model to explicitly investigate its role in cellular

metabolism. Flies with reduced *Mtch* develop cardiomyopathy and have reduced lifespan. *Mtch* knockdown flies and *MTCH2*-deleted human embryonic kidney (HEK293) cells also have impaired pyruvate oxidation due to reduced mitochondrial PDH activity, leading to a reduction of ATP production in the presence of glucose **(Figure 1.5)**. Mechanistically, reduction of *MTCH2* is associated with increased lactate production. Inhibition of PDK in cardiac *Mtch*-knockdown flies reduced lactate levels and improved lifespan as well as the substrate-dependent oxygen consumption rates. These findings demonstrate that reduction of MTCH2 increases glycolysis-derived lactate accumulation and loss of glucose-derived ATP production in the heart. The haplotype associated with relatively lower *MTCH2* expression found in the cardiomyopathy cohort may indicate maladaptive state, with relatively reduced glycolytic ATP production precisely when the heart becomes reliant on glycolysis for function.

The subsequent chapters will discuss the in-depth methods and results for examining *MTCH2* variation in human genomic data, and fly and cell models, as well as a proposed mechanism for cardiac *MTCH2*.

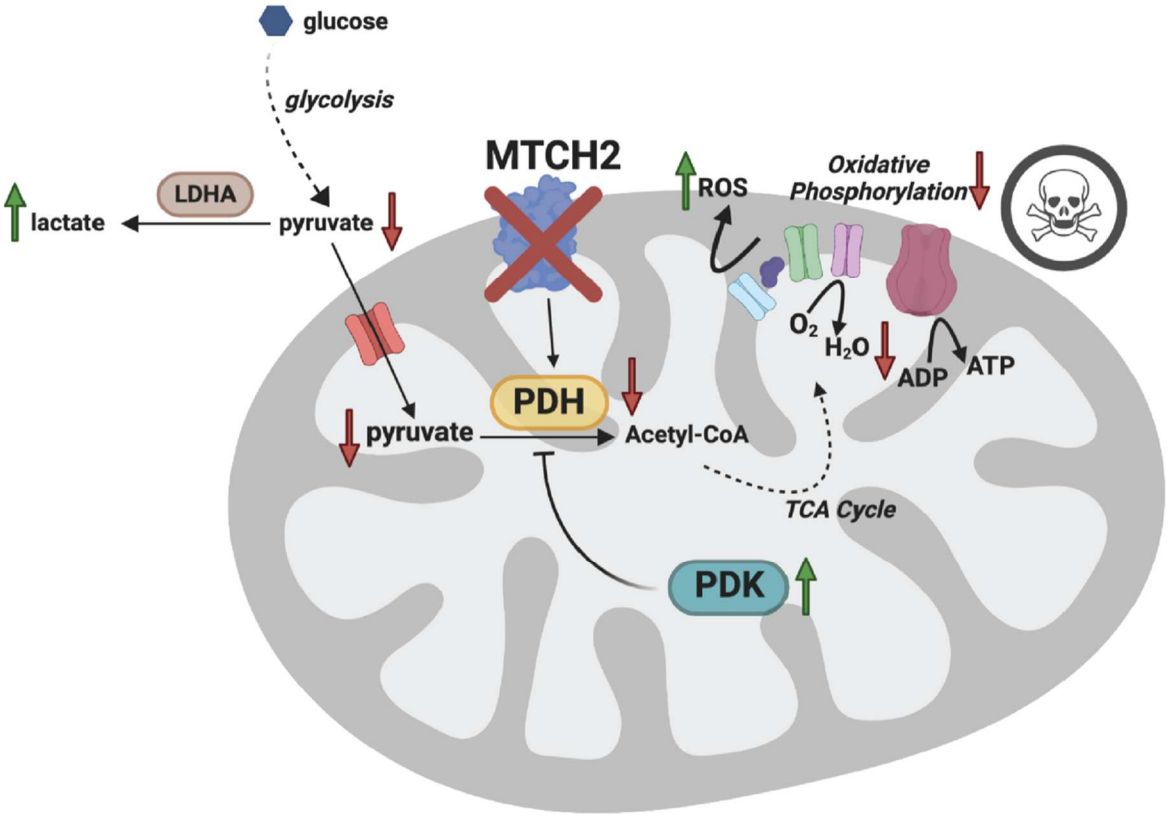

Figure 1.5: Proposed mechanism of MTCH2. Loss of *MTCH2* leads to increased lactate, reduced oxygen consumption and ATP production. Enhancing PDH activity partially corrects these deficits.

CHAPTER 2

The *MTCH2* gene has differential genetic variation between cardiomyopathy cases and controls

2.1 Overview

Cardiomyopathy is a highly heritable disorder, typically inherited in an autosomal dominant fashion. However, onset and severity of cardiomyopathy is variable, where two people with the same pathogenic disease-driving variant can experience different courses of disease. While some of this variable expressivity is attributable to environmental factors, disease variability can be influenced by additional genetic variation within the genome, otherwise known as genetic modifiers. Genetic modifiers can affect the expected phenotype of primary pathogenic variant, and can act in both protective and maladaptive manners, depending on genetic landscape and environmental factors. Because of the often small and subtle effects, genetic modifiers can be difficult to identify.

This chapter will discuss our work identifying genetic modifiers and their impact on cardiovascular disease. Specifically, it will highlight the identification of a gene, *MTCH2,* as influencing cardiac function and how variation within this gene may impact the course of heart failure. *MTCH2* was identified as having decreased nonsynonymous variation in humans with cardiomyopathy when compared to a population without heart failure. Largely driving this observation was the missense variant, rs1064608 (MTCH2 p.Pro290Ala), a variant associated with obesity and increased BMI in a previous GWAS (Turcot 2018).

This chapter contains excerpts from the Oxford University Press' Human Molecular Genetics article published in 2022, "Opposing effects of genetic variation in *MTCH2* for obesity versus heart failure," authored by Julie Fischer, Tanner Monroe, PhD, Lorenzo Pesce, PhD, Konrad Sawicki, MD PhD, Mattia Quattrocelli PhD, Rosemary Bauer, Samuel Kearns, Matthew Wolf, MD PhD, Megan Puckelwartz, PhD, and Elizabeth McNally, MD PhD. Elizabeth McNally, MD PhD, Megan Puckelwartz, PhD, Lorenzo Pesce, PhD conceived of the bootstrap search for

modifiers, and Lorenzo Pesce, PhD and Samuel Kearns performed computational and statistical analyses, all of which will be discussed in this chapter.

2.2 Introduction

2.2.1 Cardiomyopathy is influenced by genetic modifiers

Cardiomyopathy is a heterogeneous disease, where outcomes and progression are under the influence of genetic variation. For both HCM and DCM, the primary genetic mutations causing cardiomyopathy are variable in their clinical presentations, and additional genetic variation can be protective or can be deleterious to the final disease outcome. Genetic modifiers can be additive or synergistic in their interaction, traditionally referred to as genetic epistasis. Although genetic modifiers may not be pathogenic on their own, in the setting of a primary pathogenic disease-driving variant, these modifiers can exacerbate or alleviate the expected phenotype (Rahit 2020; Dipple 2000; Dipple 2001; Nadeau 2001). Identifying these variants is can help better predict disease manifestations and timing, especially where the majority of genetic diseases are not fully explained by a single mutation. Therapeutically targeting modifiers will lead us closer to precision medicine and help improve disease outcomes.

2.2.2 Preliminary analysis reveals MTCH2 has differential variation in people with cardiomyopathy compared to gnomAD.

To evaluate underlying causes of disease variability, a search for variants differentially enriched in subtypes of cardiomyopathy was carried out previously (Puckelwartz 2021). This evaluation consisted of assessing the coding region of genes, focusing on single nucleotide variants differential between in cases of HCM and DCM using a bootstrap analysis. The first phase of this analysis consisted of a resampling of missense variation in 102 cardiomyopathy-associated genes and those genes with differential variation between HCM and DCM (n=56 and n=70, respectively). This analysis identified that cardiomyopathy gene variation was greater in

DCM compared to HCM. Using a similar approach, genes with differential variation were identified between a cardiomyopathy cohort (both HCM and DCM together) and the Genome Aggregation Database (gnomAD) database (N=15708). This analysis found that the *MTCH2* had differential variation in the cardiomyopathy cohort.

2.2.3 *Using gnomAD*

When investigating genetic variation in disease, a control population is essential for comparison. The Genome Aggregation Database (gnomAD) is a resource often used to portray the genetic information of a nonselected population, therefore more reflective of the greater population (Gudmundsson 2022; de Andrade 2019). The gnomAD database contains both whole exome and genome sequencing data gathered from large-scale sequencing projects (Koch 2020). It especially serves as a useful tool when comparing variation across ancestry types, where population allele frequencies can be examined based on ancestry (Zlotogora 2018; Chakchouk 2019; Liu 2020). gnomAD provides constraint metrics for coding genes, which includes expected versus observed numbers of single nucleotide variants (SNVs) for a given gene (Fabre 2022; Schulze 2020). This is a valuable tool for variant interpretation. Genes that possess significantly fewer observed variants than expected are under greater selective pressure, where greater variant burden is not well tolerated within that genomic region. This is depicted through the Z score, where a positive Z-score represents a greater gene constraint where there are fewer observed variants compared to what is expected. Conversely, a negative Z-score represents less gene constraint, where there are more observed variants than expected, indicating the given genomic region is not likely to be under great selective pressure, and more variation is tolerated. In the case of *MTCH2,* there are fewer observed than expected synonymous and missense variants with a Z score of 1.2, indicating a mild constraint for missense variation in the human *MTCH2* gene **(Table 2.1).**

Gene constraint metrics provided by gnomAD also include the loss-of-function (LoF) constraint by reporting the probability of being LoF intolerant (pLI). Similar to a Z-score, this is calculated by accounting for the expected versus observed LoF variants. Where a pLI constraint score is close to 1, this indicates LoF variation is tolerated, and there is strong selective pressure against LoF within this genomic region. When the pLI constraint score is closer to 0, this indicates that LoF variation within the gene is tolerated. In the case of *MTCH2,* the pLI score is close to 0, indicating that loss-of-function variation is tolerated within the gene **(Table 2.1).**

Category	Expected SNVs	Observed SNVs	Constraint metrics
Synonymous	59.3	50	Z = 0.95 o/e = 0.84 (0.64-0.86)
Missense	172.5	128	Z = 1.2 o/e = 0.74 (0.64-0.86)
pLoF	23.3	7	pLI = 0.03 o/e = 0.3 (0.17-0.56)

Table 2.1: Gene constraint metrics for *MTCH2*.

2.3 Methods & Results

2.3.1 Formal evaluation of MTCH2 variation in subjects with cardiomyopathy

Intriguingly, the deviant variation between the cardiomyopathy cohort and the gnomAD database showed less variation than was expected in the *MTCH2* gene. Based on the preliminary findings that *MTCH2* showed reduced variation in the combined cardiomyopathy cohort compared to gnomAD, a database that includes individuals with disease phenotypes, we sought to further investigate *MTCH2* variation comparing *MTCH2* variation to the NUgene

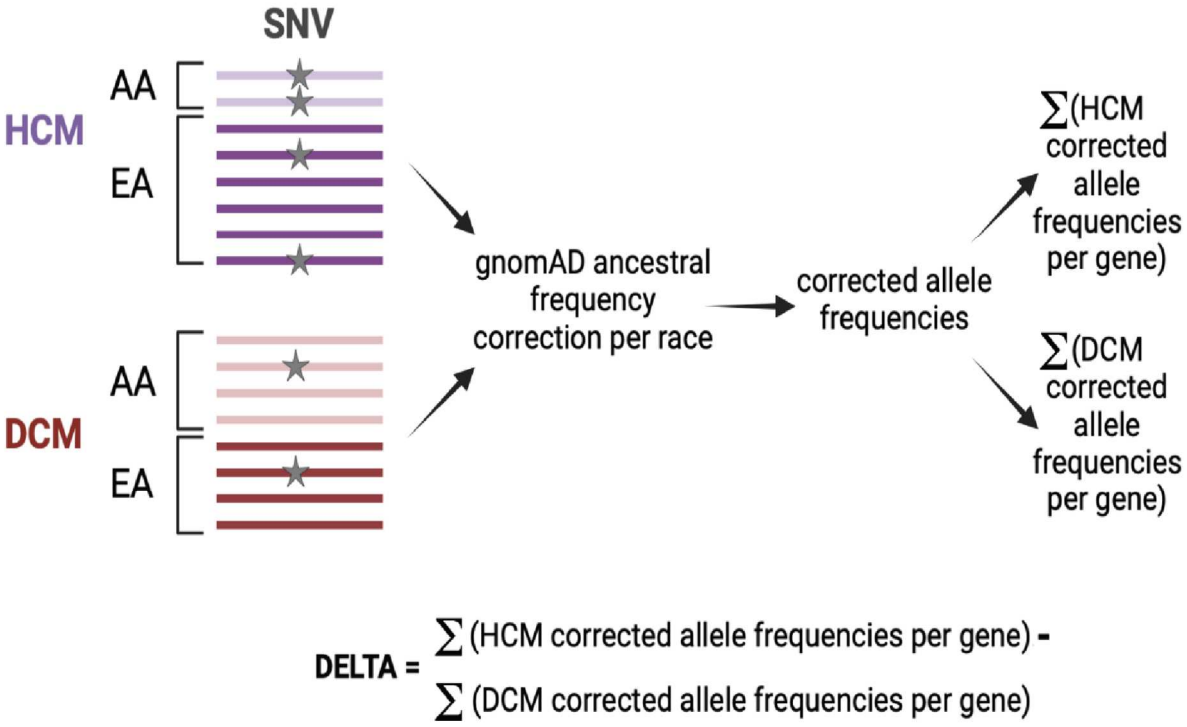

Figure 2.1 Method for identifying aberrant genetic variation in a cardiomyopathy cohort. nsSNV counts were collected in cardiomyopathy and ancestry subgroups Ancestral allele frequency correction was performed on each nsSNV in cardiac genes using gnomAD ancestral allele frequencies, and corrected frequencies were summed across each gene in each cardiomyopathy subgroup. Delta is the difference in corrected allele frequency per gene between DCM and HCM.

biobank. The NUgene Project is Northwestern's medical biobank where DNA samples are tied to electronic health records of patients in the Northwestern Medicine. Cohort selection, whole genome sequencing (WGS) and variant frequency analysis nearly 1000 NUgene participants were previously described (Pottinger 2020; Puckelwartz 2021)). For the comparison to the NUgene cohort, participants with cardiomyopathy or heart failure-related diagnosis were removed (N=772). The bootstrap analysis was applied to a 172-sample subset of the cardiomyopathy cohort using a random sampling with replacement as described previously (Puckelwartz 2021). Allele counts were aggregated by variant, race, sex, and cardiomyopathy subtype. Ancestral allele frequencies were obtained from gnomAD exome data. Expected allele numbers using ancestral gnomAD frequencies were calculated and subtracted from the observed alleles creating excess cumulative allele numbers for each gene tested. The set was

resampled 5000 times to determine confidence intervals with sufficient precision **(Figure 2.1)**. We focused on cumulative allele frequencies between 0.25 and 0.50. Calculations were performed using R functions. Significance was assessed using a false discovery rate <0.1. Comparison of variant frequencies from the NUgene Biobank and the cardiomyopathy cohort was assessed using a Chi Square Test. *cis* eQTL data were retrieved on 10/27/21 from the GTEx portal ('The Genotype-Tissue Expression (GTEx) project' 2013). Linkage disequilibrium mapping was carried out using the publicly available NCI tool, LD link, and then plotted using custom formatting (Machiela 2015).

2.3.2 *MTCH2 shows abnormal variation in people with cardiomyopathy*

Genome-wide, 184 genes were identified with a deviant cumulative allele frequency. Sixty-seven genes reached genome-wide significance for aberrant variant accumulation in the same direction for both hypertrophic cardiomyopathy (HCM) and dilated cardiomyopathy (DCM), including *MTCH2.* The *MTCH2* gene had underrepresentation of nonsynonymous single nucleotide variation (nsSNV) in the cardiomyopathy cohort (n=172) compared to the gnomAD database**.** Fewer *MTCH2* nsSNVs were identified in both DCM and HCM subjects (99.95% confidence intervals (CIs), DCM: -0.3155—0.0779; HCM: -0.3707—0.1098) **(Figure 2.2).** Results were significant for a 1% false-discovery rate across the entire protein coding genome. *MTCH2* variant analysis revealed that there was only one common (frequency range 0.25-0.50)

variant in the cardiomyopathy dataset, rs1064608. rs1064608 encodes an alanine at amino acid 290 of MTCH2, where the referent allele is a proline **(Figure 2.2 B).**

2.3.3 The *MTCH2* variant, rs1064608, has previously been associated with disease

The National Human Genome Research Institute-European Bioinformatics Institute (NHGRI-EBI) Catalog of human genome-wide association studies (GWAS), or the GWAS

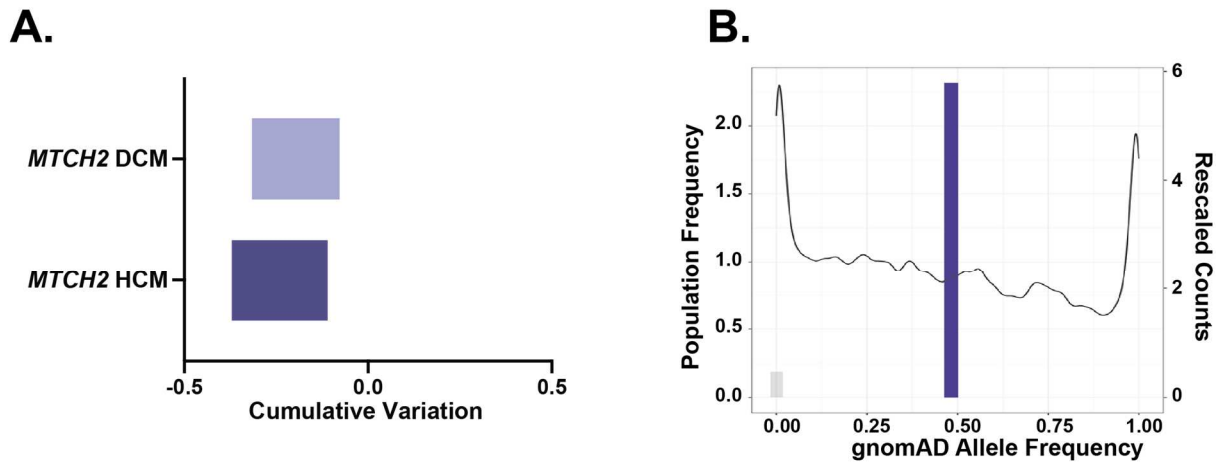

Figure 2.2 *MTCH2* variation in a human cardiomyopathy cohort. (**A**) Shown is common nsSNV variant burden in *MTCH2* in dilated cardiomyopathy (DCM) or hypertrophic cardiomyopathy (HCM) cases compared with expected gnomAD frequencies using bootstrap-based approach. The 99.95% confidence intervals are shown for *MTCH2* (DCM: -0.3155—0.0779; HCM: -0.3707—0.1098). *MTCH2* has less variation in cardiomyopathy compared to gnomAD. (**B**) The purple bar represents the normalized referent allele count of *MTCH2* p.Pro290Ala variant in the cardiomyopathy cohort (N=172), the black line represents number of variants expected at each frequency based on gnomAD genome-wide frequency prediction.

catalog, is a useful tool for investigating specific variant associations with disease. The GWAS catalog consolidates large-scale published GWAS studies such that single variants can be interrogated, and the disease traits associated with that variant as well as summary statistics for each GWAS can also be evaluated (Caliskan 2021; Buniello 2019). rs1064608 is the variant risk allele, alternate nucleotide at position 290 is a cytosine, and is associated with BMI **(Table 2.2)**. The reported association of *MTCH2* rs1064608 with BMI aligns with findings of *MTCH2* perturbation in experimental models in which MTCH2 has been manipulated (Locke 2015).

Variant and Risk Allele	P-Value	Beta	CI	Mapped Gene	Reported Trait	Trait(s)	Study Accession	Location
rs1064608-**C**	1 x 10^{-31}	0.0238 unit increase	[0.02-0.028]	*MTCH2*	Body mass index	body mass index	GCST008129	11:47618877

Table 2.2 Genome wide association studies report different rs1064608 risk alleles as being associated with BMI.

2.3.4 *Population frequencies of rs1064608*

When further investigating the population frequency of rs1064608, we found that the alternate 11-47640429-C (GRCh37) allele at this site is common in the population, with a total allele frequency of 0.4787 which is inclusive of 8734 genomes **(Table 2.3)** (Karczewski 2020). The population with the greatest allele frequency are people of East Asian descent, with an allele frequency of 0.5780.

Population	Allele Count	Allele Number	Number of Homozygotes	Allele Frequency
East Asian	474	820	72	0.5780
Latino/Admixed American	300	552	45	0.5435
European (Finnish)	1211	2282	203	0.5307
Other	355	722	59	0.4917
European (non-Finnish)	5566	11798	979	0.4718
African/African American	740	1802	32	0.4107

Ashkenazi Jewish	88	268	10	0.3284
XX	3924	7784	611	0.5041
XY	4810	10460	789	0.4598
TOTAL	**8734**	**18244**	**1400**	**0.4787**

Table 2.3 Prevalence of rs1064608 is well-represented across ancestry groups according to reported allele frequencies curated by the gnomAD database

rs1064608 is multiallelic, where the alternate allele is either C or T (SNV 11-47640429-G-C is 11-47640429-G-T). However, this is very rare and is not observed in any genomes in gnomAD but it is reported in 2 out of 249,444 exomes at a total exome allele frequency of 0.000008018.

2.3.5 *rs1064608 is in linkage disequilibrium with other GWAS variants*

There are several metabolic and cardiovascular phenotypic associations with *MTCH2* SNVs **(Table 2.4).** The most common phenotypic associations were reported changes in BMI **(Figure 2.3).** The reported traits closely align with the observed phenotypes in previously reported models of *MTCH2* dysfunction, where overexpression of *MTCH2* is associated with increased adiposity in human adipose tissue, and reduction of *MTCH2* reduces fat mass in both worms and mice, as discussed in depth in chapter 1 (Rottiers 2017; Buzaglo-Azriel 2016; Kulyté 2011).

Variant and Risk Allele	P-Value	Beta	Mapped Gene	Reported Trait	Study Accession	Location
rs10838738-**G**	5×10^{-9}	0.07 kg/m2 increase	MTCH2	Body mass index	GCST000298	11:47641497
rs3817334-**T**	2×10^{-12}	0.06 kg/m2 increase	MTCH2	Body mass index	GCST000830	11:47629441

rs3817334-**C**	6×10^{-20}	0.023 unit decrease	MTCH2	Body mass index	GCST006368	11:47629441
rs3817334-**T**	5×10^{-12}	0.0258 kg/m2 increase	MTCH2	Body mass index	GCST004557	11:47629441
rs3817334-**T**	1×10^{-11}	0.0241 kg/m2 increase	MTCH2	Body mass index	GCST004557	11:47629441
rs3817334-**T**	1×10^{-7}	0.0297 kg/m2 increase	MTCH2	Body mass index	GCST004557	11:47629441
rs3817334-**T**	3×10^{-7}	0.0269 kg/m2 increase	MTCH2	Body mass index	GCST004557	11:47629441
rs3817334-**T**	2×10^{-6}	0.0216 kg/m2 increase	MTCH2	Body mass index	GCST004557	11:47629441
rs3817334-**?**	1×10^{-6}	-	MTCH2	Body mass index (joint analysis main effects and physical activity interaction)	GCST004558	11:47629441
rs3817334-**?**	5×10^{-11}	-	MTCH2	Body mass index (joint analysis main effects and physical activity interaction)	GCST004558	11:47629441
rs3817334-**?**	1×10^{-11}	-	MTCH2	Body mass index (joint analysis main effects and physical activity interaction)	GCST004558	11:47629441
rs3817334-**T**	1×10^{-18}	0.024106821 unit increase	MTCH2	Body mass index	GCST005951	11:47629441
rs3817334-**T**	1×10^{-8}	0.0212 kg/m2 increase	MTCH2	BMI in non-smokers	GCST004499	11:47629441
rs3817334-**T**	6×10^{-6}	0.0245 kg/m2 increase	MTCH2	BMI in non-smokers	GCST004499	11:47629441
rs3817334-**T**	2×10^{-11}	0.027 kg/m2 increase	MTCH2	Body mass index	GCST002783	11:47629441

rs3817334-**T**	5×10^{-17}	0.026 kg/m2 increase	MTCH2	Body mass index	GCST002783	11:47629441
rs3817334-**T**	1×10^{-17}	0.026 kg/m2 increase	MTCH2	Body mass index	GCST002783	11:47629441
rs3817334-**T**	2×10^{-10}	0.026 kg/m2 increase	MTCH2	Body mass index	GCST002783	11:47629441
rs17788853-**A**	4×10^{-9}	0.0456 unit decrease	MTCH2	High density lipoprotein cholesterol levels	GCST90019510	11:47628066
rs3817335-**T**	3×10^{-11}	0.027965 unit increase	MTCH2	Omega-6 fatty acid levels	GCST90092933	11:47622339
rs3817335-**T**	1×10^{-8}	0.0240278 unit increase	MTCH2	Total lipid levels in lipoprotein particles	GCST90092989	11:47622339
rs59360790-**?**	2×10^{-7}	0.18308 unit increase	MTCH2, AGBL2	Body fat percentage	GCST007064	11:47647623
rs59360790-**?**	8×10^{-11}	0.17158 unit increase	MTCH2, AGBL2	Body fat percentage	GCST007064	11:47647623
rs7107356-**?**	3×10^{-10}	-	MTCH2, AGBL2	Brain region volumes	GCST009518	11:47654618
rs59360790-**?**	1×10^{-16}	0.17754 unit increase	MTCH2, AGBL2	Body fat percentage	GCST007064	11:47647623
rs10769282-**G**	3×10^{-8}	0.01524 unit decrease	MTCH2, C1QTNF4	Body fat distribution (arm fat ratio)	GCST007293	11:47604940
rs10769282-**G**	2×10^{-10}	0.02082 unit decrease	MTCH2, C1QTNF4	Body fat distribution (arm fat ratio)	GCST007293	11:47604940
rs10769282-**G**	2×10^{-12}	0.02358 unit increase	MTCH2, C1QTNF4	Body fat distribution (leg fat ratio)	GCST007295	11:47604940

rs10769282-**G**	6×10^{-9}	0.0141 unit decrease	MTCH2, C1QTNF4	Body fat distribution (trunk fat ratio)	GCST007294	11:47604940
rs10769282-**G**	5×10^{-14}	0.0183 unit decrease	MTCH2, C1QTNF4	Body fat distribution (arm fat ratio)	GCST007293	11:47604940
rs10769282-**G**	7×10^{-8}	0.01882 unit increase	MTCH2, C1QTNF4	Body fat distribution (leg fat ratio)	GCST007295	11:47604940
rs10769282-**G**	4×10^{-6}	0.01563 unit decrease	MTCH2, C1QTNF4	Body fat distribution (trunk fat ratio)	GCST007294	11:47604940
rs10769282-**G**	1×10^{-18}	0.02139 unit increase	MTCH2, C1QTNF4	Body fat distribution (leg fat ratio)	GCST007295	11:47604940
rs12363232-**?**	1×10^{-29}	-	C1QTNF4, MTCH2	Body mass index	GCST009871	11:47602338
rs78339356-**?**	9×10^{-11}	-	C1QTNF4, MTCH2	Body mass index	GCST009871	11:47599417
rs113211479-**A**	4×10^{-22}	0.024395151 unit increase	MTCH2, AGBL2	Predicted visceral adipose tissue	GCST008744	11:47648309
rs7107356-**A**	4×10^{-16}	0.309 unit decrease	MTCH2, AGBL2	Systolic blood pressure	GCST007099	11:47654618
rs7107356-**A**	3×10^{-10}	0.159 unit decrease	MTCH2, AGBL2	Pulse pressure	GCST007096	11:47654618
rs7107356-**A**	9×10^{-7}	0.265 unit decrease	MTCH2, AGBL2	Systolic blood pressure	GCST007095	11:47654618

rs12363232-**T**	4×10^{-18}	0.001991 mmol/L decrease	C1QTNF4, MTCH2	Calcium levels	GCST012398	11:47602338
rs12363232-**C**	8×10^{-15}	0.0317711 unit increase	C1QTNF4, MTCH2	Phosphoglycerides levels	GCST90092938	11:47602338
rs7107356-**?**	6×10^{-54}	-	MTCH2, AGBL2	Systolic blood pressure	GCST007087	11:47654618
rs3817334-**T**	3×10^{-6}	0.0225 kg/m2 increase	MTCH2	Body mass index	GCST004557	11:47629441
rs3817334-**T**	1×10^{-24}	0.025 unit increase	MTCH2	Body mass index	GCST004904	11:47629441
rs3817334-**T**	7×10^{-9}	0.0243 kg/m2 increase	MTCH2	Body mass index in physically active individuals	GCST004559	11:47629441
rs3817334-**T**	5×10^{-6}	0.0276 kg/m2 increase	MTCH2	Body mass index in physically active individuals	GCST004559	11:47629441
rs3817334-**T**	3×10^{-8}	0.0224 kg/m2 increase	MTCH2	Body mass index in physically active individuals	GCST004559	11:47629441
rs3817334-**T**	2×10^{-13}	0.031 unit increase	MTCH2	Body mass index	GCST006802	11:47629441
rs7120548-**?**	2×10^{-11}	0.0448821 unit decrease	MTCH2	Hypertension	GCST009685	11:47641380
rs1064608-**C**	1×10^{-31}	0.0238 unit increase	MTCH2	Body mass index	GCST008129	11:47618877
rs7107356-**A**	2×10^{-10}	0.149 unit decrease	MTCH2, AGBL2	Diastolic blood pressure	GCST007094	11:47654618
rs10838738-**G**	5×10^{-9}	0.07 kg/m2 increase	MTCH2	Body mass index	GCST000298	11:47641497

Table 2.4. *MTCH2* single nucleotide variants in the GWAS catalog.

We examined GWAS variants in **Table 2.4** associated with cardiac or metabolic phenotypes and whether they were in linkage disequilibrium (LD) with rs1064608. Figure 2.2 A shows the position of MTCH2 nsSNVs (blue), as well as MTCH2 variants identified from genome-wide association studies (GWAS) associated with metabolic and cardiovascular phenotypes (yellow), including body mass index (BMI), hypertension, and high-density lipoprotein (HDL) levels (Willer 2009; Pottinger 2020; Fernandez-Caggiano 2020; Sinnott-Armstrong 2021). rs1064608 (p.P290A) was previously identified in a GWAS for BMI and is in near total LD with rs10839738 (R^2 = 0.997), which is a lead index SNP identified in a GWAS for BMI (Turcot 2018; Hindorff 2009). LD mapping revealed the co-inheritance pattern between rs1064608 and an additional GWAS variant rs3817334 (R^2 = 0.501) **(Figure 2.4 B).**

Figure 2.3 *MTCH2* variation is associated with disease. The *MTCH2* variants, rs1064608, rs3817334, and rs10838738 are associated with BMI and obesity. *Denotes expression quantitative trait loci that alter *MTCH2* expression.

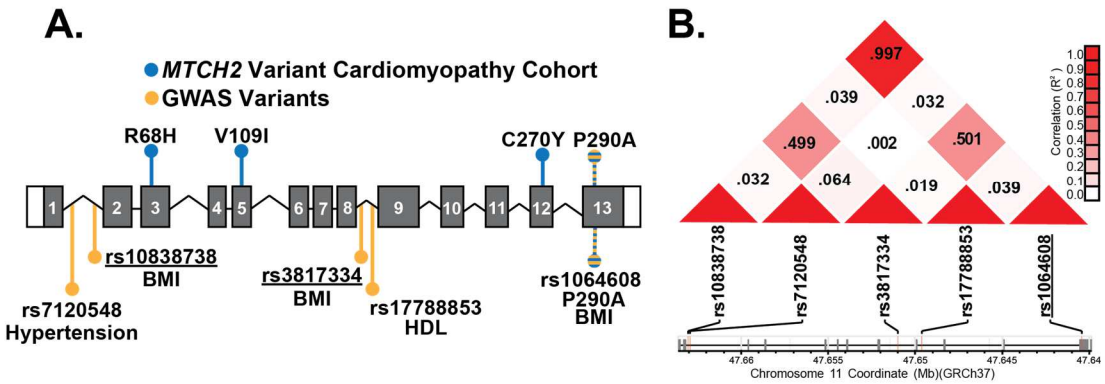

Figure 2.4 rs1064608 is in linkage disequilibrium with other GWAS variants (**A**)The top pins (blue) show the position of *MTCH2* variants from a cardiomyopathy cohort, and the bottom pins (yellow) depict *MTCH2* variants identified in GWAS for cardiac and metabolic phenotypes. The blue and yellow striped pin represents rs1064608 (*MTCH2* p.Pro290Ala) identified in a GWAS for BMI. (**B**) Linkage disequilibrium plot of the 5 GWAS SNPs from **A** reveals strong LD between rs1064608 and the two SNPs previously associated with BMI (rs10838738 and rs3817334).

2.3.5 Linkage disequilibrium analysis associates rs1064608 with the MTCH2 cis eQTL rs10838738 and lower MTCH2 expression

The Genotype Tissue Expression (GTEx) Project is an open-access database in which tissue-specific gene expression can be assessed ('The Genotype-Tissue Expression (GTEx) project' 2013). We used GTEx data to determine if either of the MTCH2 GWAS SNPs for BMI were also expression quantitative trait loci (eQTL). Both SNVs (rs1064608, rs3817334) were associated with significantly altered expression of *MTCH2* in skeletal muscle **(Figure 2.5 A).** The rs1064608 referent allele (p.Pro290) was overrepresented in the cardiomyopathy cohort

(N=172) when compared to a general cohort derived from the Northwestern medical biobank (N=772) with an overall allele frequency of 0.776 in the cardiomyopathy cohort compared to 0.714 in the control cohort, respectively (P<0.024, Chi Square Test, **Figure 2.5 B**). The rs1064608 alternate allele (p.Pro290Ala) was previously associated with BMI, and this allele is underrepresented in people with cardiomyopathy **(Table 2.4)**. The rs1064608 alternate allele (alanine at position 290) and rs10838738 *cis* eQTL for increased *MTCH2* expression are in near complete LD, suggesting that presence of the rs1064608 alternate allele is linked to increased *MTCH2* expression, and the rs1064608 referent allele (proline at position 290) is associated with reduced *MTCH2* expression. Thus, it is the variant linked to lower expression that was

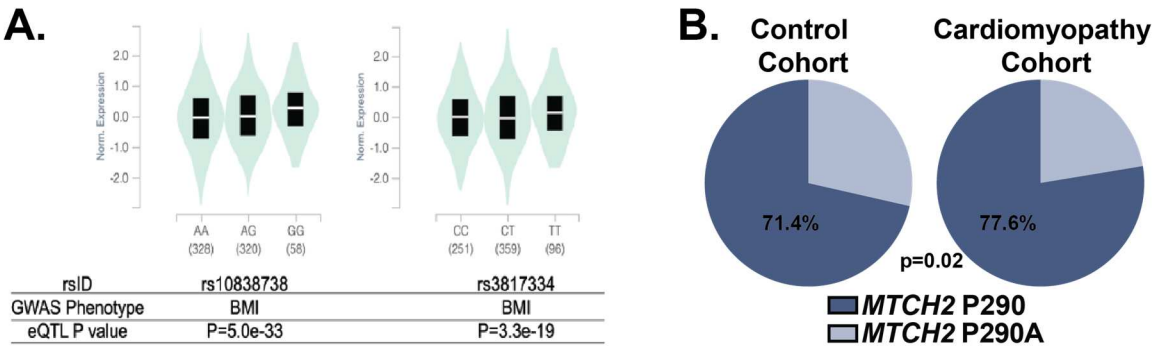

Figure 2.5 Linkage disequilibrium analysis associates rs1064608 with the *MTCH2 cis* eQTL rs10838738 and lower *MTCH2* expression. (**A**) GTEx shows two *MTCH2* SNPs that are expression quantitative trait loci (eQTL) in skeletal muscle and have genome-wide significant association with BMI (underlined in **2.3A**). **(B**) In a control cohort derived from the Northwestern NUgene medical biobank, the referent allele, MTCH2 Pro290, is found in 71.4% of biobank participants without heart failure (dark blue, left) compared to 77.6% of subjects in a cardiomyopathy cohort (dark blue, right). Control N=772, cardiomyopathy cohort N=172 *P=0.02

overrepresented cardiomyopathy cases compared to controls. This finding suggests *MTCH2* reduction is protective for obesity but may not be beneficial in the setting of heart failure. Therefore, we hypothesized that lower *MTCH2* expression may be maladaptive in the heart.

2.4 Discussion

2.4.1 MTCH2 variation and metabolic outcomes in humans.

GWAS identified *MTCH2* SNPs with expression, obesity, and lean body mass (Willer 2009; Renström 2009; Bauer 2009). In humans, mice, worms, fish, and flies, there is a consistent relationship that upregulation of *MTCH2* associates with obesity while *MTCH2* downregulation is associated more with lean body mass (Willer 2009; Buzaglo-Azriel 2016; Rottiers 2017; Landgraf 2016). Although lean body mass is beneficial for most cardiovascular traits, the substrate dependence in heart failure may represent an exception. In cardiomyopathy patients, we found overrepresentation of a SNP and haplotype linked to lower *MTCH2* expression. This type of inheritance, with high risk-allele population frequency is plausibly explained by antagonistic pleiotropy, wherein a risk allele for one condition may be protective in another (Carter 2011). Antagonistic pleiotropy is well described in traits associated with protection from infection like sickle cell and malaria and APOL1 and trypanosoma infection (Piel 2010; Vanhollebeke 2006). In these examples, genetic variation that protects against infection creates risk for other disorders like anemia or chronic kidney disease. In the case of *MTCH2* variation, genetic alleles that protect against high fat diet-induced obesity may be disadvantageous for a failing myocardium since the failing heart is more reliant on glucose as a fuel source.

2.4.2 Modeling MTCH2 dysfunction

Using WGS, we found that the variant, rs1064608, was underrepresented in a cardiomyopathy cohort. This variant encodes a Pro290Ala change near the N terminus of the

MTCH2 protein. This means that Pro290 was more frequently observed in people with cardiomyopathy and Ala290 was more frequently observed in people without cardiomyopathy. We expect that there are key conformational differences in secondary protein structure between these two variants. Because of the unique cyclic structure, proline residue changes are known to alter protein folding and “turns” in the local secondary structure, as steric restrictions from other residues do not permit the same angled turns in polypeptide chains as proline residues do (Morgan 2013; Melnikov 2016). Conformational changes caused by alterations in proline residues are known to affect function of transmembrane proteins such as MTCH2 (Meier 2005; Glatzová 2021; Tie 2008). This could mean that there are key functional differences in MTCH2 between people with cardiomyopathy and people without.

Another possibility is that people with Pro290 express less *MTCH2,* which could worsen outcomes of heart failure. The genetic variant causing Ala290 in people without cardiomyopathy is in near complete LD with another variant, rs10839738, which is a known eQTL for increased *MTCH2* expression in human skeletal muscle. Therefore, we expect that people with Ala290 express more *MTCH2* transcript, and people with Pro290 express less *MTCH2* transcript. In this case, those with Pro290 expressing less *MTCH2* transcript are more likely to be people with cardiomyopathy. Therefore, we sought to model reduced *MTCH2* expression and determine the cardiac consequences to conclude whether *MTCH2* is essential to heart function. We hypothesized that reduced *MTCH2* expression is maladaptive in the setting of heart failure. To test this, we generated a model of *MTCH2* dysfunction using a cardiac-specific knockdown of the *MTCH2* ortholog, *Mtch*, in fly hearts, as well as a *MTCH2* knockout model in a human cell line. The next chapter will discuss our findings and the consequences of dysfunctional *MTCH2* on metabolic pathways and cardiac function.

CHAPTER 3

Reduction of *MTCH2* impairs metabolism in a substrate-specific manner

3.1 Overview

Genome wide association studies (GWAS) previously identified *MTCH2* variants as being implicated in metabolic phenotypes such as obesity, BMI, weight distribution, and lean body mass (Kulyté 2011; Wang 2012; Rask-Andersen 2019). Work from others showed that deletion of the mouse *Mtch2* gene from both heart and skeletal muscle protects against high fat diet induced obesity but also produces a hypercontractile cardiac phenotype, which we hypothesize is maladaptive in heart failure (Buzaglo-Azriel 2016). Our laboratory used whole genome sequencing (WGS) to look for single nucleotide polymorphisms (SNPs) with differential variation in a cardiomyopathy cohort compared to those without cardiac disease. From this analysis, the *MTCH2* gene was found to have different patterns of nonsynonymous variation in cardiomyopathy genomes compared to a general nonselected population. Specifically, *MTCH2* was identified as having decreased nonsynonymous variation in humans with cardiomyopathy when compared to a population without heart failure. Largely driving this observation was the missense variant, rs1064608 (MTCH2 p.Pro290Ala), a variant associated with increased BMI in a previous GWAS (Turcot et al. 2018). We identified the referent allele of rs1064608 (p.Pro290) as being overrepresented in cardiomyopathy cases compared to controls, and linkage disequilibrium analysis associated this variant with the *MTCH2* cis eQTL rs10838738 and lower *MTCH2* expression. Therefore, p.Pro290, which is overrepresented in people with cardiomyopathy should also be linked to reduced *MTCH2* expression. We hypothesize that reduced *MTCH2* expression is maladaptive in the setting of heart failure. To investigate this

hypothesis, we generated models of *MTCH2* reduction using *Drosophila* and HEK293 cells. This chapter will discuss our experiments and findings in these models, and the potential implications of *MTCH2* variation in people with cardiomyopathy.

This chapter contains excerpts from the Oxford University Press' Human Molecular Genetics article published in 2022, "Opposing effects of genetic variation in *MTCH2* for obesity versus heart failure," authored by Julie Fischer, Tanner Monroe, PhD, Lorenzo Pesce, PhD, Konrad Sawicki, MD PhD, Mattia Quattrocelli PhD, Rosemary Bauer, Samuel Kearns, Matthew Wolf, MD PhD, Megan Puckelwartz, PhD, and Elizabeth McNally, MD PhD. Matthew Wolf, MD PhD conducted OCT imaging for analysis, and Julie Fischer, Rosemary Bauer, and Mattia Quattrocelli PhD conducted other experimental analyses. Lorenzo Pesce, PhD, Tanner Monroe, PhD and Konrad Sawicki, MD PhD provided expert opinion and experimental guidance. Megan Puckelwartz, PhD, and Elizabeth McNally, MD PhD supervised the project.

3.2 Introduction

The phenotypic expression of genetically-mediated cardiomyopathy is variable, often attributed to genetic modifiers (Rahit 2020; Puckelwartz 2021). Our lab performed whole genome sequencing in cardiomyopathy patients in an attempt to identify genetic modifiers in cardiac genes that may be altering disease phenotype. In cardiomyopathy patients, we found overrepresentation of a SNP and haplotype linked to lower *MTCH2* expression. Based on this finding in conjunction with the previous literature that *MTCH2* has a role in regulating oxidative phosphorylation and lipid metabolism, we sought to identify how *MTCH2* is functioning in cardiovascular metabolism (Kulyté 2011; Buzaglo-Azriel 2016). We used *Drosophila* to model *MTCH2* dysfunction. *Drosophila* are an advantageous disease model as fly genetics can be easily manipulated to examine functional consequences. Flies are used to model genetic cardiomyopathies, where fly phenotypes recapitulate what is observed in human hearts (Wolf 2012). We further validated our fly findings in a human cell model. Together, these data

demonstrate that *MTCH2* in an integral component of substrate-specific metabolism, and therapies targeting pathways affected by *MTCH2* dysfunction may alleviate malignant phenotypes observed in cardiomyopathy patients with aberrant *MTCH2* variation.

3.3 Methods & Results

3.3.1 Determining MTCH2 orthologs & fly husbandry

We first sought to model *MTCH2* reduction in *Drosophila melanogaster* as an exploratory approach to investigate its effect on heart tube function. Because there was no previous literature on *MTCH2* in flies, we conducted a homolog search of *MTCH2* in FlyBase: a database for *Drosophila* genetics and molecular biology. The homology search results yielded two predicted potential *MTCH2* fly orthologs: *Mtch* and CG10920. *Mtch* provided the better match score (15/15), whereas the match score for CG10920 was 10/15. The match score is computed by the Drosophila RNAi Screening Center (DRSC) integrative ortholog prediction tool generated by Harvard Medical School (Hu 2021). We conducted a sequence comparison and alignment using Clustal Omega and the Basic Local Alignment Search Tool (BLAST) by the National Center for Biotechnology Information (NCBI) to determine which *Drosophila* gene was a better *MTCH2* ortholog (Sievers 2014). From these methods, we concluded that *Drosophila Mtch* was most similar to human *MTCH2,* and CG10920 was more similar to the *MTCH2* paralog *MTCH1.* From here, we proceeded using *Mtch* as the *Drosophila* ortholog of *MTCH2.*

To investigate the effects of *MTCH2* reduction, I generated and examined tissue-specific knockdowns of the *Drosophila MTCH2* ortholog, *Mtch*. This was accomplished using the GAL4/UAS system (Nishihara 2007). This is a binary system where a GAL4 driver line is engineered to express GAL4, a yeast protein. GAL4 is exclusively expressed by a tissue-specific promoter. This GAL4 driver line is crossed to an upstream activating sequence (UAS)

line. GAL4 preferentially binds the UAS DNA sequence to activate transcription of RNAi hairpins that will knockdown the gene of interest in the progeny of these crosses (Ni 2008; Perkins 2015). We used the *tinC* cardiomyocyte-specific promoter to drive expression in the heart (Zarndt 2017; Wolf 2006). Using this system, we were able to knockdown *Mtch* in the fly heart tube **(Figure 3.1).**

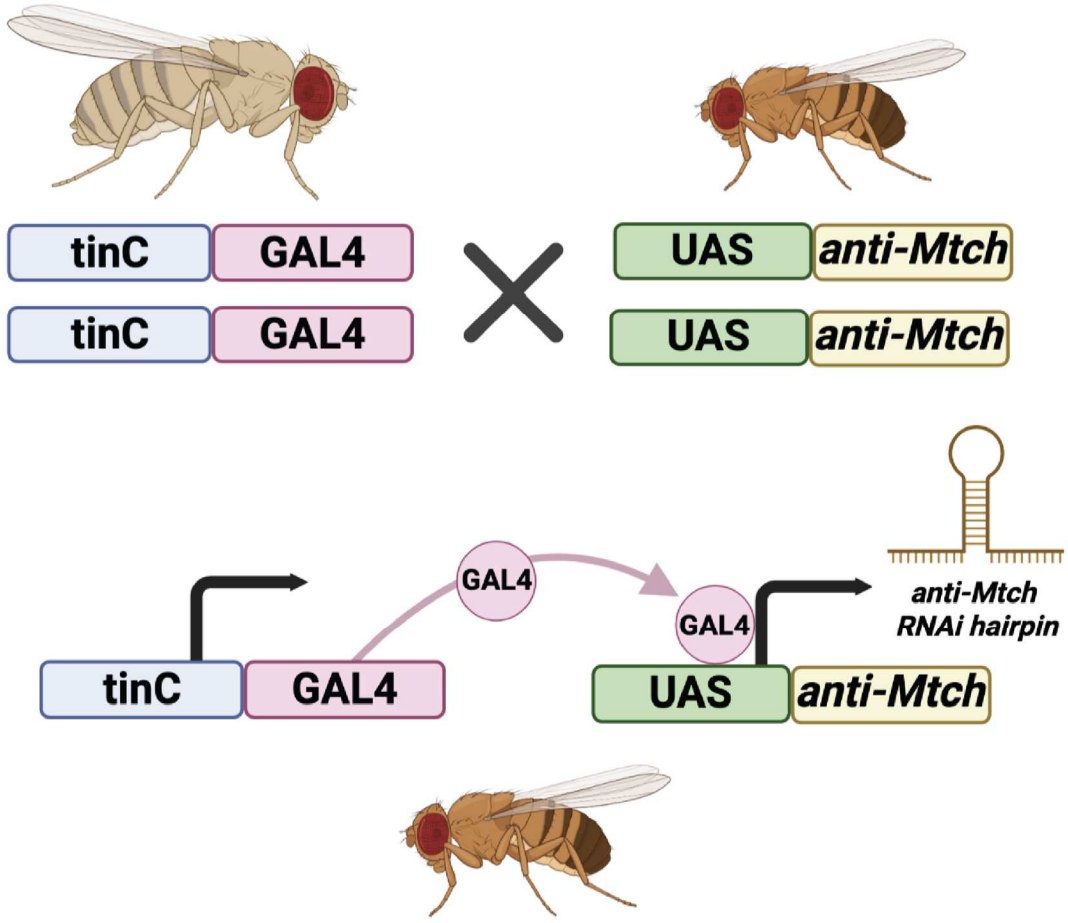

Figure 3.1 GAL4/UAS system employed in flies. tinC-GAL4 drivers express GAL4 specifically in fly cardiomyocytes. GAL4 binds UAS sequence which activates expression of anti-*Mtch* RNAi hairpins.

Fly stocks were obtained from Indiana University's Bloomington *Drosophila* Stock Center **(Table 3.1)** Fly lines were established using the GAL4/UAS system, and controls were

determined by previous standards that conducted similar crosses (Viswanathan 2016; Petersen 2022; Perkins 2015). The tinC-GAL4 transgenic fly line was crossed to a line expressing a *Mtch* RNAi hairpin under a GAL4-binding UAS, or, as an isogenic control, to a line expressing a nontargeting hairpin under the same UAS (Bloomington Drosophila Stock Center). Cardiac-specific *Mtch* knockdowns were identified by the nomenclature "*Mtch-tinC"* to indicate *Mtch* was targeted where the tinC promoter was active, since *tinC* is myocardial-specific and therefore an appropriate driver to reduce expression in the heart tube (Wolf 2006; Zarndt 2017; Novak 2015). Flies were maintained on 12 hr light/dark cycles, at 50% humidity, and fed a Jazz-Mix (Fisherbrand) diet at 25°C. Separation and collection of all flies were conducted by brief anesthetization with CO_2. All experiments were performed on 3-week-old flies, unless otherwise noted, using equal numbers of male and female flies.

Fly Line	Strain	Vendor	Catalog Number
UAS-Control	y[1] v[1]; P{y[+t7.7]=CaryP}attP40	Bloomington Drosophila Stock Center	36304
UAS-Mtch	y[1] v[1]; P{y[+t7.7] v[+t1.8]=TRiP.HMS01902}attP40	Bloomington Drosophila Stock Center	38986
tinC-GAL4	w[1118]; P{y[+t7.7] w[+mC]=GMR93F03-GAL4}attP2	Bloomington Drosophila Stock Center	40657

Table 3.1 *Drosophila* lines used

3.3.2 Validation of cardiac-specific Mtch knockdown & RT-qPCR in flies

To ensure that knockdown of *Drosophila Mtch* was cardiac-specific, we assessed *Mtch* transcript expression in three different tissues: whole hearts, whole abdomens and whole heads. Here, we anticipated that that if the knockdown strategy was indeed cardiac specific, we would only detect a reduction of *Mtch* expression in the heart tubes, as the knockdown should only occur where the tinC promoter is active. *Mtch* expression was determined via Reverse

Transcriptase quantitative Polymerase Chain Reaction (RT-qPCR) and normalized to α*Tub84B,* a ubiquitous housekeeping gene that we anticipated to be unaffected by *Mtch* knockdown **(Table 3.2)**

Gene	Primer F	Primer R
Mtch	CTGCCCAACCGCCAATTATG	AAGCTTGTCATACCGGAGCC
α*Tub84B*	TGTCGCGTGTGAAACACTTC	AGCAGGCGTTTCCAATCTG

Table 3.2 Primers used to validate *Mtch* knockdowns

This was conducted on isolated whole heart tubes, whole heart-containing abdomens, and whole heads of both the *Mtch-tinC* flies and control flies. Whole heart tubes were dissected from flies anesthetized with CO_2 by methods previously described in Vogler and Ocorr and excess cuticle was removed (Vogler 2009). Similarly, whole abdomens and whole heads were dissected from flies anesthetized with CO_2. All tissues were sourced from equal numbers of male and females of three weeks of age (N=20 total) and were collected into microcentrifuge tubes. Tissues were snap-frozen in liquid nitrogen and immediately homogenized in TRIzol™ Reagent (ThermoFisher Scientific) with a disposable pellet pestle (Millipore Sigma) and Pellet Pestle Motor hand homogenizer (Kimble). RNA was isolated from homogenates adapted from The Center for Genomics and Bioinformatics' Extraction of Total RNA from *Drosophila* (Bogart & Andrews, 2006). Final RNA concentration was quantified using a NanoDrop 2000 Spectrophotometer (ThermoFisher Scientific). cDNA was synthesized from isolated RNA using qScript cDNA SuperMix (QuantaBio), and relative fluorescence was captured using iTaq Universal SYBR Green Supermix (BIO-RAD) and measured with CFX96 Touch Deep Well Real-Time PCR System (BIO-RAD).

Expression of all genes was analyzed relative to *αTub84B* using a Student's t-test of the average ±SEM. Gene expression was quantified by generating a relative expression value (R value). R values were determined using the following equation:

$$R=[(\text{Efficiency value for gene of interest})^{\Delta Cq \text{ for gene of interest}}]/$$
$$[(\text{ Efficiency value for normalization gene})^{\Delta Cq \text{ for normalization gene}}]$$

This was repeated 6 times, where each datapoint represents a cohort of 20 flies, comprised of 10 males and 10 females.

These RNA isolation and quantification methods were applied for all gene expression analyses in flies, and specific primer sequences are listed below in **Table 3.3**. Primers were validated to ensure specificity by repeating the RT-qPCR methods above but with serial dilutions of cDNA template. Cq means for each dilution were plotted against the dilution value, and a trendline was added using Microsoft excel. qPCR primers were considered to have good efficiency if the slope trendline produced an R^2 between 0.95 and 1 and a slope very close to -3.3. Efficiency values were calculated from the slope by using the Thermo Fisher qPCR Efficiency Calculator.

Gene	Primer F	Primer R
Mtch	CTGCCCAACCGCCAATTATG	AAGCTTGTCATACCGGAGCC
α*Tub84B*	TGTCGCGTGTGAAACACTTC	AGCAGGCGTTTCCAATCTG
Ldh	AGAGAAGTGGAACGAGCTGC	ATGCCATGTTCGCCCAAAAC
Pdha	ACACAGATGCAGACGATCCG	GCCATTGCCTCCGTAGAAGT
Pdhb	AAGGTTTCCCGTGGACTGTG	CCCATCTCTGTGATTGGCGT

Pdk	ACGTGGAGCAGAGCTAACAC	ACTCTCTTCGCAGGACGTTG
Pdp	AATGTACAAACAAGCCGCCG	GAGAACGTGGTGGATTCCGT
ATPCL	GTCTTCGAAAGATGCGCGAC	CGCAAATAGCGGTCATGTGG
ACC	AGAAATCGTGCGGAACCAGT	CTGGAGTTGTCACTCTGCGT
SREBP	CACCGACAAGCACAGGTAGT	GATCGTGATTCTGGCGTTGC
Mondo	AAACGGGAGTAGGTGCTTCG	ACCATAAACTGGCCGGAGTG
Pepck1	GCTGGACGAGCTATCTTCCC	TGATGGGGTCAGTACGGGAT
Pepck2	AAGGGGTACAGTTGTGCTCG	GGAAGTTCGAGTTCCGGTGT
foxo	TGGATGGTCCAGAATGTGCC	AGTTCTTCCATCCGGCACTG
kdn	GCCACCAATTCTGACCGAGA	CACACCGGAATGGGCATCTA
mAcon1	ACTGCGAGTACGATGAGCTG	TCTCGCCTAGCTTGCTGATG
Idh	CAAGTGCGCCACAATCACTC	TGGGCGACTTCCACATCTTC
Nc73EF	CTCAACGACGCGATTTCGAC	TGGTTGCCGTTAGCTCTTGT
ScsbetaA	GTGAACCGGCCAATTTCCTG	GGCAATGACATCACAACGCA
SdhA	CATCATGCTGCTGTGTTCCG	TCCTCGCGAACCTTGAAGTC
Fum1	TGGCAAGCTATACGACGACC	GGTGGGGAAGGTATCGTTGG
Mdh2	CCACTCTGTCGATGGCCTAC	TCGTAGTCGTTGAGCTTGGG
mtDNA (fly)	GCCGCTCCTTTCCATTTTTGATTTCC	TGCCAGCAGTCGCGGTTATACCA
Trxr-2	AGAATACAGTTGCGTCGGCA	TCTTTACGGTCAAGCCGGTC
spargel	ACTGCTCAACCATAACCGGG	GCGATGGACCGATAGACCTG

Table 3.3 Primers used to assess gene expression in flies

3.3.3 Optical Coherence Tomography imaging methods

Adult heart tube contractility was analyzed using a Thorlabs Telesto II OCT system (Thorlabs, Inc.) and methods previously described (Wolf 2006; Yu 2013). Male and female files were collected three to five days after eclosion, briefly anesthetized with CO2, and embedded in a soft gel support, and then allowed to fully awaken, which was assessed by body movement. Animals were first imaged in B-mode in the longitudinal orientation to identify the A1 segment of

the heart chamber. They were then imaged transversely in M-mode for 3 sec, and multiple M-modes were recorded for each fly. Animals were then re-imaged in B-mode to ensure proper orientation of the heart tube. M-modes were processed in ImageJ by referencing to a 150μm standard. End-diastolic dimension (EDD), end-systolic dimension (ESD), and heart rate were calculated directly from the processed M-mode traces using three consecutive heart beats. Percent fractional shortening (FS) was calculated as (EDD-ESD) / EDD x 100. Performing and analyzing the OCT experiments was conducted by persons blinded to the animal group genotype assignments.

Each fly was imaged in the longitudinal long axis to identify the anterior conical chamber and then the imaging plane was turned 90° to obtain the short axis image. Then, M-mode images were obtained. The live camera of the OCT system was used to confirm the A1 segment, and OCT imaging uses multiple planes to assure the positioning of the anterior conical chamber.

3.3.4 Longevity Analysis in Flies

Equal numbers of male (N=60) and female (N=60) flies were collected on the day of pupal eclosion and divided into groups of 20 per vial and placed on JazzMix food. Dead flies were counted in each vial daily to mark survival, and food was changed every third day. This was repeated until all flies were dead. Statistical analysis was conducted using Kaplan-Meier test of the average ± SEM.

3.3.5 Measuring Circulating Lactate and Glucose

Circulating lactate and glucose were both measured from whole-fly hemolymph extraction at 3 weeks of age. Hemolymph was isolated by decapitation methods and

centrifugation-based filtering (Tennessen 2014). Single data points were generated from a cohort consisting of equal numbers of male (N=30) and female (N=30) flies. Lactate was measured from isolated hemolymph using Lactate Plus Meter Test Strips (Nova Biomedical). Circulating glucose in the hemolymph was measured using the Glucose (GO) Assay Kit (Millipore Sigma), and absorbance was measured at 540nm using the Synergy™ HTX Multi-detection Microplate Reader (BioTek; BTS1LF), to detect the proportion of hemolymph glucose.

3.3.6 Glycogen Measurement

Total glycogen content was measured in whole abdominal segments of equal numbers of male (N=60) and female (N=60) flies at three weeks of age. Single data points were generated from a cohort consisting of 40 flies each. Glycogen was assessed using the Colormetric Glycogen Assay Kit (Abcam), and sample glycogen was measured at OD 570nm using the Synergy™ HTX Multi-detection Microplate Reader (BioTek; BTS1LF) and compared to the standard curve generated from serial dilutions of the Glycogen Standard (Abcam).

3.3.7 Triglyceride Quantification in Flies

Triglycerides were quantified in dissected abdomens of *Drosophila* using equal numbers of male (N=10) and female (N=10) flies at three weeks of age. Single data points were generated from a cohort consisting of 20 flies each. Triglycerides were assessed via colorimetric quantification using Infinity™ Triglycerides Liquid Stable Reagent and compared to a standard curve. Absorbance was measured at 500nm using the Synergy™ HTX Multi-detection Microplate Reader (BioTek; BTS1LF) to calculate triglyceride content and values were normalized to body weight.

3.3.8 Adiposity Assessment Using a Buoyancy Test

Adiposity was assessed by submerging PBS-rinsed third instar larvae into a PBS-based 20% sucrose solution (Millipore Sigma). Single data points were generated from a cohort of N=10 larvae. The percent of floating larvae was recorded as a reflection of buoyancy to evaluate adiposity (Reis 2010; Hazegh 2016).

3.3.9 Measurement of Food Consumption in Flies

Food intake was assessed over a 24-hour period in 3-week-old cohorts of male (N=10) and female (N=10) flies. To measure food intake, 3mM sucrose (Millipore Sigma) was administered into a 5µl glass capillary that was fed into vials with fly cohorts placed on 2% agar, and the amount consumed from the capillary was measured after 24 hours according to the capillary feeding assay as previously described (Diegelmann 2017).

3.3.10 Measurement of Oxygen Consumption Rate and Proton Production Rate in Flies

Seahorse (Agilent) experiments were modeled after similar fly-based experiments (Bawa 2020; Neville 2018). Oxygen consumption rate (OCR) and proton production rate (PPR) were measured using a Seahorse XFe96 Analyzer (Agilent). The day prior to all experiments, the Agilent Seahorse XFe96 cartridge was hydrated with 200µl of calibrant solution overnight at 37 °C. All experiments were conducted on decapitated flies to permit substrate permeation into fly tissues, bypassing the hydrophobic fly cuticle, which was demonstrated to be effective compared to non-decapitated flies, which do not permit substrate permeation. Plates containing internally exposed fly carcasses were briefly centrifuged such that fly carcasses were fully submerged in solution. Tissue culture plates were incubated with nutrient-supplemented media at 37°C for one hour. Experiments were simultaneously conducted at 25°C to ensure phenotypes were not temperature specific**.** Nutrient-supplemented media contained either a final concentration of 10mM glucose or 1mM BSA-palmitate. All plates contained wells with

nutrient-supplement media but lacking fly carcasses to account for background correction. Examination of proton production rate was assessed in the presence of 10mM glucose. Each well contained equal numbers of 3-week-old male (N=10) and female (N=10) flies. Each data point consisted of the average of three basal OCR measurements or PPR measurements of the same well to generate the overall OCR or PPR for that well.

3.3.11 Metabolomic Analysis and Flux Analysis

Metabolite abundance was assessed in whole abdominal segments via targeted metabolomics. Abdomens of 20 males and 20 females were snap frozen for hydrophilic metabolome isolation. Samples were homogenized via ultra-sonification (Branson Sonifier 250) in 80% methanol using HPLC grade water (Millipore Sigma). Supernatant of homogenized samples were then dried with a speed vacuum (Thermo Scientific Savant *SpeedVac* DNA130), and remaining metabolome-containing pellet was submitted to mass spectrometry analysis. Metabolomics services were performed by the Metabolomics Core Facility at Robert H. Lurie Comprehensive Cancer Center of Northwestern University. All results were normalized to sample dry mass and total iron content. Flux analysis was conducted by starving 3-week-old flies for 4 hours on 2% agar and feeding 10% $^{13}C_6$ (Milipore Sigma) for 4 hours to label TCA intermediates, or 15 minutes to label glycolytic intermediates. Abdomens of 20 males and 20 females were promptly dissected after labeled carbon feeding, and snap frozen for hydrophilic metabolome isolation, conducted identically as described above.

3.3.12 Drosophila Drug Treatments

Flies were collected from pupal eclosion and placed on Jazz Mix food supplemented with 20μg/ml dicholoroacetic acid (DCA) (Millipore Sigma). Flies were put on fresh food with DCA every 3 days. Longevity was measured as described above. To assess the effects of PDK and PDH inhibition on circulating lactate levels, DCA and 6,8-bis(benzylthio)octanoic acid (BOA)

were administered to 3-week-old flies in Jazz Mix food at a final concentration of either 20μg/ml for DCA or 5mM for BOA for 3 days prior to experimental analysis. Lactate was assessed in these flies via decapitation methods as described above. To measure the change in oxygen consumption rate in flies in the presence of DCA, DCA was administered at 200μg/ml in JazzMix food to 3-week-old flies for three days prior to experimental analysis. Flies were then decapitated and placed into wells with equal numbers of males (N=10) and females (N=10). OCR was assessed with a final concentration of 10mM glucose supplemented to each well. Measurements were taken identically as described in the OCR measurement above. 150nM methyl viologen dichloride hydrate (Paraquat) (Millipore Sigma) was provided on a 25mm Whatman® filter paper (Millipore Sigma) soaked in 10mM glucose, and flies were exposed overnight in vials containing nothing but the soaked filter paper. The number of dead flies was counted 24 hours later to calculate a mortality rate for each cohort.

3.3.13 Cell Lines and Culturing

HEK293 cells (ATCC) were cultured in Dulbecco's Modified Eagle's Medium (ThermoFisher Scientific) with 10% Fetal Bovine Serum and 1% Penicillin/Streptomycin (ThermoFisher Scientific). All cells were maintained at 37°C with 5% CO_2 in a humidified incubator.

3.3.14 Clustered regularly interspaced short palindromic repeats (CRISPR)-mediated MTCH2 knockouts

gRNA 3'-CTTTCACGTACATGAGCGGC-5' targeting exon 1 of *MTCH2* was cloned into the Cas9-expressing pSpCas9(BB)-2A-Puro (PX459) V2.0 (Addgene) vector by Blue Heron Biotech, LLC (Bothell, Washington). HEK293 cells were transfected with 1μg of this custom vector, or an empty Cas9 vector lacking a gRNA sequence for controls, using FuGENE® HD

Transfection Reagent (Promega). Transfected cells were allowed 24 hours of recovery before undergoing 3-day selection with 1μg/mL, 2.5μg/mL, and 4μg/mL puromycin. Single cell colonies were isolated following puromycin selection and sequenced at 50,000 reads using Amplicon-EZ (GENEWIZ) to confirm *MTCH2* deletion.

3.3.15 Gene Expression in Human Cells

RNA was isolated from control and knockout cells that were snap-frozen in liquid nitrogen and immediately homogenized in TRIzol™ Reagent (ThermoFisher Scientific) with a disposable pellet pestle (Millipore Sigma) and Pellet Pestle Motor hand homogenizer (Kimble). RNA was isolated from homogenates adapted from the TRIzol™ Reagent User Guide Protocol (Invitrogen). Final RNA concentration was quantified using a NanoDrop 2000 Spectrophotometer (ThermoFisher Scientific). cDNA was synthesized from isolated RNA using qScript cDNA SuperMix (QuantaBio), and relative fluorescence was captured using iTaq Universal SYBR Green Supermix (BIO-RAD) and measured with CFX96 Touch Deep Well Real-Time PCR System (BIO-RAD).

Gene expression was analyzed relative to *RNA18S5* (18s rRNA). Statistical differences between populations were assessed using a Student's t-test of the average ± SEM, unless otherwise noted and indicated based on data distribution. Gene expression was quantified by generating an R value, otherwise known as a relative expression value. R values were determined using the following equation:

$$R=[(\text{Efficiency value for gene of interest})^{\Delta Cq \text{ for gene of interest}}]/$$
$$[(\text{ Efficiency value for normalization gene})^{\Delta Cq \text{ for normalization gene}}]$$

This was repeated 6 times, where each datapoint represents an 80% confluent well of a cultured 6-well plate.

These RNA isolation and quantification methods were applied for all gene expression analysis in HEK cells, and specific primer sequences are listed below in **Table 3.4.** Primers were validated to ensure specificity by repeating the RT-qPCR methods above but with serial dilutions of cDNA template. The Cq means for each dilution were plotted against the dilution value, and a trendline was added using Microsoft excel. qPCR primers were considered to have good efficiency if the slope trendline produced an R^2 between 0.95 and 1 and a slope very close to -3.3. Efficiency values were calculated from the slope by using the ThermoFisher qPCR Efficiency Calculator.

Gene	Forward Primer	Reverse Primer
MTCH2	GAGAATGAAAGGCCCGCAAG	CATTCCTGGTGAAGGGCGAG
RNA18S5 (18s)/RNR5	TGTGCCGCTAGAGGTGAAATT	TGGCAAATGCTTTCGCTTT
PDHA1	CGCAGAGCTTACAGGACGAA	CCATTGCCCCCGTAGAAGT
PDHA2	GGCGGAGGGGCTTAAATACT	AAACCGCGAATGAATTTCTG
PDHB	GGGGCATACAAGGTTAGTCG	ATTCCAGCAAAGCCCATCTC
PDK1	CCGCTCTCCATGAAGCAGTT	TTGCCGCAGAAACATAAATGAG
PDK2	GATCCAGCAATGCCTGTGAG	CGGGAAGCAGGTTGATCTC
PDK4	CCCGAGAGGTGGAGCATTT	GCATTTTCTGAACCAAAGTCCAGTA
DLAT	TCCAACTCCCCAGCCTTTAG	GCAAGAGGGCTAACAAACACC
LDHA	GGTTGGTGCTGTTGGCATGG	TGCCCCAGCCGTGATAATGA

Table 3.4 Primer sequences for assessing gene expression in human cells

3.3.16 Protein Preparation and Western Blotting

Total protein was isolated from control and HEK293 *MTCH2* deleted cells using RIPA buffer supplemented with 8M urea and quantitated with the Pierce™ BCA Protein Assay kit (Thermo Fisher Scientific). Fifteen μg of lysate was incubated at RT with 4X Laemmli Sample Buffer (Bio-Rad) and 2-mercaptoethanol (Millipore-Sigma) for 20 min, and then separated on 4-15% Mini-Protean TGX Stain-Free Protein Gel (Bio-Rad). Separated proteins were transferred to Immobilon-P PVDF membrane and incubated with primary antibodies diliuted at 1:1000 in StartingBlock T20 (TBS) Blocking buffer (ThermoFisher Scientific). Antibodies used included: anti-MTCH2 polyclonal antibody (Proteintech; Cat # 16888-1-AP), cytochrome C monoclonal Antibody (ThermoFisher Scientific; Cat # 33-8500). Secondary antibodies were from Jackson ImmunoResearch and diluted 1:2500. Antibodies are further specified in **Table 3.5.** All antibodies were diluted in StartingBlock T20 (TBS) Blocking buffer (ThermoFisher Scientific). Signals were detected with SuperSignal West Pico Plus chemiluminescent substrate (ThermoFisher Scientific) and imaged using Invitrogen iBright.

Antibody	Vendor	Catalog Number	Protein Size (kDa)	Host	Class/Clonality
anti-MTCH2	Proteintech	16888-1-AP	33	Rabbit	Polyclonal
Anti-Cytochrome C	ThermoFisher Scientific	33-8500	15	Mouse	Monoclonal
Peroxidase AffiniPure Anti-Rabbit IgG	Jackson ImmnoResearch Inc.	111-035-144	n/a	Goat	Polyclonal
Peroxidase AffiniPure Anti-Mouse IgG	Jackson ImmnoResearch Inc.	115-035-003	n/a	Goat	Polyclonal

Table 3.5 Antibodies used for assessing protein expression in human cells

3.3.17 Quantification of Mitochondrial DNA in Human Cells

To quantify mitochondrial DNA (mtDNA), total DNA (DNA) was isolated from control and edited HEK293 cells using the Gentra Puregene® DNA Purification Kit (QIAGEN) and treated with RNAse A Solution to remove ambient RNA. DNA was hydrated with Invitrogen™ UltraPure™ DNase/RNase-Free Distilled Water (ThermoFisher Scientific) and quantified with the NanoDrop2000 Spectrophotometer (ThermoFisher Scientific). DNA was measured using quantitative PCR, where relative fluorescence was measured using iTaq Universal SYBR Green Supermix (BIO-RAD) in a CFX96 Touch Deep Well Real-Time PCR System (BIO-RAD). Primers were designed to capture the mitochondrial-encoded gene, mitochondrially encoded tRNA leucine 1 (*MT-TL1*), and nuclear-encoded gene, *RNR5.* Relative expression of *MT-TL1* compared to *RNR5* was assessed and analyzed using a Student's t-test of the average ± SEM. Primer sequences are specified in **Table 3.6.**

Gene	Forward Primer	Reverse Primer
RNA18S5 (18s)/RNR5	TGTGCCGCTAGAGGTGAAATT	TGGCAAATGCTTTCGCTTT
mtDNA/ MT-TL1 (human)	CACCCAAGAACAGGGTTTGT	TGGCCATGGGTATGTTGTTA

Table 3.6 Primer sequences for quantifying mtDNA in human cells

3.3.18 Analysis of Oxygen Consumption Rate and Proton Production Rate in Human Cells

Oxygen consumption rate (OCR) and proton production rate (PPR) were measured using a Seahorse XFe96 Analyzer (Agilent). All experiments were conducted with a seeding density of 10,000 cells/well. Cells were allowed to incubate with nutrient-supplemented media at 37°C with 5% CO_2 for 1 hour. Nutrient-supplemented media in OCR experiments contained either a final concentration of 50mM glucose or 1mM BSA-palmitate. PPR media consisted of a final concentration of 50mM glucose. All DCA experiments were conducted using media

supplemented with 100uM DCA and 50mM glucose. Each data point represented a single well of cells, which consisted of the average of three basal OCR or PPR measurements of the same well to generate the overall OCR or PPR for that data point. All measurements were normalized to cell count.

3.3.19 Mitochondrial Isolation and Measurement of Pyruvate Dehydrogenase Activity

Pyruvate dehydrogenase activity was assessed in both whole cell lysate and isolated mitochondria from cultured HEK293 cells. Confluent cells in a 10cm plate were harvested and pelleted via centrifugation. Cells were homogenized with a dounce-homogenizer and allowed to swell in the hypotonic buffer as described. Swollen cells were centrifuged with homogenization buffer to remove nuclei and cell membrane fragments from the homogenate to achieve a pellet containing isolated mitochondria. PDH activity was measured using the colorimetric Pyruvate dehydrogenase Activity Assay Kit (Millipore Sigma), and absorbance at 450nm ($A_{450)}$ of samples was recorded at baseline and in 5 min increments up to 3 hours using Synergy™ HTX Multi-detection Microplate Reader (BioTek; BTS1LF) to record the change in A_{450} over time as a reflection of PDH activity. All measurements were normalized to mitochondrial count.

3.3.20 Mitochondrial Imaging

MTCH2$^{-/-}$ and control (unedited) HEK293 were cultured with fresh Dulbecco's Modified Eagle's Medium (ThermoFisher Scientific) with 10% Fetal Bovine Serum and 1% Penicillin/Streptomycin (ThermoFisher Scientific) containing 100nM MitoTracker Green FM (ThermoFisher Scientific) to probe for mitochondria, regardless of mitochondrial membrane potential, and with 100nM Image-iT TMRM Reagent (ThermoFisher Scientific), a probe that selectively sequesters in healthy mitochondrial with active membrane potential. Cells were

allowed to incubate this media with probes for 30min at 37°C with 5% CO_2 in a humidified incubator and imaged for fluorescence using a KEYENCE BZ-X810 fluorescence microscope.

3.3.21 Statistics

Longevity assessments were conducted with the Kaplan-Meier method, where individual data points were representative of the average of three different fly culture replicates. All other statistical differences between populations were assessed using a Student's t-test of the average ± SEM or a Wilcoxon rank-sum test with Holm correction for multiple comparisons.

3.3.22 Key Resources

Reagents & Materials	**Vendor**	**Catalog Number**
JazzMix	Fisher Scientific	**AS153**
Drosophila Vial, Narrow	VWR	75813-144
TRIzol™ Reagent	ThermoFisher Scientific	15596026
qScript cDNA SuperMix	QuantaBio	**95048**
iTaq Universal SYBR Green Supermix	BIO-RAD	**1725124**
Infinity™ Triglycerides Liquid Stable Reagent	ThermoFisher Scientific	**TR22421**
Glucose (GO) Assay Kit	Millipore Sigma	GAGO20
D-(+)-Glucose	Millipore Sigma	G7021
Sucrose	Millipore Sigma	S8501
BSA-Palmitate Saturated Fatty Acid Complex (5 mM)	Cayman Chemical	29558
HPLC grade H_2O	Millipore Sigma	70733
D-Glucose-$^{13}C_6$	Millipore Sigma	389374
Dicholoroacetic acid (DCA)	Millipore Sigma	D54702
6,8-Bis(benzylthio)-octanoic acid (BOA)	Millipore Sigma	SML0404
Methyl viologen dichloride hydrate (Paraquat)	Millipore Sigma	856177
Whatman® qualitative filter paper, Grade 1	Millipore Sigma	WHA1001325
DMEM – Dulbecco's Modified Eagle Medium 1X (glucose, glutamine, and pyruvate)	ThermoFisher Scientific	11995-073

Fetal Bovine Serum	ThermoFisher Scientific	26140079
Penicillin/Streptomycin (5,000 U/mL)	ThermoFisher Scientific	15070-063
FuGENE® HD Transfection Reagent	Promega	E2311
Pierce™ BCA Protein Assay Kit	ThermoFisher Scientific	23225
4x Laemmli Sample Buffer	BIO-RAD	1610747
2-Mercaptoethanol	Millipore Sigma	M6250
4–15% Mini-PROTEAN® TGX Stain-Free™ Protein Gels, 10 well, 30 µl	BIO-RAD	4568083
Spectra™ Multicolor Broad Range Protein Ladder	ThermoFisher Scientific	26634
Immobilon-P PVDF Membrane	Millipore Sigma	IPVH00010
StartingBlock T20 (TBS) Blocking Buffer	ThermoFisher Scientific	37543
Cytochrome C Monoclonal Antibody	ThermoFisher Scientific	33-8500
Gentra Puregene® DNA Purification Kit	QIAGEN	158767
Invitrogen™ UltraPure™ DNase/RNase-Free Distilled Water	ThermoFisher Scientific	10-977-015
PDH Activity Assay Kit	Millipore Sigma	MAK183-1KT
Peroxidase AffiniPure Goat Anti-Mouse IgG (H+L)	Jackson ImmunoResearch Laboratories, INC.	115-035-003
Peroxidase AffiniPure Goat Anti-Rabbit IgG (H+L)	Jackson ImmunoResearch Laboratories, INC.	111-035-144
SuperSignal™ West Pico PLUS Chemiluminescent Substrate	ThermoFisher Scientific	34579
PhosSTOP™ Phosphatase Inhibitor Tablets	Millipore Sigma	4906837001
cOmplete™, Mini, EDTA-free Protease Inhibitor Cocktail	Millipore Sigma	11836170001
MTCH2 Polyclonal Antibody	Proteintech	16888-1-AP

Table 3.7 Reagents and materials used in experiments described in methods section

3.4 Results

3.4.1 Cardiac-specific reduction of Mtch reduces lifespan and alters cardiac dynamics in flies.

Cardiac-specific reduction of Mtch reduces lifespan and alters cardiac dynamics in flies. In mice, global deletion of *Mtch2* is embryonic lethal (Bahat 2018). To evaluate the role of *MTCH2* in the heart, we generated cardiac-specific reduction of the MTCH2 ortholog, *Mtch*, in *Drosophila melanogaster* using RNAi-mediated knockdown. Cardiac specificity was achieved using a fly line expressing an anti-*Mtch* RNAi hairpin under the cardiac-exclusive promoter, *tinC* (Wolf 2006; Zarndt 2017). Control flies were isogenic to *Mtch* knockdowns and expressed a nontargeting hairpin under the *tinC* promoter. *Mtch-tinC* flies had a 50% reduction in cardiac *Mtch* expression compared to controls, consistent with partial loss of function **(Figure 3.2A-C)**

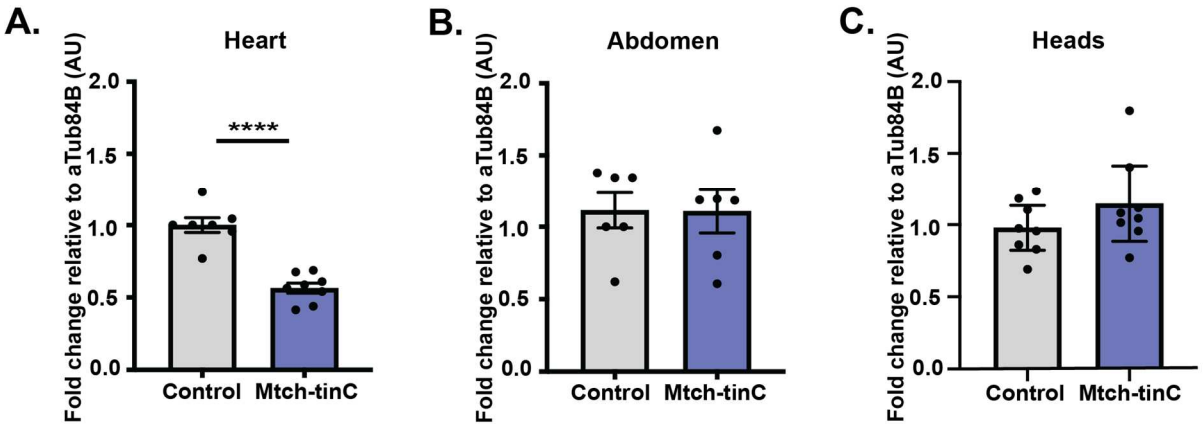

Figure 3.2 *Mtch*-tinC flies have cardiac-specific reduction in *Mtch* transcript levels (**A-C**) In Mtch-tinC flies, *Mtch* expression was reduced in heart tubes (N=7, ****P<0.0001), but *Mtch* expression was unchanged in abdominal tissue after heart tube removal (N=6, P>0.05) and unchanged in whole heads of Mtch-tinC flies (N=8, P>0.05). Average ± SEM, black dots represent group of 20 flies. Gene expression values were normalized to αTub84B.

Optical coherence tomography was applied to evaluate heart tube function, demonstrating that *Mtch* cardiac depletion produced marked reduction in cardiac function, seen as an increase in both end-diastolic and end-systolic diameter of heart tubes (**Figure 3.3 A, B, and F)**. This reduction in fractional shortening occurred in *Mtch* mutants as early as the first week of life and was maintained throughout adulthood (**Figure 3.3 C-F)**.

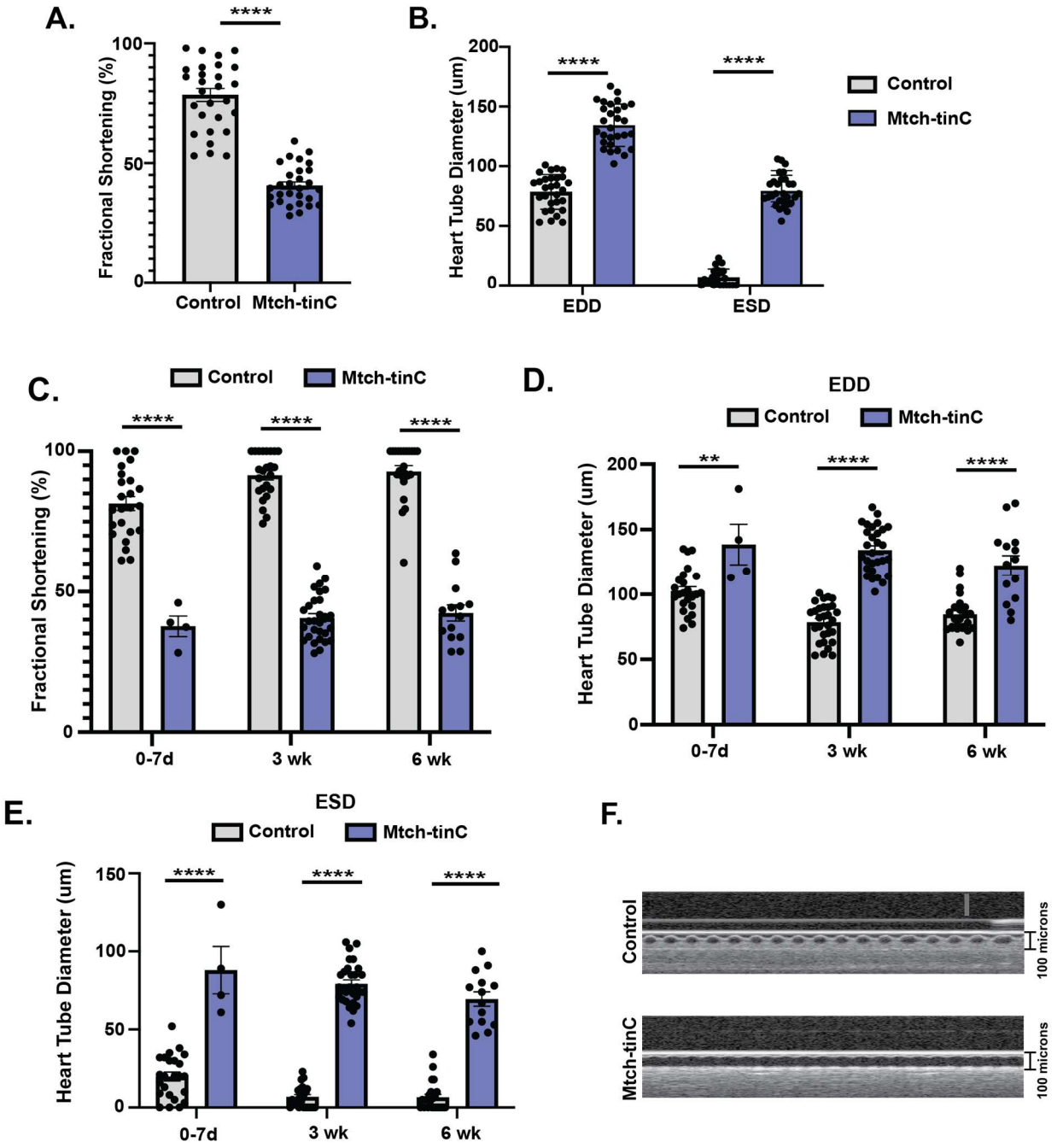

Figure 3.3 Heart tube function was impaired in cardiac *Mtch* knockdown flies. (**A-B**) Fractional shortening (FS) was reduced in the heart tube of Mtch-tinC flies assessed by optical coherency tomography (****P<0.0001, black dots represent each individual fly, N=29). The right panel shows end-diastolic diameter (EDD) and end-systolic diameter (ESD) of heart tubes EDD (****P<0.0001), ESD (****P<0.0001, *N*=29, black dots represent each individual fly). **(C)** FS was reduced in the heart tube of *Mtch-tinC* flies of all ages tested (purple) as assessed by optical coherency tomography (N=29) ****P<0.0001, black dots represent each individual fly. (**D-E).** EDD and ESD were increased *Mtch-tinC* flies of all ages tested (purple) (N=29) EDD ****P<0.0001, ESD ****P<0.0001) (**F**) Images from of 3-week-old flies using optical coherence tomography. Panels reveal degree of contraction of the heart tube. Top panel is imaging from control fly, bottom panel shows a Mtch-tinC fly with reduced function as evidenced by the lack of contraction.

Cardiac-specific reduction of *Mtch* significantly shortened lifespan compared to control flies, resulting in a reduction of the 50% survival rate **(Figure 3.4)**. Overall, partial reduction of *Mtch* in the fly heart adversely affected heart tube function and reduced overall longevity.

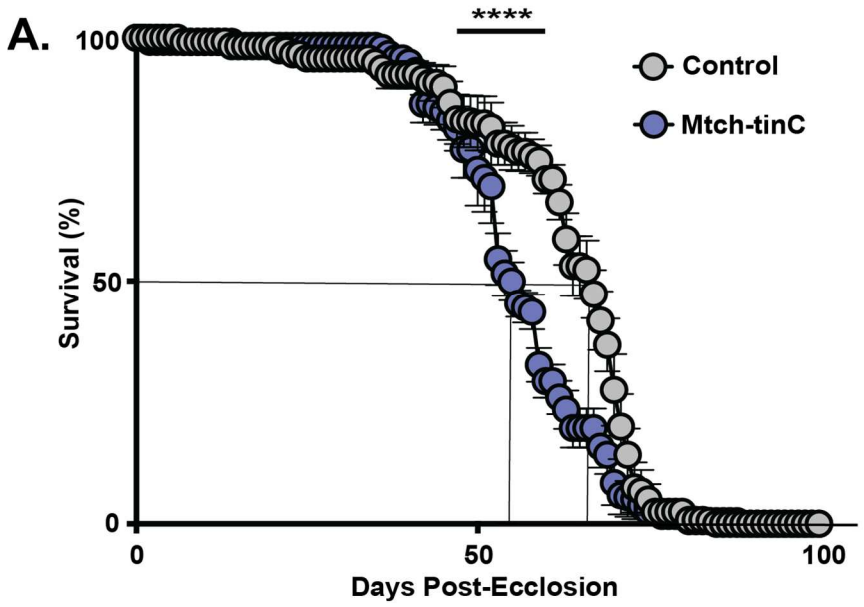

Figure 3.4 Cardiac-specific knockdown of *Mtch* reduces lifespan in flies. Kaplan–Meier curve showing *Mtch-tinC* flies had reduced longevity (N=120 per genotype), ****P<0.0001, Kaplan–Meir estimate). Unless stated otherwise, all comparisons were made using a two-tailed student's *t*-test. All experiments used equal numbers of 3-week-old males and females. Dark gray = *Mtch-tinC*; light gray = control.

3.4.2 Depletion of cardiac Mtch in flies alters substrate stores.

To assess energy storage in cardiac *Mtch* knockdowns, we measured adiposity in *Mtch* knockdown larvae using a buoyancy test(Reis 2010). Cardiac *Mtch* knockdowns had reduced abdominal triglyceride content and were significantly less buoyant than controls, indicating less overall adiposity and fat content **(Figure 3.5 A and B)**. These findings align with GWAS identifying lower *MTCH2* expression associated with reduced adiposity in humans. Food consumption was similar in *Mtch* knockdown and control flies, suggesting calorie intake was not

responsible for shifts in adiposity **(Figure 3.5 C).** There was excess glycogen content in the heart tube-containing abdomen of 3-week-old adult mutant flies compared to controls **(Figure 3.5 D)** with no change in circulating glucose relative to controls **(Figure 3.5 E).** The reduced body fat content and greater abdominal glycogen storage in cardiac *Mtch* knockdowns suggested the predominantly carbohydrate rich diet normally fed to flies was shifted more towards glycolysis and less from oxidative phosphorylation.

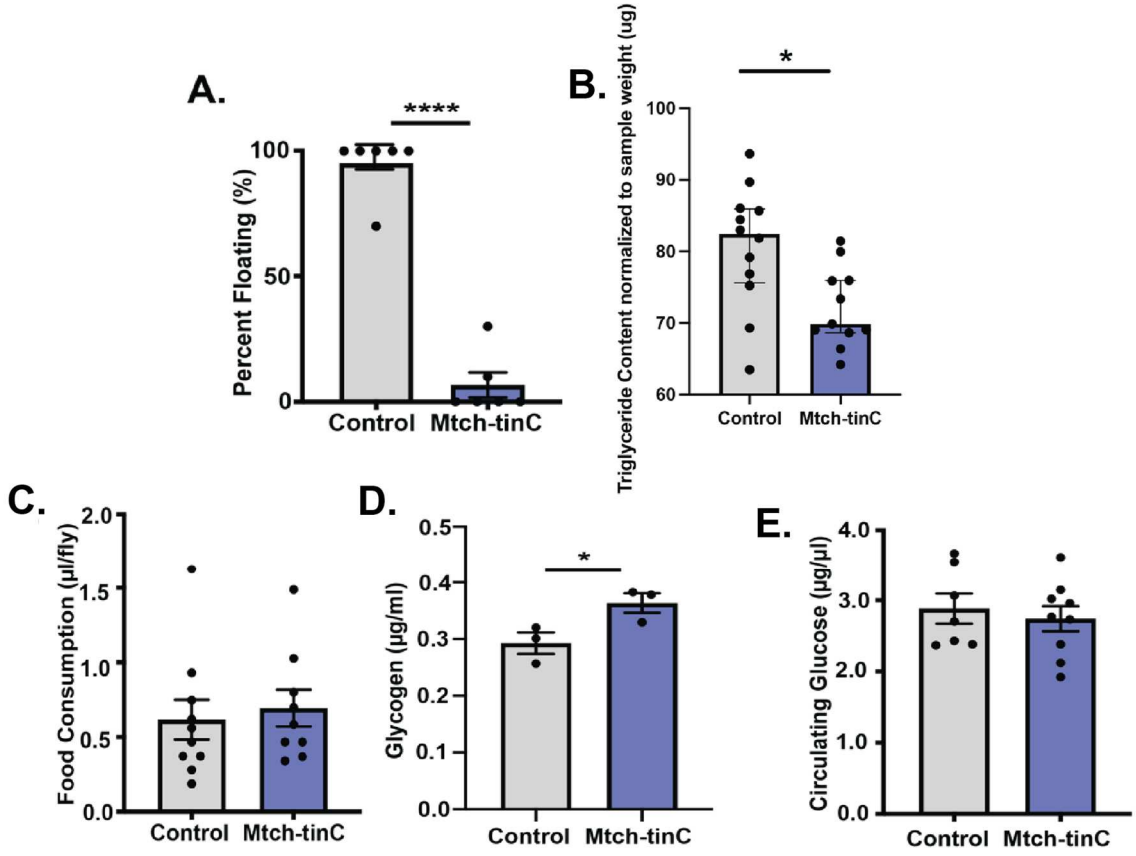

Figure 3.5 Cardiac *Mtch* knockdowns had reduced adiposity and increased glycogen content. (**A**) *Mtch-tinC* larvae had reduced adiposity based on buoyancy of third instar larvae (average ± SEM, N=6, each black dot represents 10 flies, ****P<0.0001). (**B**) Whole abdominal triglyceride content was reduced in cardiac *Mtch* knockdown flies. (N=12). Each dot represents triglyceride quantification of a cohort of 20 flies, each normalized to sample weight and using equal numbers of males and females at 3 weeks of age. (P=0.01). **(C)** Food consumption over a 24h period was unchanged in 3-week-old Mtch-tinC flies (N=8, each black dot represents 20 flies, P>0.05). (**D**) Glycogen content was greater in the heart-containing abdomen of *Mtch-tinC* flies (*N* = 120, *P=0.0491). (**E**) Circulating glucose levels were unchanged in the hemolymph of *Mtch- tinC* flies (N=8, each black dot is 60 flies, P>0.05). All comparisons were made using a two-tailed Student's *t*-test. Unless stated otherwise, all experiments used equal numbers of 3-week-old males and females. Dark gray = *Mtch-tinC*; light gray = control.

3.4.3 Cardiac Mtch dysfunction increases glycolytic lactate accumulation in flies.

At baseline, cardiac *Mtch* knockdowns had significantly higher circulating lactate levels than control flies, consistent with the shift towards glycolysis with *Mtch* reduction and similar to what was reported in mice lacking Mtch2 in skeletal and cardiac muscle (**Figure 3.6 A**). Cardiac *Mtch* knockdowns also had an increased ratio of lactate to pyruvate, consistent with greater conversion of pyruvate to lactate (**Figure 3.6 B**). These findings were corroborated with whole body proton production rate (PPR), another indicator of glycolytic output, in the presence of 10mM glucose in which cardiac *Mtch* knockdowns had higher whole-body PPR (**Figure 3.6 C**). Although lactate was increased in *Mtch* knockdowns, expression of lactate dehydrogenase mRNA itself was unchanged in these flies (**Figure 3.6 D**). The lactate accumulation seen in *Mtch* reduction suggested glycolysis as a major source of ATP, rather than the normal use of oxidative phosphorylation.

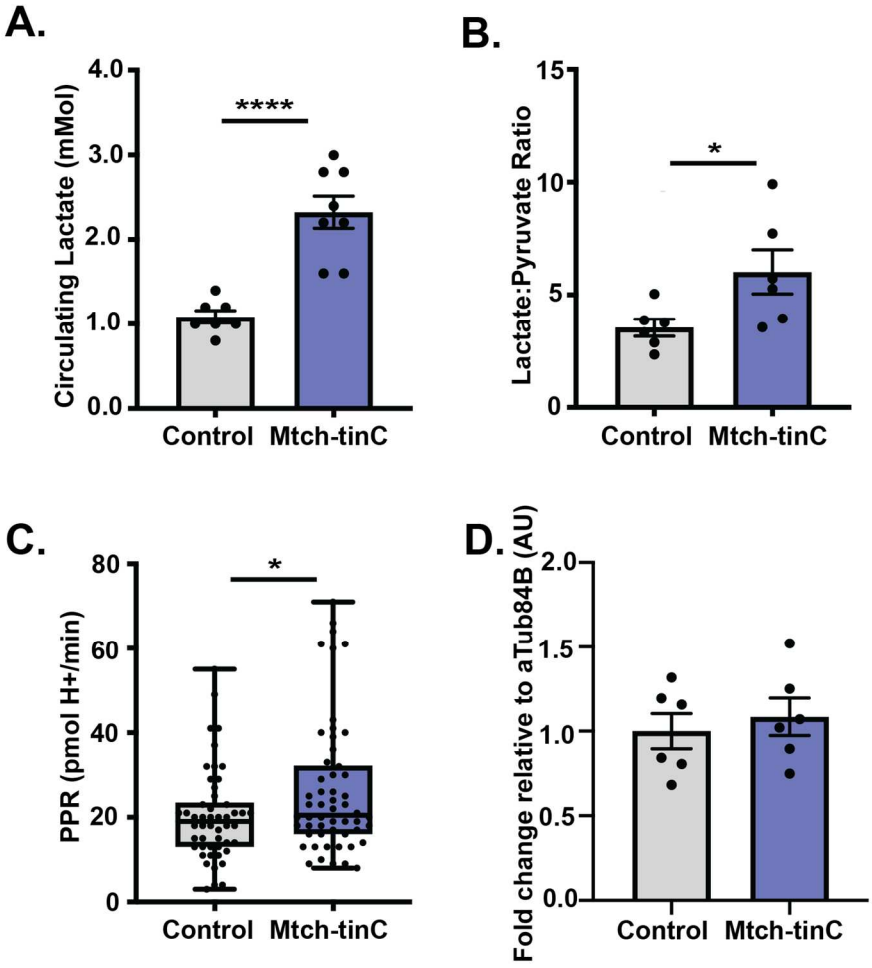

Figure 3.6 Increased circulating lactate in cardiac *Mtch* knockdown *Drosophila*. (**A**) Circulating lactate was increased in the hemolymph of *Mtch-tinC* flies (average ± SEM, N=8 groups, each dot is 60 flies, ****P<0.0001). (**B**) Ratio of normalized lactate:pyruvate metabolite counts in the heart-containing abdomen was elevated in *Mtch-tinC* flies, measured by LCMS-based targeted metabolite profiling (N=6, each black dot is 30 flies, ****P<0.0001). (**C**) Whole-body PPR was increased *in Mtch-tinC* flies (N=51, each black dot is 20 flies, *P=0.02). (**D**) *Ldh* expression was unchanged in heart- containing abdomen in *Mtch-tinC* flies (N=6, each black dot is 20 flies, P>0.05). The increase of lactate to pyruvate and PPR suggests increased glycolysis. Gene expression values are normalized to α*Tub84B*. All com- parisons were made using a two-tailed Student's *t*-test. Unless stated otherwise, all experiments used equal numbers of 3-week-old males and females. Dark gray = *Mtch-tinC*; light gray = control.

3.4.5 Cardiac Mtch dysfunction lowers the rate of glucose oxidation and energy production in flies.

We measured oxygen consumption rate (OCR) in the presence of glucose or the fatty acid palmitate. Cardiac *Mtch* knockdown flies had lower OCR in the presence of glucose, but not palmitate, demonstrating a substrate-specific impairment in OCR (**Figure 3.7 A**). To determine whether this glucose-specific reduction in OCR associated with lower oxidative phosphorylation, we examined the ratio of ATP:ADP metabolites in the presence of 10mM glucose. Using targeted metabolomics, we found that cardiac *Mtch* knockdowns also had a reduction in ATP:ADP in the presence of glucose (**Figure 3.7 B**), suggesting compromised energy production when glucose is the substrate. We exposed flies to ^{13}C M+6 labeled glucose (each of the 6 carbons in glucose is a ^{13}C isotope instead of ^{12}C) to trace the flux of glucose molecules through glycolysis and pyruvate oxidation to identify the disruption in glucose oxidation (**Figure 3.7 C**). Ratio of M+3 labeled lactate to M+2 labeled citrate can be used to infer the relative amount 13C M+6 labeled glucose contributing to glycolysis versus oxidation through the tricarboxylic acid (TCA) cycle. This ratio was higher in *Mtch* knockdowns relative to controls, demonstrating glucose in *Mtch* knockdowns was shifted towards being metabolized via glycolysis rather than oxidized to fuel the tricarboxylic acid (TCA) cycle (**Figure 3.7 D**). Furthermore, the amount of M+2 labeled citrate (citrate derived from ^{13}C M+6 labeled glucose metabolism) generated from M+3 labeled pyruvate (pyruvate derived from 13C M+6 labeled glucose metabolism) was lower in *Mtch* knockdowns compared to controls, indicating the entry of glucose derivatives into the TCA cycle was partially blocked in *Mtch* knockdowns (**Figure 3.7 E**). The rate of glycolysis was unchanged in *Mtch* knockdowns, and the amount of glycolytic intermediates diverted to the pentose phosphate pathway (PPP) was negligible, suggesting that the disruption in glucose metabolism was in glycolysis and PPP metabolism (**Figure 3.8 A-C**). When examining percent composition of labeled TCA species, there were no significant differences in labeled TCA metabolite ratios nor in the ratio of M+2:M+4 citrate (citrate derived

from 13C M+6 labeled glucose metabolism where M+2 citrate is representative of citrate metabolism the first turn of the TCA cycle, and M+4 citrate is representative of M+2 citrate being further metabolized in a subsequent turn of the TCA cycle), suggesting that the efficiency of the TCA cycle itself was unchanged in *Mtch* knockdowns (**Figure 3.8 D**). Interestingly, the assessment of pooled labeled and unlabeled metabolites showed that total levels of TCA metabolites were unchanged between *Mtch* knockdowns and controls (**Figure 3.7 F**).

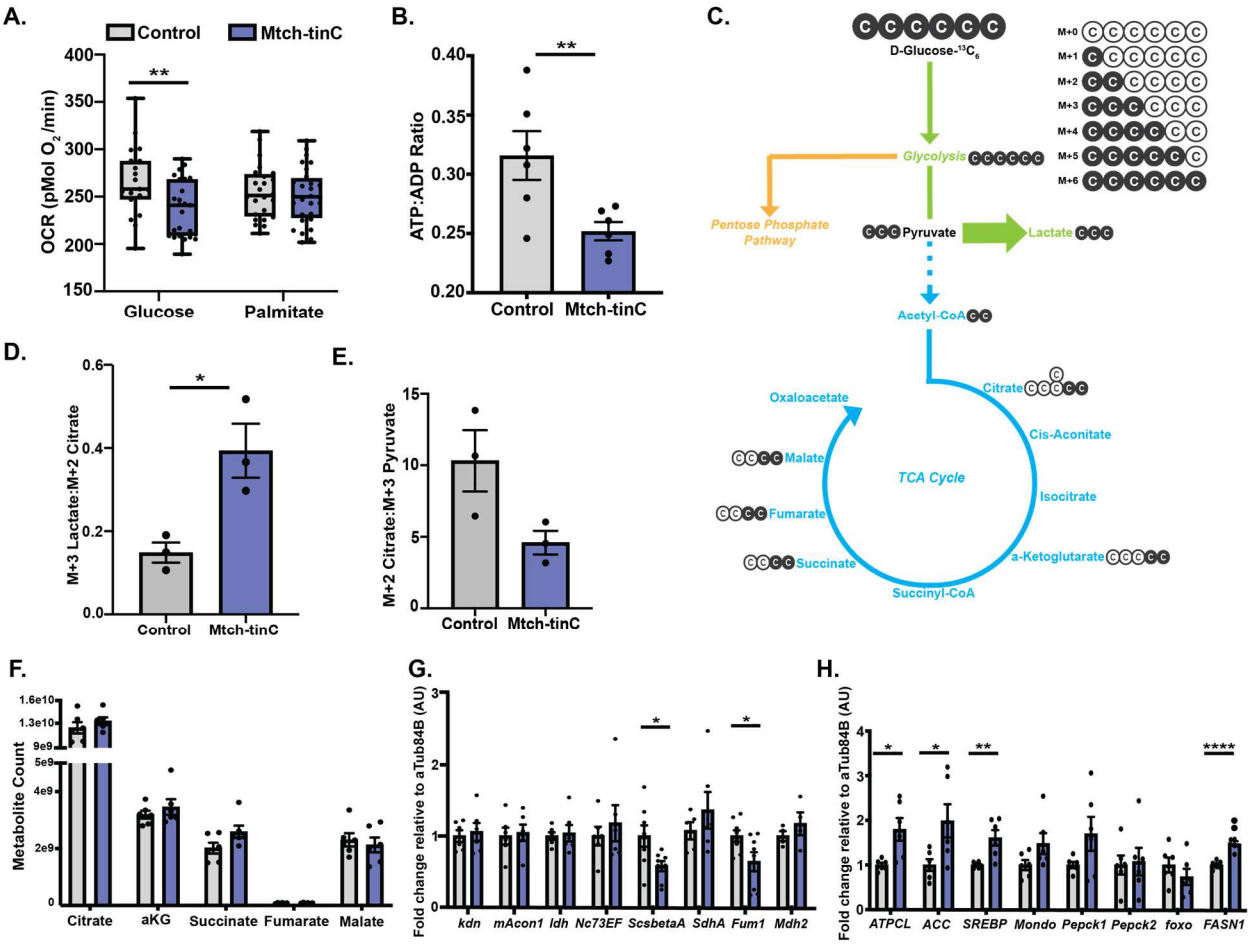

Figure 3.7 Cardiac *Mtch* knockdown in *Drosophila* obstructed glucose oxidation and energy production. (**A**) Whole-body basal OCR was reduced in cardiac *Mtch*-knockdowns given glucose but not palmitate (average ± SEM, N=20, each black dot represents 20 flies, **P=0.006). (**B**) *Mtch-tinC* flies had reduced energy generation, measured by the ratio of normalized ATP:ADP metabolite counts (N=6 groups, each black dot is 30 flies, *P=0.02). (**C**) Metabolite flux profiling traced the fate of consumed ^{13}C M+6 labeled glucose. (**D**) Glucose had a greater fate to lactate production in *Mtch-tinC* flies, assessed from ratio of normalized labeled lactate:pyruvate metabolite counts (average ± SEM, N= 6, each black dot represents 30 flies, *P=0.0242) (green arrow in **C**). (**E**) Amount of pyruvate shuttled to the citric acid cycle was lower in *Mtch-tinC* flies (N=3, each black dot represents 30 flies, P=0.07) (blue dashed arrow in **C**). (**F**) Measurement of total normalized citric acid cycle metabolites was unchanged in *Mtch-tinC* flies (N=6, each black dot represents 30 flies, citrate (P=0.34), α keto glutarate (P=0.40), succinate (P=0.07), fumarate (P=0.61), malate (P=0.63)). (**G**) Expression of genes encoding the citric acid cycle enzymes showed selective reduction of *ScsbetaA* (*P=0.02) and *Fum1* (*P=0.04) (N=6, each black dot represents 20 flies). (**H**) Expression of genes implicated in fatty acid metabolism showed selective reduction of *ATPCL* (*P=0.01), *ACC* (*P=0.03), *SREBP* (**P=0.006) and *FASN1* (****P<0.0001) (N=6, each group represents 20 flies). Gene expression values are normalized to α*Tub84B*. All comparisons were made using a two-tailed student's t-test. Unless stated otherwise, all experiments used equal numbers of 3-week-old males and females. Purple = *Mtch-tinC*; gray = control.

The mRNA expression of most TCA enzymes was unchanged in cardiac *Mtch* knockdowns in the presence of glucose with the exception that *ScsbetaA* (succinate-CoA ligase) and *Fum1* (fumarase) were reduce (**Figure 3.7 G**). The reduction in glucose-derived citrate in the TCA cycle in the face of unchanged total TCA metabolite levels suggests that other metabolic pathways may be compensating to fuel the TCA cycle in cardiac *Mtch* knockdowns. In support of compensation, we found an upregulation of *ATPCL, ACC, SREBP*, and *FASN1*, key genes involved in fatty acid synthesis, in cardiac *Mtch* knockdowns compared to controls (**Figures 3.7 H**). This upregulation may help maintain the TCA cycle and oxygen consumption in the presence of palmitate. However, this upregulation is adequate since longevity was compromised in cardiac *Mtch* knockdown flies (**Figure 3.4 G**). These findings point to pyruvate oxidation, and therefore acetyl-CoA entry into the TCA cycle, as a potential dysregulated step in glucose metabolism in cardiac *Mtch* knockdowns.

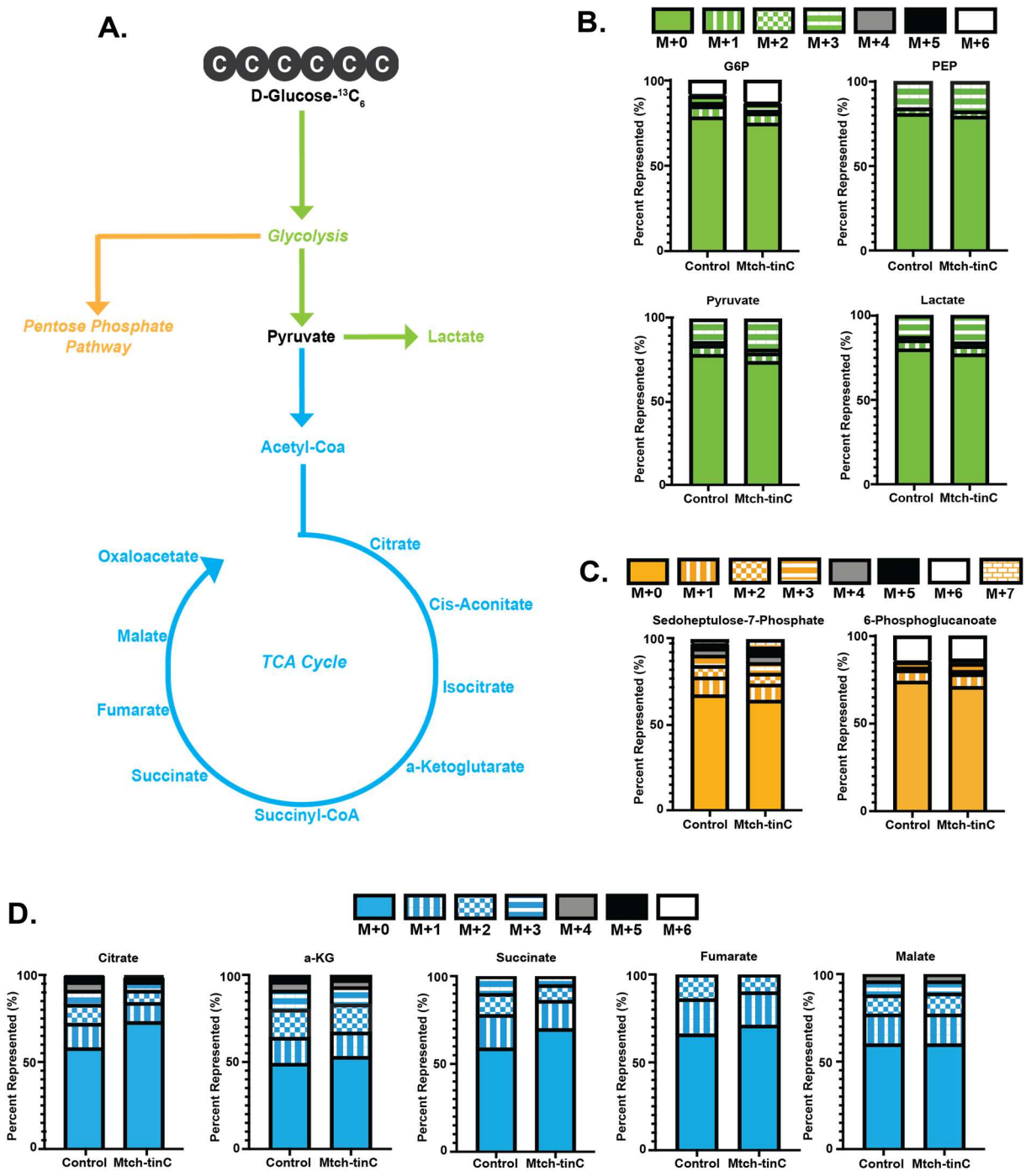

Figure 3.8 Cardiac *Mtch* knockdown does not alter the rate of metabolic processes. (**A**) Metabolite profiling using fluxomics traced the fate of consumed ^{13}C M+6 labeled glucose. (**B**) Labeled glycolytic intermediate quantification in the presence of labeled glucose showed no significant alteration of glycolytic rate between Control and *Mtch-tinC* flies. (**C**) Labeled pentose phosphate pathway (PPP) intermediate quantification in the presence of labeled glucose showed no significant alteration of PPP rate between Control and *Mtch-tinC* flies. (**D**) Labeled TCA intermediates in the presence of labeled glucose showed no significant alteration of TCA rate between Control and *Mtch-tinC* flies. Unless stated otherwise, all experiments used equal numbers of 3-week-old males and females (average±SEM, N=3 cohorts of 30 flies).

3.4.6 Enhanced Pyruvate Dehydrogenase (PDH) activity through inhibition of Pyruvate Dehydrogenase Kinase (PDK) offsets Mtch reduction.

PDK inhibits PDH, preventing pyruvate to acetyl-CoA conversion, and resulting in more lactic acid production. mRNA expression of *Pdha* (pyruvate Dehydrogenase A), *PdhB* (pyruvate dehydrogenase B), *Pdk* (pyruvate dehydrogenase kinase), and *Pdp* (pyruvate dehydrogenase phosphatase) was unchanged in *Mtch* knockdown heart-containing abdomens (**Figure 3.9 A**). We investigated whether PDK inhibition could alleviate the block in glucose oxidation observed in cardiac *Mtch* knockdowns by treating flies the first day of pupal eclosion with 20 μg/ml dichloroacetic acid (DCA), a chemical inhibitor of PDK and known activator of PDH (Khan, Allende-Vega, 2017). DCA treatment rescued survival of cardiac *Mtch* knockdowns (**Figure 3.9 B**). Additionally, DCA treatment restored glucose oxidation in *Mtch* knockdowns, as demonstrated by a reduction in circulating lactate levels and increase in OCR in the presence of glucose (**Figure 3.9 C and D**). As a positive control, flies were treated for 3 days with 6,8-bis(benzylthio)octanoic acid (BOA), a small molecule inhibitor of PDH (Rabin-Court 2019). BOA treatment increased circulating lactate levels in control flies to the level observed in untreated *Mtch* knockdowns, and at the same time, BOA treatment did not alter lactate levels in cardiac *Mtch* knockdowns (**Figure 3.9 E**). These findings are consistent with *Mtch* knockdowns having a high basal level of inhibited PDH, resulting in excess lactate production.

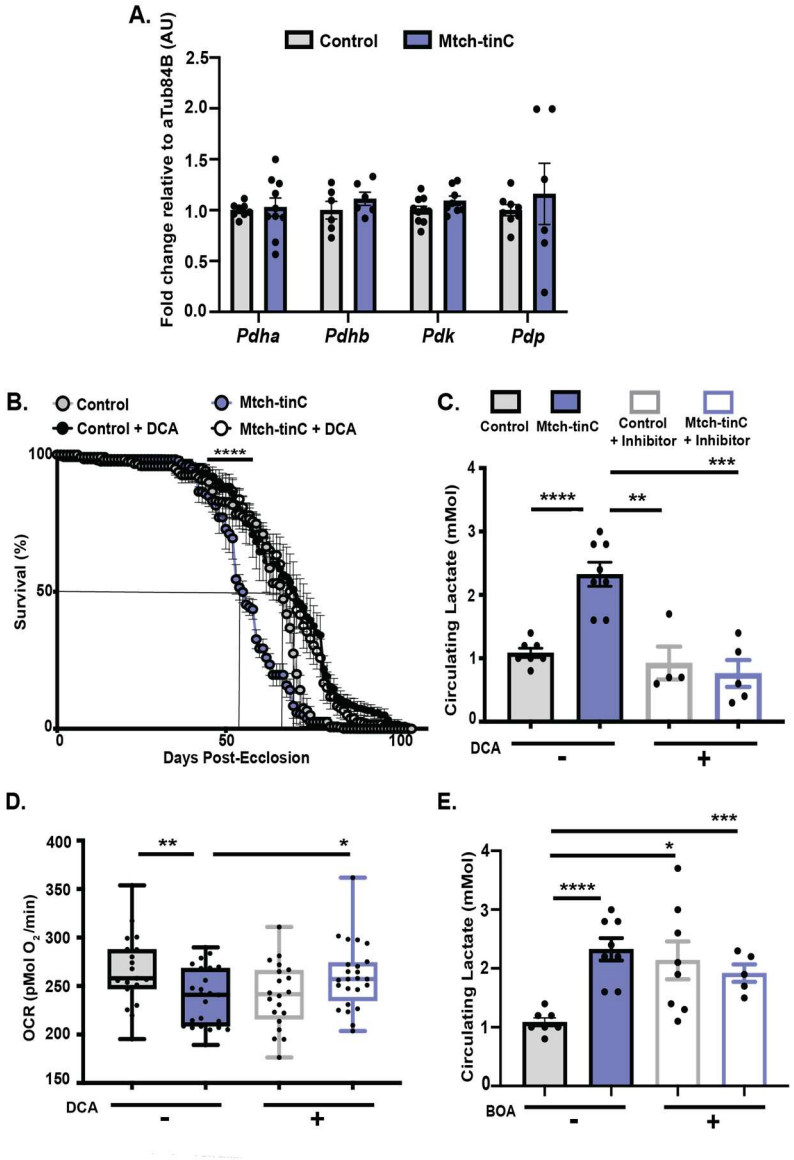

Figure 3.9 Chemical inhibition of PDK in *Drosophila Mtch* knockdowns improved lifespan and elevated lactate levels. (**A**) Gene expression of enzymes involved in pyruvate metabolism are unchanged under cardiac knockdown of *Mtch* (N=6, each black dot represents 20 flies). (**B**) Longevity analysis of flies given PDK inhibitor (DCA) post-eclosion. PDK inhibition improved lifespan in *Mtch-tinC* flies (average ± SEM, N=120, *Mtch-tinC* minus DCA vs *Mtch-tinC* given DCA, *P<0.0001, Kaplan–Meier estimate). (**C**) Circulating lactate measured in flies given either glucose diet or glucose diet supplemented with PDK inhibitor (DCA, clear column). PDK inhibition lowered lactate levels in *Mtch-tinC* flies (N=8, each black dot represents 60 flies, Control minus DCA vs *Mtch-tinC* minus DCA, ****P<0.0001, *Mtch-tinC* minus DCA vs Control given DCA, **P=0.0015, Control given DCA vs *Mtch-tinC* given DCA, ***P=0.0002)). (**D**) Measurement of whole-body basal OCR under glucose conditions given either glucose without PDK inhibitor or glucose supplemented with PDK inhibitor (DCA). PDK inhibition improved *Mtch-tinC* OCR (N=20 wells of 20 flies, control DCA vs *Mtch-tinC* minus DCA, **P=0.0060, *Mtch-tinC* minus DCA vs *Mtch-tinC* given DCA, *P=0.0159. (**E**) Circulating lactate measured from hemolymph of flies given either glucose diet or glucose diet supplemented with PDH inhibitor (BOA) (N=8 groups of 60 flies). PDH inhibition does not affect *Mtch-tinC* lactate levels. Control minus inhibitor vs *Mtch-tinC* minus inhibitor, ****P<0.0001, Control minus BOA vs Control given BOA, *P=0.0104, *Mtch-tinC* minus BOA vs *Mtch-tinC* given BOA, ***P=0.0003 two-tailed Student's *t*-test *P* value. Unless stated otherwise, all comparisons were made using a two-tailed Student's t-test. All experiments used 3-week-old equal numbers of males and females. Purple = *Mtch-tinC*; gray = control.

3.4.7 Mitochondrial dysfunction in cardiac Mtch knockdowns.

To determine if mitochondrial function was compromised cardiac *Mtch* knockdowns, we employed targeted metabolomics to measure the ratio of oxidized glutathione (GSSG) to reduced glutathione (GSH), a common indicator of oxidative stress. GSSG:GSH was significantly elevated in cardiac *Mtch* knockdowns, indicating that *Mtch* knockdowns have higher levels of reactive oxygen species (ROS) (**Figure 3.10 A**). To determine if *Mtch* knockdowns were tolerant to exogenous oxidative stress, we treated flies for 24 hours with 150nM paraquat, a ROS-inducing toxin, finding that cardiac *Mtch* knockdowns experienced a greater mortality rate and therefore greater susceptibility to exogenous ROS than control flies (**Figure 3.10 B**). We examined expression of *Trxr-2*, which encodes a ROS-neutralizing enzyme. *Trxr-2* expression was reduced in *Mtch* knockdown heart-containing abdomens (**Figure 3.10 C**). However, when we assessed gene expression of other ROS-neutralizing enzymes, catalase and *SOD2*, no change was observed in *Mtch* knockdowns (**Figure 3.10 D and E**). We found the mitochondrial genome encoded expression of the *ND2* transcript increased relative to the nuclear genome-encoded αTub84B transcript in cardiac *Mtch* knockdowns with unchanged *PGC1*α expression (**Figure 3.10 F and G**). We interpret this relative increase in mitochondrial transcriptional expression to reflect enhanced but inadequate mitochondrial biogenesis since OCR and ATP production were impaired in the presence of glucose (**Figure 3.7 A and B**). Gene expression of known regulators of mitochondrial fission and fusion were not altered in cardiac *Mtch* knockdowns (**Figure 3.10 H**), and mitochondrial cristae were intact in *Drosophila* cardiac *Mtch* knockdown heart tubes (**Figure 3.10 I**).

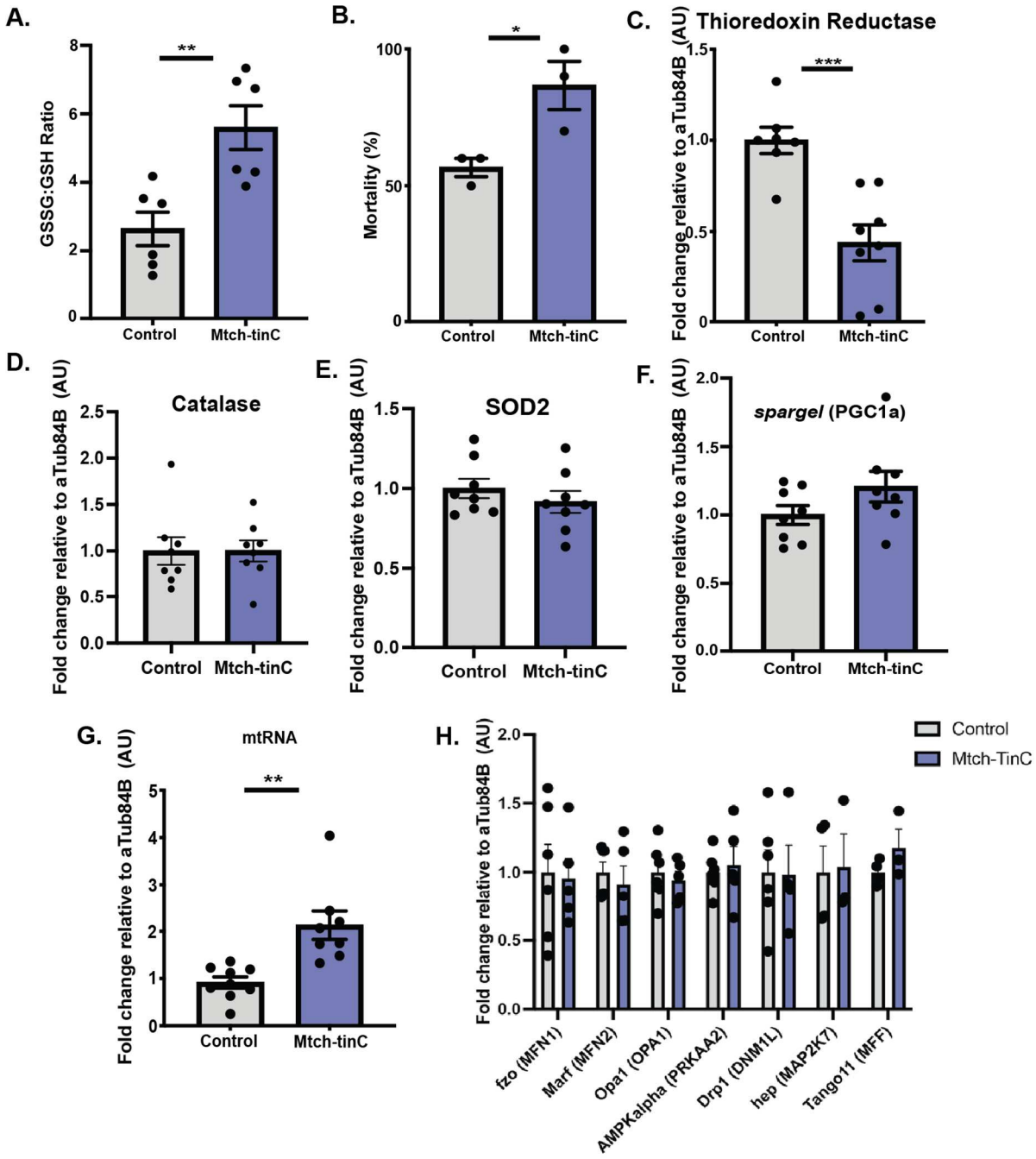
A.
GSSG:GSH Ratio
**
Control
Mtch-tinC
B.
Mortality (%)
*
Control
Mtch-tinC
C.
Thioredoxin Reductase
Fold change relative to aTub84B (AU)
***
Control
Mtch-tinC
D.
Catalase
Fold change relative to aTub84B (AU)
Control
Mtch-tinC
E.
SOD2
Fold change relative to aTub84B (AU)
Control
Mtch-tinC
F.
spargel (PGC1a)
Fold change relative to aTub84B (AU)
Control
Mtch-tinC
G.
mtRNA
Fold change relative to aTub84B (AU)
**
Control
Mtch-tinC
H.
Control
Mtch-TinC
Fold change relative to aTub84B (AU)
fzo (MFN1)
Marf (MFN2)
Opa1 (OPA1)
AMPKalpha (PRKAA2)
Drp1 (DNM1L)
hep (MAP2K7)
Tango11 (MFF)
I.
200 nm
200 nm

Figure 3.10 Mitochondrial dysfunction in cardiac *Mtch* knockdown *Drosophila*. (**A**) Ratio of oxidized glutathione: reduced glutathione was elevated in the heart-containing abdomen of *Mtch-tinC* flies measured by LCMS-based targeted metabolite profiling (average ± SEM, N=6, each black dot represents 30 flies, **P=0.0043). (**B**) *Mtch-tinC* flies were more susceptible to death after 24h exposure to paraquat, a ROS-inducing toxin (N=6, each black dot represents 30 flies, *P=0.0335). (**C**) Gene expression of mitochondrial thioredoxin reductase (*Trxr-2*) was lower in *Mtch-tinC* flies (N=6, each black dot represents 20 flies, ***P=0.0006). Gene expression values are normalized to α*Tub84B*. (**D-F**) Gene expression of Catalase, SOD2, and *spargel* (PGC1α) is unchanged under cardiac knockdown of *Mtch,* (N=6, each black dot represents 20 flies). (**G**) *Mtch-tinC* flies had greater expression of mitochondrial-specific mRNA relative to nuclear- specific mRNA in the presence of glucose (N=8, each black dot represents 20 flies, **P=0.001). (**H**) Expression of genes regulated in mitochondrial fission and fusion are unchanged. (**I**) Cristae structure of *Mtch* knockdowns appear unchanged. Unless stated otherwise, all comparisons were made using a two-tailed Student's *t*-test. All experiments used equal numbers of 3-week-old males and females. Purple = *Mtch-tinC*; light gray = control.

3.4.8 Deletion of MTCH2 in human cells reduces oxygen consumption rate and pyruvate dehydrogenase activity

To investigate the role of *MTCH2* in human cells, we used gene editing to target exon 1 of *MTCH2* in human embryonic kidney (HEK) 293 cells, resulting in a homozygous frameshift deletion. *MTCH2*$^{-/-}$ cells expressed no detectable MTCH2 protein and reduction of the *MTCH2* transcript (**Figure 3.11 A-C**). Similar to cardiac *Mtch* knockdown flies, *MTCH2*$^{-/-}$ cells supplemented with 50mM glucose had a greater basal PPR than unedited cells. Additionally, *MTCH2*$^{-/-}$ cells had reduced OCR in the presence of glucose, but not palmitate, demonstrating the same substrate-dependent impairment seen in cardiac *Mtch* flies (**Figure 3.11 D-E**). OCR was impaired under high glucose (50mM) conditions, and no difference was seen under 10mM glucose, suggesting that *MTCH2*$^{-/-}$ cells are susceptible to high glucose conditions (**Figure 3.11 F**). To evaluate mitochondria membrane potential, we stained control and *MTCH2*$^{-/-}$ HEK cells for MitoTracker Green, a mitochondrial marker, and TMRM, a marker of mitochondrial membrane potential that sequesters in active and functional mitochondria (**Figure 3.11 G**). We found that *MTCH2*$^{-/-}$ cells had lost TMRM signal, indicating loss of mitochondrial membrane potential and dysfunctional mitochondria. Supplementation of *MTCH2*$^{-/-}$ cells with 50mM glucose and DCA was sufficient to increase OCR in *MTCH2*$^{-/-}$ cells, confirming that PDH activation can override the loss of *MTCH2*$^{-/-}$ (**Figure 3.11 H**). We found increased mitochondrial DNA relative to nuclear DNA (nDNA) in *MTCH2*$^{-/-}$ cells (**Figure 3.11 I**), despite no change in OCR and ATP production in the presence of glucose, as would be expected with increased mitochondria (**Figure 3.11 J**). These data suggest *MTCH2*$^{-/-}$ cells undergo a compensatory but inadequate mitochondrial biogenesis. Interestingly, the expression of PDK1 and PDK4 were increased in *MTCH2*$^{-/-}$ cells compared to control cells (**Figure 3.11 K-L)**. Accordingly, PDH activity was reduced in mitochondria of *MTCH2*$^{-/-}$ cells. However, reduced PDH activity was not seen in whole cell lysates, confirming that the reduction of PDH activity in *MTCH2*$^{-/-}$ cells is

mitochondria-specific (**Figure 3.11 M-N**). These findings demonstrate that inhibition of PDK alleviates *MTCH2* knockdown and knockout phenotypes in both fly hearts and human cells.

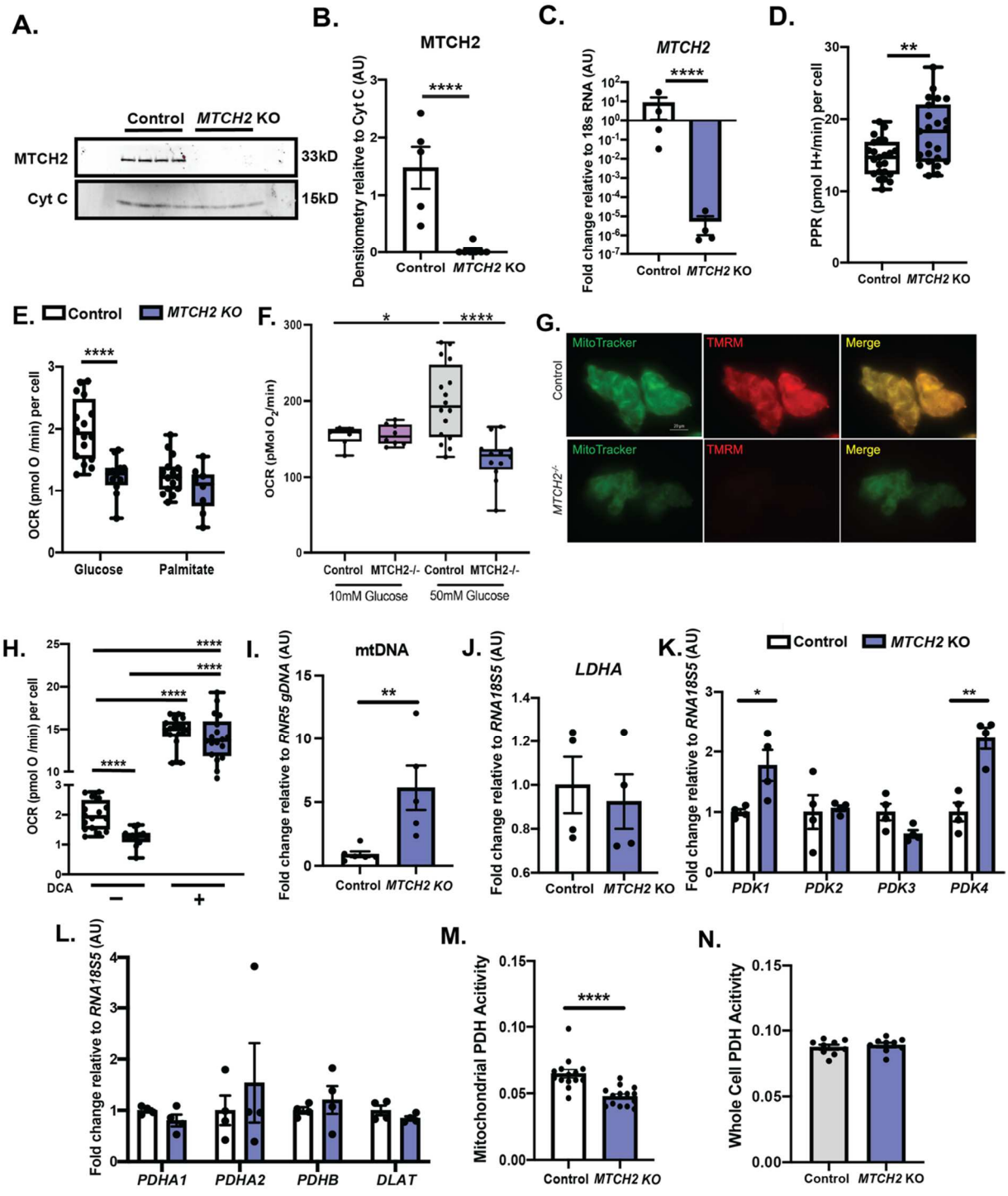

Figure 3.11 Deletion of *MTCH2* in HEK293 cells reduced OCR and pyruvate dehydrogenase activity. (**A**) Immunoblot of MTCH2 protein in control (unedited) and *MTCH2*$^{-/-}$ cells (*MTCH2 KO*), relative to mitochondrial cytochrome C. (**B**) Quantification of immunoblot band density relative to mitochondrial cytochrome C protein (average ± SEM, N=6 wells of cultured cells, ****P,0.0001). (**C**) *MTCH2* mRNA was reduced in *MTCH2*$^{-/-}$ cells compared to control (N=4, ****P<0.0001). (**D**) Basal PPR of cells supplemented with 50 mm glucose (N=23 wells, **P=0.002). (**E**) Basal OCR of control and *MTCH2*$^{-/-}$ cells supplemented with 50 mm glucose or 1 mm palmitate, normalized to cell count (N=18 wells, ****P<0.0001). (**F**) Basal OCR in the presence of 50 mm glucose media supplemented with 100 µm DCA PDK inhibitor, normalized to cell count (N=18 wells Control minus DCA vs *MTCH2* KO minus DCA, ****P<0.0001; Control minus DCA vs Control plus DCA, ****P<0.0001; Control minus DCA vs *MTCH2* KO plus DCA, ****P<0.0001; *MTCH2* KO minus DCA vs *MTCH2* KO plus DCA, ****P<0.0001). (**G)** Loss of mitochondrial membrane potential in *MTCH2*$^{-/-}$ human cells. Mitochondria were marked in control and *MTCH2*$^{-/-}$ cells using MitoTracker Green (green). The same mitochondria when stained with TMRM (red) showed a loss of signal, consistent with loss of mitochondria membrane potential. (N=3 wells per genotype). **(H**) Basal OCR in the presence of 50 mm glucose media supplemented with 100 µm DCA PDK inhibitor, normalized to cell count (N=18 wells Control minus DCA vs *MTCH2* KO minus DCA, ****P<0.0001; Control minus DCA vs Control plus DCA, ****P<0.0001; Control minus DCA vs *MTCH2* KO plus DCA, ****P<0.0001; *MTCH2* KO minus DCA vs *MTCH2* KO plus DCA, ****P<0.0001). (**I**) mtDNA in control vs *MTCH2*$^{-/-}$ cells (N=6 wells, **P=0.009). **(J)** Gene expression of *LDHA* in Control (white*) MTCH2*$^{-/-}$ cells (purple) (average ± SEM, N=4 wells of distinct cultures). **(K)** Gene expression PDK isoforms (N=4) *PDK1** P=0.0260, PDK4 **P=0.002. **(L)** Gene expression PDH subunits and isoforms (N=4, each black dot represents 20 flies). (**M**) Pyruvate dehydrogenase activity in mitochondria isolated from control and *MTCH2*$^{-/-}$ cells, normalized to mitochondrial count (N=14 wells, ****P<0.0001). (**N**) Pyruvate dehydrogenase activity in whole cell lysates, normalized to mitochondrial count (N=14 wells). Purple = *Mtch-tinC*; gray = control. Gene expression values are normalized to *RNA18S5*.

3.5 Discussion

Cardiac *Mtch* knockdown flies and *MTCH2*$^{-/-}$ cells both displayed increased lactate. We found that chemical inhibition of PDK with DCA, a PDH inhibitor, reduced lactate levels in *MTCH2* mutants, and in flies with cardiac *Mtch* knockdown, lactate reduction was sufficient to extend lifespan. In human heart failure, DCA treatment was shown to improve myocardial lactate consumption with concomitant improvement in mechanical work of the left ventricle, but DCA treatment may not exert its effect by improving noninvasive measures of heart function (Lewis 1998; Matsuhashi 2015). In rodents, DCA treatment can be used to prevent heart failure outcomes through its action on PDK and also through epigenetic remodeling (Matsuhashi 2015; Kato 2010). Regulation of PDH through PDK is critical in tissues with high energy demand, such as the heart (Cluntun 2021). PDH converts pyruvate to acetyl coenzyme A (CoA) in the mitochondria, and PDH activity is inhibited by phosphorylation via PDK. PDH activity is known to be reduced in heart failure, and deletion of mitochondrial pyruvate carriers in the heart worsens heart failure phenotypes (Cluntun 2021; Zhang 2020). A block of pyruvate oxidation could itself account for the increase in lactate seen in *MTCH2* mutants. Alternatively, agents that inhibit PDK activity may simply be working indirectly to overcome mitochondrial defects arising from loss of MTCH2. Loss of MTCH2 increased mtDNA content, but increased mtDNA did not reflect enhanced mitochondrial biogenesis and function but is more consistent with an ineffective compensatory mechanism, which is further supported by reduced mitochondrial membrane potential in the absence of MTCH2. Recent work showed that deletion of *MTCH2* produced hyperfragmented mitochondria, consistent with MTCH2 having a key role in maintaining normal mitochondria structure and function (Labbé 2021). All of these mechanisms, excess lactate itself, reduced pyruvate oxidation or other mitochondrial impairment would be maladaptive in the setting of heart failure. Collectively, these data support the human GWAS demonstrating a link between *MTCH2* and adiposity. Under high fat conditions, reduced *MTCH2* promotes lean body mass and be protective from obesity. Intriguingly, *MTCH2* variants

linked to increased BMI in adults associate with lower birth weight with each BMI-increasing *MTCH2* allele associated with a 13g decrease in birthweight (Kilpeläinen 2011). The conditions that support rapid fetal growth are similar to the failing heart with an increased dependence on glucose as a fuel source. The substrate dependence of MTCH2 levels is an important consideration when considering its related phenotypes.

Collectively, we found that *MTCH2* is a critical component of glucose metabolism and is essential to mitochondrial function. The similar findings between human cells and *Drosophila* support a highly conserved mechanism, and we showed that cardiac *MTCH2* hindered glucose oxidation by a reduction in mitochondrial PDH activity, where mutant phenotypes were rescued by blocking the PDH inhibitor, PDK. These findings highlight the PDK-PDH axis as a potential therapeutic target for heart failure in people with genetic variants that are thought to reduce *MTCH2* expression., especially at stages of disease where the heart is more reliant on glucose as a substrate.

CHAPTER 4

Discussion

4.1 Overview

MTCH2 is a mitochondrial membrane protein that is implicated in disease. SNPs in *MTCH2* have been previously associated with obesity, and animal models of in which *MTCH2* expression has been reduced demonstrate reduction in adiposity and an increase in energy expenditure (Willer 2009; Buzaglo-Azriel 2016; Rottiers 2017; Kulyté 2011). Through genomic profiling, we identified *MTCH2* possesses aberrant variation in people with cardiomyopathy. Using a fly and human cell model, I showed that *MTCH2* influences metabolism in a substrate-specific manner. Specifically, in the presence of glucose, but not fatty acids, loss of *MTCH2* leads to reduction in pyruvate oxidation and increase in lactate production, accompanied by an ATP deficit. These phenotypes reflect reduction in mitochondrial PDH activity, where glucose-derived acetyl-CoA is not being used to fuel the TCA cycle. This chapter will discuss the potential mechanism by which PDH activity is reduced in the mitochondria under *MTCH2* dysfunction, and what role *MTCH2* may normally serve in a healthy cell.

This chapter contains excerpts from the Oxford University Press' Human Molecular Genetics article published in 2022, "Opposing effects of genetic variation in *MTCH2* for obesity versus heart failure," authored by Julie Fischer, Tanner Monroe, PhD, Lorenzo Pesce, PhD, Konrad Sawicki, MD PhD, Rosemary Bauer, Samuel Kearns, Matthew Wolf, MD PhD, Megan Puckelwartz, PhD, and Elizabeth McNally, MD PhD. Components of the discussion from this manuscript are incorporated into this chapter, which was written by Julie Fischer in collaboration with Megan Puckelwartz, PhD, and Elizabeth McNally, MD PhD.

4.2 Discussion

4.2.1 MTCH2 variation and metabolic outcomes in humans.

GWAS identified *MTCH2* SNPs with expression, obesity, and lean body mass (Willer 2009; Renström 2009; Bauer 2009). In humans, mice, worms, fish, and flies, there is a consistent relationship that upregulation of *MTCH2* associates with obesity while *MTCH2* downregulation is associated more with lean body mass (Willer 2009; Buzaglo-Azriel 2016; Rottiers 2017; Kulyté 2011). Although lean body mass is beneficial for most cardiovascular traits, the substate dependence in heart failure may represent an exception. In cardiomyopathy patients, we found overrepresentation of a SNP and haplotype linked to lower *MTCH2* expression. This type of inheritance, with high risk-allele population frequency is plausibly explained by antagonistic pleiotropy, wherein a risk allele for one condition may be protective in another (Carter 2011). Antagonistic pleiotropy is well described in traits associated with protection from infection like sickle cell and malaria and APOL1 and trypanosoma infection (Piel 2010; Vanhollebeke 2006). In these examples, genetic variation that protects against infection creates risk for other disorders like anemia or chronic kidney disease. In the case of *MTCH2* variation, genetic alleles that protect against high fat diet-induced obesity may be disadvantageous for a failing myocardium since the failing heart is more reliant on glucose as a fuel source.

The relationship between *MTCH2* level and metabolism is consistent and conserved across diverse species. In experimental models, excess lactate appears is a molecular signature of reduced *MTCH2* activity. Elevated lactate was seen in mice lacking Mtch2 in heart and skeletal muscle and is also seen in cardiac *Mtch* knockdown flies, which only lack *Mtch* in the fly heart tube (Buzaglo-Azriel 2016; Fischer 2022). Reduction of *Mtch* in the fly heart tube was sufficient to cause increased lactate, but it should be noted the fly heart tube contributes significantly to the overall mass of the organism since this structure extends into the abdomen. We also observed reduced adiposity in *Drosophila* with cardiac *Mtch* knockdown, which

parallels the resistance to high fat diet in the *Mtch2* heart/skeletal mouse mutant and is also similar to *C. elegans* with *mtch-1* reduction (Rottiers 2017). The human *MTCH2* haplotype linked to lower expression tags its expression in skeletal muscle supporting that skeletal muscle may be an important source for mediating this effect. Additionally, the protein coding SNP Pro290Ala, which is in linkage disequilibrium, may itself also contribute to reduced function **(Figure 4.1)**. Protein modeling revealed subtle differences between the Pro290 and Ala290 alleles in the carboxy-terminal final transmembrane, and this change could also contribute to impaired MTCH2 protein function.

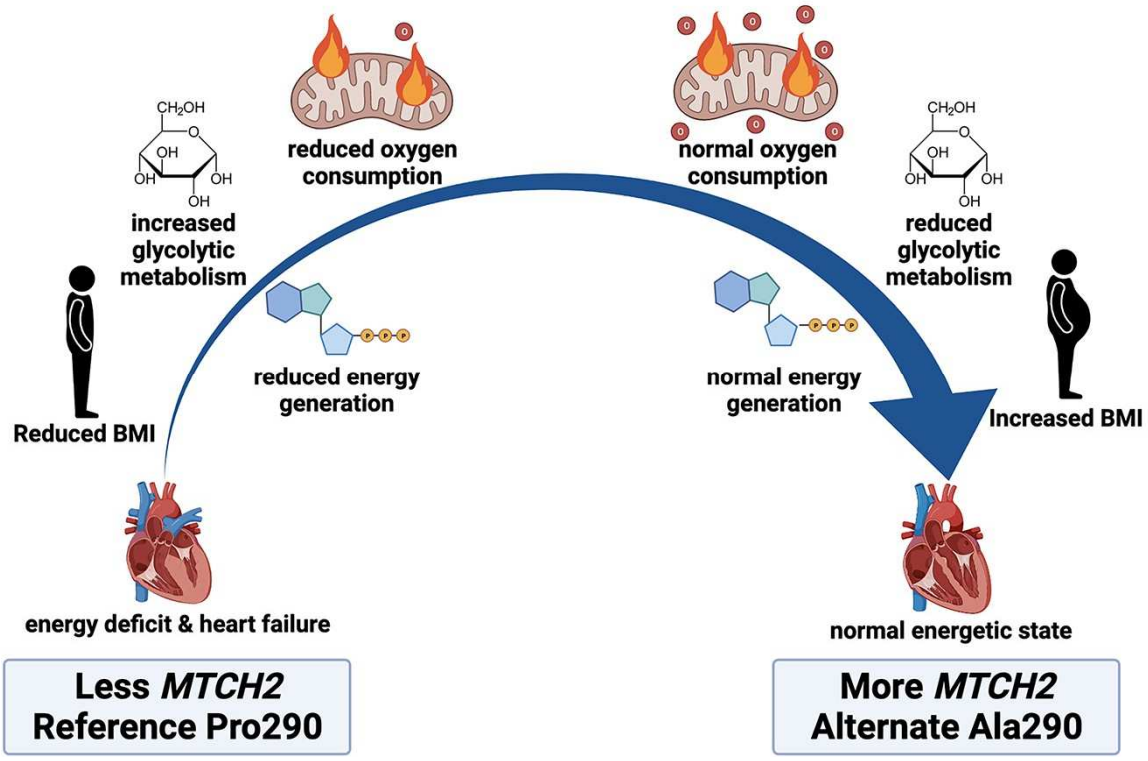

Figure 4.1. **rs1064608 is a variant in *MTCH2* that leads to a Pro290Ala change at the protein level**. This variant is underrepresented in people with cardiomyopathy, therefore Pro290 is more commonly observed in people with heart failure. Conversely, Ala290 is more likely observed in people without cardiomyopathy, and Ala290 is associated with greater *MTCH2* expression, as the variant causing Ala290 is in near complete LD with an eQTL for increased *MTCH2* expression, as observed in human skeletal muscle. Therefore, the Pro290 associated variant observed in people with cardiomyopathy is associated with reduced *MTCH2* expression. Functional models of *MTCH2* reduction have shown this leads to reduced adiposity, increased glycolytic metabolism, and reduced glucose oxidation, marked by a reduction in energy generation.

4.2.2 Loss of MTCH2 in cells increases lactate and shows altered activity of mitochondrial pyruvate dehydrogenase.

Cardiac *Mtch* knockdown flies and *MTCH2*$^{-/-}$ cells displayed increased lactate as a major finding in the basal state. We found that chemical inhibition of the PDH inhibitor, PDK, reduced lactate levels in *MTCH2* mutants, and in flies with cardiac *Mtch* knockdown, lactate reduction was sufficient to extend lifespan. In human heart failure, DCA treatment was shown to improve myocardial lactate consumption with concomitant improvement in mechanical work of the left ventricle, but DCA treatment may not exert its effect by improving noninvasive measures of heart function (Bersin 1994; Lewis 1998). In rodents, DCA treatment can be used to prevent heart failure outcomes through its action on PDK and also through epigenetic remodeling (Matsuhashi 2015; Kato 2010). Regulation of PDH through PDK is critical in tissues with high energy demand, such as the heart (Cluntun 2021). PDH converts pyruvate to acetyl coenzyme A (CoA) in the mitochondria, and PDH activity is inhibited by phosphorylation via PDK. PDH activity is known to be reduced in heart failure, and deletion of mitochondrial pyruvate carriers in the heart worsens heart failure phenotypes (Fernandez-Caggiano 2020; Cluntun 2021; McCommis 2020; Zhang 2020). A block of pyruvate oxidation could itself account for the increase in lactate seen in *MTCH2* mutants. Alternatively, agents that inhibit PDK activity may simply be working indirectly to overcome mitochondrial defects arising from loss of MTCH2. Loss of MTCH2 increased mtDNA content, but increased mtDNA did not reflect enhanced mitochondrial biogenesis and function but is more consistent with an ineffective compensatory mechanism, which is further supported by reduced mitochondrial membrane potential in the absence of MTCH2.

Recent work showed that deletion of *MTCH2* produced hyperfragmented mitochondria, consistent with MTCH2 having a key role in maintaining normal mitochondria structure and function (Labbé 2021). All of these mechanisms, excess lactate itself, reduced pyruvate oxidation or other mitochondrial impairment would be maladaptive in the setting of heart failure.

Collectively, these data support the human GWAS demonstrating a link between *MTCH2* and adiposity. Under high fat conditions, reduced *MTCH2* promotes lean body mass and be protective from obesity. Intriguingly, MTCH2 variants linked to increased BMI in adults associate with lower birth weight with each BMI-increasing *MTCH2* allele associated with a 13g decrease in birthweight (Kilpeläinen 2011). The conditions that support rapid fetal growth are similar to the failing heart with an increased dependence on glucose as a fuel source. The substrate dependence of MTCH2 levels is an important consideration when considering its related phenotypes.

4.2.3 Consideration of MTCH2 as a lactate transporter

It has been well documented that lactate production in increased during heart failure, where the failing heart is characterized by high levels of glycolysis and reduced reliance on fatty acids and oxidative metabolism compared to the healthy adult heart (Zymliński 2018; Tran 2019). Lactate is often thought of as a waste product from lactate dehydrogenase (LDH) acting on pyruvate to generate cytosolic lactate in a series of anerobic reactions. However, the reaction of LDH synthesizing lactate from pyruvate is a reversible reaction where lactate can be converted back to pyruvate. Additionally, lactate can be transported from the cytosol, both into the mitochondria and extracellularly via monocarboxylate transporters (MCTs). MCT1, 2, 3, and 4 are known to transport monocarboxylate metabolites, such as lactate, pyruvate, and some ketone bodies, where MCT1 and 4 are thought to be mainly responsible for import and export of lactate (Halestrap 1999; Halestrap 2004). MCT1 has been suggested to be mostly involved in intracellular import of monocarboxylates, whereas MCT4 has been mostly described as being an exporter of lactate, however the roles of each have not been fully defined (Doherty 2013). In a rat heart failure model, it has been shown that MCT1 and MCT4 are upregulated at the protein level in cardiomyocytes (Jóhannsson 2001; Zhu 2013). This suggests that not only is lactate production increased during heart failure but import and export of lactate is elevated as well.

Lactate taken up by the cell can be converted to metabolic fuel, as mentioned previously. Lactate can be reconverted to pyruvate, which can then undergo oxidation to increase ATP synthesis (Bonen 2000; Hui 2017). Additionally, this reaction generated NADH, which can be used as reductive power to fuel the electron transport chain. This recycling of lactate occurs in healthy cells, where is taken up by the cell and into mitochondria by MCT transporters, and this reaction is increased with exercise and muscular stress, as shown in human blood samples after high-stress exercise, and it is thought that this similarly occurs during heart failure (Stanley 1986; Mazzeo 1986; Dong 2021). Furthermore, ^{13}C-labeled lactate has been shown to incorporate into TCA metabolites in nearly all tissues in mice, solidifying the role of lactate as a notable fuel source (Hui 2017). Interestingly, in a fed state, glucose was shown to contribute to the TCA cycle mostly through catabolism to lactate and then reverted to TCA cycle metabolites in the heart of these same mice. In skeletal muscle, lactate and direct glucose oxidation appeared to contribute equally to TCA metabolites, suggesting that lactate is critical to normal tissue fuel but even greater in the heart. Because *Mtch* mutant flies have greater circulating lactate and less carbohydrate-derived TCA metabolites, this could support a hypothesis of MTCH2 being a lactate transporter, where loss of *MTCH2* prevents lactate recycling for TCA fuel and therefore an energy deficit.

Elevated lactate has been previously associated with *MTCH2* dysfunction, where knockout of *Mtch2* in the skeletal and cardiac muscle in mice and our cardiac-specific *Mtch* knockdown in flies each demonstrate increased lactate production (Buzaglo-Azriel 2016; Fischer 2022). While it has not been explored, one possibility is that MTCH2 serves as a lactate transporter. It is known MTCH2 is a member of the SLC25 family, which transport nutrients and ions across mitochondrial membranes (Gutiérrez-Aguilar 2013). Therefore, MTCH2 likely serves as a solute carrier, although the potential solutes transported are undefined (Ruprecht 2020). It is possible that under cardiac stress, lactate production increases and cannot be recycled as fuel under *MTCH2* dysfunction. One way to assess this would be to starve *Mtch* knockdown flies

or *MTCH2*$^{-/-}$ HEK cells and provide media supplemented with ^{13}C isotope-labeled lactate, followed by metabolomic flux tracing. This would show whether lactate can traverse the mitochondrial membrane and be used as fuel under *MTCH2* reduction. If lactate cannot reenter mitochondria, it is likely MTCH2 plays a role in mitochondrial lactate transport.

4.2.4 Possible compensatory reactions occurring under loss of MTCH2

A common phenotype observed with *MTCH2* reduction is reduced adiposity, where this has been demonstrated in mice, worms, human cells, and flies (Fischer 2022; Buzaglo-Azriel 2016; Rottiers 2017). Our studies have shown that *MTCH2* influences metabolism in a substrate-specific manner. Interestingly, we found that cardiac-specific *Mtch* knockdown in flies increased transcriptional expression of genes implicated in fatty acid syntheses. Cardiac *Mtch* knockdown flies also display reduction in oxygen consumption exclusively in the presence of glucose, but not the fatty acid palmitate. Furthermore, these flies showed a reduction in glucose-derived TCA metabolites, but no change in overall TCA metabolites, suggesting that the TCA cycle is being replenished by non-carbohydrate substrates. From these results, we suspect that compensatory reactions are occurring under *MTCH2* reduction in attempt to fulfill energetic needs. Potential modes of compensation could be through ketolysis or anaplerosis. We know that loss of *MTCH2* leads to reduced adiposity, and this could mean that fat reserves are being utilized for fuel in this case. Because *MTCH2* mutants cannot adequately oxidize glucose, this may trigger starvation mode, promoting ketolysis of fats. This can replenish the acetyl-coA pool for maximum ATP production. Additionally, anaplerosis could also be replenishing metabolite pools in *MTCH2* mutants, where TCA intermediates are replenished through amino acid metabolism (Des Rosiers 2011). This could be delineated by supplementing our *MTCH2*$^{-/-}$ HEK cell cultures with ^{13}C isotope labeled glutamine or aspartate, to determine if TCA cycle metabolites incorporate labeled carbons, which would indicate that anaplerosis is occurring as a potential compensatory reaction.

4.2.5 Is MTCH2 exclusively an outer mitochondrial membrane protein?

In 2005, the Gross Lab originally discovered that MTCH2 plays a role in tBID recruitment by the cross-linking and biochemical purification of the mitochondrial complex that forms with tBID in hematopoietic FL5.12 cells (Grinberg 2005). When analyzed, it was discovered that MTCH2 is a part of this complex, providing evidence that MTCH2 is an outer mitochondrial membrane (OMM) protein. Because of this, MTCH2 is considered an unusual member of the SLC25 family in that it encodes an outer, rather than inner, mitochondrial membrane protein. However, although it has been demonstrated through protease sensitivity assays that MTCH2 localizes to the OMM, it is unknown if MTCH2 has the ability to dissociate from the OMM or localize. This is the only study and context in which MTCH2 localization has been examined. Because it's known some mitochondrial membrane proteins, such as PDH, can traverse membranes, it is possible that MTCH2 does not exclusively sit at the OMM. Immunofluorescence imaging of MTCH2 under different nutrient and stress conditions will answer whether MTCH2 is a mobile mitochondrial protein, like PDH. Furthermore, the structure of MTCH2 has only been computationally hypothesized, and not experimentally validated. Studies have suggested MTCH2 has anywhere from 3-6 transmembrane domains (Gross 2005; Grinberg 2005; Fischer 2022). Structure determination through crystallography would help better assess where MTCH2 may reside within the cell.

4.3 Concluding remarks

Understanding how genetic background impacts disease is a complex yet essential task. Genetic variants can elicit different effects depending on disease context. In this thesis, I discussed in chapter 2 how a variant in *MTCH2* potentially has alternative consequences in obesity versus heart failure settings. In chapter 3, I discussed functional validation of this gene

in a fly cardiac and human cell model, and what this could mean for people with heart failure. Specifically, our variant of interest rs1064608, is underrepresented in people with cardiomyopathy, which likely is associated with reduced *MTCH2* expression, as rs1064608 is in near complete LD with an eQTL for increased *MTCH2* expression, as observed in human skeletal muscle. We found that reduced *MTCH2* leads to recued mitochondrial PDH activity, therefore reducing pyruvate oxidation and ATP synthesis. Consequentially, glucose metabolism is forced toward lactate production. Chemically alleviating PDH to promote its activity improved mutant phenotypes. These findings emphasize that *MTCH2* is essential to cardiac function and metabolism, and that variation within *MTCH2* is common in the population. Pursuing therapies to improve oxidative metabolism in people with reduced *MTCH2* dysfunction may prevent and improve outcomes of heart failure.

REFERENCES

Ahmadpour, S. T., K. Mahéo, S. Servais, L. Brisson, and J. F. Dumas. 2020. 'Cardiolipin, the Mitochondrial Signature Lipid: Implication in Cancer', *Int J Mol Sci*, 21.

Allikian, M. J., G. Bhabha, P. Dospoy, A. Heydemann, P. Ryder, J. U. Earley, M. J. Wolf, H. A. Rockman, and E. M. McNally. 2007. 'Reduced life span with heart and muscle dysfunction in Drosophila sarcoglycan mutants', *Hum Mol Genet*, 16: 2933-43.

Archer, S. L., Y. H. Fang, J. J. Ryan, and L. Piao. 2013. 'Metabolism and bioenergetics in the right ventricle and pulmonary vasculature in pulmonary hypertension', *Pulm Circ*, 3: 144-52.

Ardehali, H., H. N. Sabbah, M. A. Burke, S. Sarma, P. P. Liu, J. G. Cleland, A. Maggioni, G. C. Fonarow, E. D. Abel, U. Campia, and M. Gheorghiade. 2012. 'Targeting myocardial substrate metabolism in heart failure: potential for new therapies', *Eur J Heart Fail*, 14: 120-9.

Bahat, A., A. Goldman, Y. Zaltsman, D. H. Khan, C. Halperin, E. Amzallag, V. Krupalnik, M. Mullokandov, A. Silberman, A. Erez, A. D. Schimmer, J. H. Hanna, and A. Gross. 2018. 'MTCH2-mediated mitochondrial fusion drives exit from naïve pluripotency in embryonic stem cells', *Nat Commun*, 9: 5132.

Bar-Lev, Y., S. Moshitch-Moshkovitz, G. Tsarfaty, D. Kaufman, J. Horev, J. H. Resau, and I. Tsarfaty. 2016. 'Mimp/Mtch2, an Obesity Susceptibility Gene, Induces Alteration of Fatty Acid Metabolism in Transgenic Mice', *PLoS One*, 11: e0157850.

Barp, A., L. Bello, L. Politano, P. Melacini, C. Calore, A. Polo, S. Vianello, G. Sorarù, C. Semplicini, B. Pantic, A. Taglia, E. Picillo, F. Magri, K. Gorni, S. Messina, G. L. Vita, G. Vita, G. P. Comi, M. Ermani, V. Calvo, C. Angelini, E. P. Hoffman, and E. Pegoraro. 2015. 'Genetic Modifiers of Duchenne Muscular Dystrophy and Dilated Cardiomyopathy', *PLoS One*, 10: e0141240.

Bartlett, K., and S. Eaton. 2004. 'Mitochondrial beta-oxidation', *Eur J Biochem*, 271: 462-9.

Bauer, F., C. C. Elbers, R. A. Adan, R. J. Loos, N. C. Onland-Moret, D. E. Grobbee, J. V. van Vliet-Ostaptchouk, C. Wijmenga, and Y. T. van der Schouw. 2009. 'Obesity genes identified in genome-wide association studies are associated with adiposity measures and potentially with nutrient-specific food preference', *Am J Clin Nutr*, 90: 951-9.

Bawa, S., D. S. Brooks, K. E. Neville, M. Tipping, M. A. Sagar, J. A. Kollhoff, G. Chawla, B. V. Geisbrecht, J. M. Tennessen, K. W. Eliceiri, and E. R. Geisbrecht. 2020. 'Drosophila TRIM32 cooperates with glycolytic enzymes to promote cell growth', *Elife*, 9.

Baz-Lopez, D, V D Bruno, T W Johnson, R Ascione, and E Sammut. 2021. 'Distinct metabolic transcriptional patterns and Warburg effect in porcine model of ischaemic cardiomyopathy', *European Heart Journal*, 42.

Bersin, R. M., C. Wolfe, M. Kwasman, D. Lau, C. Klinski, K. Tanaka, P. Khorrami, G. N. Henderson, T. de Marco, and K. Chatterjee. 1994. 'Improved hemodynamic

function and mechanical efficiency in congestive heart failure with sodium dichloroacetate', *J Am Coll Cardiol*, 23: 1617-24.

Bertero, E., and C. Maack. 2018. 'Metabolic remodelling in heart failure', *Nat Rev Cardiol*, 15: 457-70.

Bhide, S., A. S. Trujillo, M. T. O'Connor, G. H. Young, D. E. Cryderman, S. Chandran, M. Nikravesh, L. L. Wallrath, and G. C. Melkani. 2018. 'Increasing autophagy and blocking Nrf2 suppress laminopathy-induced age-dependent cardiac dysfunction and shortened lifespan', *Aging Cell*, 17: e12747.

Bolfer, L., A. H. Estrada, C. Larkin, T. J. Conlon, F. Lourenco, K. Taggart, S. Suzuki-Hatano, and C. A. Pacak. 2020. 'Functional Consequences of PDK4 Deficiency in Doberman Pinscher Fibroblasts', *Sci Rep*, 10: 3930.

Bonen, A. 2000. 'Lactate transporters (MCT proteins) in heart and skeletal muscles', *Med Sci Sports Exerc*, 32: 778-89.

Bosshart, P. D., D. Kalbermatter, S. Bonetti, and D. Fotiadis. 2019. 'Mechanistic basis of L-lactate transport in the SLC16 solute carrier family', *Nat Commun*, 10: 2649.

Broce, I. J., C. H. Tan, C. C. Fan, I. Jansen, J. E. Savage, A. Witoelar, N. Wen, C. P. Hess, W. P. Dillon, C. M. Glastonbury, M. Glymour, J. S. Yokoyama, F. M. Elahi, G. D. Rabinovici, B. L. Miller, E. C. Mormino, R. A. Sperling, D. A. Bennett, L. K. McEvoy, J. B. Brewer, H. H. Feldman, B. T. Hyman, M. Pericak-Vance, J. L. Haines, L. A. Farrer, R. Mayeux, G. D. Schellenberg, K. Yaffe, L. P. Sugrue, A. M. Dale, D. Posthuma, O. A. Andreassen, C. M. Karch, and R. S. Desikan. 2019. 'Dissecting the genetic relationship between cardiovascular risk factors and Alzheimer's disease', *Acta Neuropathol*, 137: 209-26.

Brooks, G. A. 2021. 'Role of the Heart in Lactate Shuttling', *Front Nutr*, 8: 663560.

Bugger, H., M. Schwarzer, D. Chen, A. Schrepper, P. A. Amorim, M. Schoepe, T. D. Nguyen, F. W. Mohr, O. Khalimonchuk, B. C. Weimer, and T. Doenst. 2010. 'Proteomic remodelling of mitochondrial oxidative pathways in pressure overload-induced heart failure', *Cardiovasc Res*, 85: 376-84.

Buniello, A., J. A. L. MacArthur, M. Cerezo, L. W. Harris, J. Hayhurst, C. Malangone, A. McMahon, J. Morales, E. Mountjoy, E. Sollis, D. Suveges, O. Vrousgou, P. L. Whetzel, R. Amode, J. A. Guillen, H. S. Riat, S. J. Trevanion, P. Hall, H. Junkins, P. Flicek, T. Burdett, L. A. Hindorff, F. Cunningham, and H. Parkinson. 2019. 'The NHGRI-EBI GWAS Catalog of published genome-wide association studies, targeted arrays and summary statistics 2019', *Nucleic Acids Res*, 47: D1005-d12.

Buroker, N. E., X. H. Ning, and M. Portman. 2008. 'Cardiac PPARalpha Protein Expression is Constant as Alternate Nuclear Receptors and PGC-1 Coordinately Increase During the Postnatal Metabolic Transition', *PPAR Res*, 2008: 279531.

Buzaglo-Azriel, L., Y. Kuperman, M. Tsoory, Y. Zaltsman, L. Shachnai, S. L. Zaidman, E. Bassat, I. Michailovici, A. Sarver, E. Tzahor, M. Haran, C. Vernochet, and A. Gross. 2016. 'Loss of Muscle MTCH2 Increases Whole-Body Energy Utilization and Protects from Diet-Induced Obesity', *Cell Rep*, 14: 1602-10.

Caliskan, M., C. D. Brown, and J. C. Maranville. 2021. 'A catalog of GWAS fine-mapping efforts in autoimmune disease', *Am J Hum Genet*, 108: 549-63.

Cammarato, A., C. H. Ahrens, N. N. Alayari, E. Qeli, J. Rucker, M. C. Reedy, C. M. Zmasek, M. Gucek, R. N. Cole, J. E. Van Eyk, R. Bodmer, B. O'Rourke, S. I.

Bernstein, and D. B. Foster. 2011. 'A mighty small heart: the cardiac proteome of adult Drosophila melanogaster', *PLoS One*, 6: e18497.

Carter, A. J., and A. Q. Nguyen. 2011. 'Antagonistic pleiotropy as a widespread mechanism for the maintenance of polymorphic disease alleles', *BMC Med Genet*, 12: 160.

Chakchouk, I., D. Zhang, Z. Zhang, L. C. Francioli, R. L. P. Santos-Cortez, I. Schrauwen, and S. M. Leal. 2019. 'Disparities in discovery of pathogenic variants for autosomal recessive non-syndromic hearing impairment by ancestry', *Eur J Hum Genet*, 27: 1456-65.

Chen, L., Q. Gong, J. P. Stice, and A. A. Knowlton. 2009. 'Mitochondrial OPA1, apoptosis, and heart failure', *Cardiovasc Res*, 84: 91-9.

Chen, Z., M. Liu, L. Li, and L. Chen. 2018. 'Involvement of the Warburg effect in non-tumor diseases processes', *J Cell Physiol*, 233: 2839-49.

Choma, M. A., S. D. Izatt, R. J. Wessells, R. Bodmer, and J. A. Izatt. 2006. 'Images in cardiovascular medicine: in vivo imaging of the adult Drosophila melanogaster heart with real-time optical coherence tomography', *Circulation*, 114: e35-6.

Clémençon, B., M. Babot, and V. Trézéguet. 2013. 'The mitochondrial ADP/ATP carrier (SLC25 family): pathological implications of its dysfunction', *Mol Aspects Med*, 34: 485-93.

Cluntun, A. A., R. Badolia, S. Lettlova, K. M. Parnell, T. S. Shankar, N. A. Diakos, K. A. Olson, I. Taleb, S. M. Tatum, J. A. Berg, C. N. Cunningham, T. Van Ry, A. J. Bott, A. T. Krokidi, S. Fogarty, S. Skedros, W. I. Swiatek, X. Yu, B. Luo, S. Merx, S. Navankasattusas, J. E. Cox, G. S. Ducker, W. L. Holland, S. H. McKellar, J. Rutter, and S. G. Drakos. 2021. 'The pyruvate-lactate axis modulates cardiac hypertrophy and heart failure', *Cell Metab*, 33: 629-48.e10.

Connaughton, S., F. Chowdhury, R. R. Attia, S. Song, Y. Zhang, M. B. Elam, G. A. Cook, and E. A. Park. 2010. 'Regulation of pyruvate dehydrogenase kinase isoform 4 (PDK4) gene expression by glucocorticoids and insulin', *Mol Cell Endocrinol*, 315: 159-67.

Cornelis, M. C., E. B. Rimm, G. C. Curhan, P. Kraft, D. J. Hunter, F. B. Hu, and R. M. van Dam. 2014. 'Obesity susceptibility loci and uncontrolled eating, emotional eating and cognitive restraint behaviors in men and women', *Obesity (Silver Spring)*, 22: E135-41.

D'Oria, R., R. Schipani, A. Leonardini, A. Natalicchio, S. Perrini, A. Cignarelli, L. Laviola, and F. Giorgino. 2020. 'The Role of Oxidative Stress in Cardiac Disease: From Physiological Response to Injury Factor', *Oxid Med Cell Longev*, 2020: 5732956.

Dahl-Halvarsson, M., M. Olive, M. Pokrzywa, K. Ejeskär, R. H. Palmer, A. E. Uv, and H. Tajsharghi. 2018. 'Drosophila model of myosin myopathy rescued by overexpression of a TRIM-protein family member', *Proc Natl Acad Sci U S A*, 115: E6566-e75.

Dai, C., Q. Li, H. I. May, C. Li, G. Zhang, G. Sharma, A. D. Sherry, C. R. Malloy, C. Khemtong, Y. Zhang, Y. Deng, T. G. Gillette, J. Xu, D. T. Scadden, and Z. V. Wang. 2020. 'Lactate Dehydrogenase A Governs Cardiac Hypertrophic Growth in Response to Hemodynamic Stress', *Cell Rep*, 32: 108087.

Das, D., R. Aradhya, D. Ashoka, and M. Inamdar. 2008. 'Macromolecular uptake in Drosophila pericardial cells requires rudhira function', *Exp Cell Res*, 314: 1804-10.

de Andrade, K. C., M. N. Frone, T. Wegman-Ostrosky, P. P. Khincha, J. Kim, A. Amadou, K. M. Santiago, F. P. Fortes, N. Lemonnier, L. Mirabello, D. R. Stewart, P. Hainaut, L. P. Kowalski, S. A. Savage, and M. I. Achatz. 2019. 'Variable population prevalence estimates of germline TP53 variants: A gnomAD-based analysis', *Hum Mutat*, 40: 97-105.

Des Rosiers, C., F. Labarthe, S. G. Lloyd, and J. C. Chatham. 2011. 'Cardiac anaplerosis in health and disease: food for thought', *Cardiovasc Res*, 90: 210-9.

Dhatariya, K. K., N. S. Glaser, E. Codner, and G. E. Umpierrez. 2020. 'Diabetic ketoacidosis', *Nat Rev Dis Primers*, 6: 40.

Diegelmann, S., A. Jansen, S. Jois, K. Kastenholz, L. Velo Escarcena, N. Strudthoff, and H. Scholz. 2017. 'The CApillary FEeder Assay Measures Food Intake in Drosophila melanogaster', *J Vis Exp*.

Dipple, K. M., and E. R. McCabe. 2000. 'Phenotypes of patients with "simple" Mendelian disorders are complex traits: thresholds, modifiers, and systems dynamics', *Am J Hum Genet*, 66: 1729-35.

Dipple, K. M., J. K. Phelan, and E. R. McCabe. 2001. 'Consequences of complexity within biological networks: robustness and health, or vulnerability and disease', *Mol Genet Metab*, 74: 45-50.

Dodd, M. S., H. J. Atherton, C. A. Carr, D. J. Stuckey, J. A. West, J. L. Griffin, G. K. Radda, K. Clarke, L. C. Heather, and D. J. Tyler. 2014. 'Impaired in vivo mitochondrial Krebs cycle activity after myocardial infarction assessed using hyperpolarized magnetic resonance spectroscopy', *Circ Cardiovasc Imaging*, 7: 895-904.

Doenst, T., T. D. Nguyen, and E. D. Abel. 2013. 'Cardiac metabolism in heart failure: implications beyond ATP production', *Circ Res*, 113: 709-24.

Doherty, J. R., and J. L. Cleveland. 2013. 'Targeting lactate metabolism for cancer therapeutics', *J Clin Invest*, 123: 3685-92.

Dong, S., L. Qian, Z. Cheng, C. Chen, K. Wang, S. Hu, X. Zhang, and T. Wu. 2021. 'Lactate and Myocardiac Energy Metabolism', *Front Physiol*, 12: 715081.

Duee, E. D., and P. V. Vignais. 1965. '[Exchange between extra- and intramitochondrial adenine nucleotides]', *Biochim Biophys Acta*, 107: 184-8.

Duffy, J. B. 2002. 'GAL4 system in Drosophila: a fly geneticist's Swiss army knife', *Genesis*, 34: 1-15.

Eramo, M. J., V. Lisnyak, L. E. Formosa, and M. T. Ryan. 2020. 'The 'mitochondrial contact site and cristae organising system' (MICOS) in health and human disease', *J Biochem*, 167: 243-55.

Fabre, A., and J. Mancini. 2022. 'No preferential mode of inheritance for highly constrained genes', *Intractable Rare Dis Res*, 11: 25-28.

Fernandez-Caggiano, M., A. Kamynina, A. A. Francois, O. Prysyazhna, T. R. Eykyn, S. Krasemann, M. G. Crespo-Leiro, M. G. Vieites, K. Bianchi, V. Morales, N. Domenech, and P. Eaton. 2020. 'Mitochondrial pyruvate carrier abundance mediates pathological cardiac hypertrophy', *Nat Metab*, 2: 1223-31.

Fillmore, N., J. L. Levasseur, A. Fukushima, C. S. Wagg, W. Wang, J. R. B. Dyck, and G. D. Lopaschuk. 2018. 'Uncoupling of glycolysis from glucose oxidation accompanies the development of heart failure with preserved ejection fraction', *Mol Med*, 24: 3.

Fillmore, N., and G. D. Lopaschuk. 2013. 'Targeting mitochondrial oxidative metabolism as an approach to treat heart failure', *Biochim Biophys Acta*, 1833: 857-65.

Fischer, J. A., T. O. Monroe, L. L. Pesce, K. T. Sawicki, M. Quattrocelli, R. Bauer, S. D. Kearns, M. J. Wolf, M. J. Puckelwartz, and E. M. McNally. 2022. 'Opposing effects of genetic variation in MTCH2 for obesity versus heart failure', *Hum Mol Genet*.

Fransson, U., A. H. Rosengren, F. C. Schuit, E. Renström, and H. Mulder. 2006. 'Anaplerosis via pyruvate carboxylase is required for the fuel-induced rise in the ATP:ADP ratio in rat pancreatic islets', *Diabetologia*, 49: 1578-86.

Gacita, A. M., D. E. Fullenkamp, J. Ohiri, T. Pottinger, M. J. Puckelwartz, M. A. Nobrega, and E. M. McNally. 2021. 'Genetic Variation in Enhancers Modifies Cardiomyopathy Gene Expression and Progression', *Circulation*, 143: 1302-16.

Gao, S., G. Li, Y. Shao, Z. Wei, S. Huang, F. Qi, Y. Jiao, Y. Li, C. Zhang, and J. Du. 2021. 'FABP5 Deficiency Impairs Mitochondrial Function and Aggravates Pathological Cardiac Remodeling and Dysfunction', *Cardiovasc Toxicol*, 21: 619-29.

'The Genotype-Tissue Expression (GTEx) project'. 2013. *Nat Genet*, 45: 580-5.

Gertz, E. W., J. A. Wisneski, W. C. Stanley, and R. A. Neese. 1988. 'Myocardial substrate utilization during exercise in humans. Dual carbon-labeled carbohydrate isotope experiments', *J Clin Invest*, 82: 2017-25.

Ghanem, N., C. El-Baba, K. Araji, R. El-Khoury, J. Usta, and N. Darwiche. 2021. 'The Pentose Phosphate Pathway in Cancer: Regulation and Therapeutic Opportunities', *Chemotherapy*, 66: 179-91.

Gibala, M. J., M. E. Young, and H. Taegtmeyer. 2000. 'Anaplerosis of the citric acid cycle: role in energy metabolism of heart and skeletal muscle', *Acta Physiol Scand*, 168: 657-65.

Gibb, A. A., and B. G. Hill. 2018. 'Metabolic Coordination of Physiological and Pathological Cardiac Remodeling', *Circ Res*, 123: 107-28.

Glatzová, D., H. Mavila, M. C. Saija, T. Chum, L. Cwiklik, T. Brdička, and M. Cebecauer. 2021. 'The role of prolines and glycine in the transmembrane domain of LAT', *Febs j*, 288: 4039-52.

Green, E. M., H. Wakimoto, R. L. Anderson, M. J. Evanchik, J. M. Gorham, B. C. Harrison, M. Henze, R. Kawas, J. D. Oslob, H. M. Rodriguez, Y. Song, W. Wan, L. A. Leinwand, J. A. Spudich, R. S. McDowell, J. G. Seidman, and C. E. Seidman. 2016. 'A small-molecule inhibitor of sarcomere contractility suppresses hypertrophic cardiomyopathy in mice', *Science*, 351: 617-21.

Griffin, T. M., K. M. Humphries, M. Kinter, H. Y. Lim, and L. I. Szweda. 2016. 'Nutrient sensing and utilization: Getting to the heart of metabolic flexibility', *Biochimie*, 124: 74-83.

Grinberg, M., M. Schwarz, Y. Zaltsman, T. Eini, H. Niv, S. Pietrokovski, and A. Gross. 2005. 'Mitochondrial carrier homolog 2 is a target of tBID in cells signaled to die by tumor necrosis factor alpha', *Mol Cell Biol*, 25: 4579-90.

Gross, A. 2005. 'Mitochondrial carrier homolog 2: a clue to cracking the BCL-2 family riddle?', *J Bioenerg Biomembr*, 37: 113-9.

Gudmundsson, S., M. Singer-Berk, N. A. Watts, W. Phu, J. K. Goodrich, M. Solomonson, H. L. Rehm, D. G. MacArthur, and A. O'Donnell-Luria. 2022. 'Variant interpretation using population databases: Lessons from gnomAD', *Hum Mutat*, 43: 1012-30.

Guo, Z. 2015. 'Pyruvate dehydrogenase, Randle cycle, and skeletal muscle insulin resistance', *Proc Natl Acad Sci U S A*, 112: E2854.

Gutiérrez-Aguilar, M., and C. P. Baines. 2013. 'Physiological and pathological roles of mitochondrial SLC25 carriers', *Biochem J*, 454: 371-86.

Haas, J., K. S. Frese, B. Peil, W. Kloos, A. Keller, R. Nietsch, Z. Feng, S. Müller, E. Kayvanpour, B. Vogel, F. Sedaghat-Hamedani, W. K. Lim, X. Zhao, D. Fradkin, D. Köhler, S. Fischer, J. Franke, S. Marquart, I. Barb, D. T. Li, A. Amr, P. Ehlermann, D. Mereles, T. Weis, S. Hassel, A. Kremer, V. King, E. Wirsz, R. Isnard, M. Komajda, A. Serio, M. Grasso, P. Syrris, E. Wicks, V. Plagnol, L. Lopes, T. Gadgaard, H. Eiskjær, M. Jørgensen, D. Garcia-Giustiniani, M. Ortiz-Genga, M. G. Crespo-Leiro, R. H. Deprez, I. Christiaans, I. A. van Rijsingen, A. A. Wilde, A. Waldenstrom, M. Bolognesi, R. Bellazzi, S. Mörner, J. L. Bermejo, L. Monserrat, E. Villard, J. Mogensen, Y. M. Pinto, P. Charron, P. Elliott, E. Arbustini, H. A. Katus, and B. Meder. 2015. 'Atlas of the clinical genetics of human dilated cardiomyopathy', *Eur Heart J*, 36: 1123-35a.

Halestrap, A. P., and D. Meredith. 2004. 'The SLC16 gene family-from monocarboxylate transporters (MCTs) to aromatic amino acid transporters and beyond', *Pflugers Arch*, 447: 619-28.

Halestrap, A. P., and N. T. Price. 1999. 'The proton-linked monocarboxylate transporter (MCT) family: structure, function and regulation', *Biochem J*, 343 Pt 2: 281-99.

Hamilton, D. J. 2013. 'Mechanisms of disease: is mitochondrial function altered in heart failure?', *Methodist Debakey Cardiovasc J*, 9: 44-8.

Hartley, P. S., K. Motamedchaboki, R. Bodmer, and K. Ocorr. 2016. 'SPARC-Dependent Cardiomyopathy in Drosophila', *Circ Cardiovasc Genet*, 9: 119-29.

Hasanuzzaman, M., M. R. H. Raihan, A. A. C. Masud, K. Rahman, F. Nowroz, M. Rahman, K. Nahar, and M. Fujita. 2021. 'Regulation of Reactive Oxygen Species and Antioxidant Defense in Plants under Salinity', *Int J Mol Sci*, 22.

Hazegh, K. E., and T. Reis. 2016. 'A Buoyancy-based Method of Determining Fat Levels in Drosophila', *J Vis Exp*.

Heid, I. M., A. U. Jackson, J. C. Randall, T. W. Winkler, L. Qi, V. Steinthorsdottir, G. Thorleifsson, M. C. Zillikens, E. K. Speliotes, R. Mägi, T. Workalemahu, C. C. White, N. Bouatia-Naji, T. B. Harris, S. I. Berndt, E. Ingelsson, C. J. Willer, M. N. Weedon, J. Luan, S. Vedantam, T. Esko, T. O. Kilpeläinen, Z. Kutalik, S. Li, K. L. Monda, A. L. Dixon, C. C. Holmes, L. M. Kaplan, L. Liang, J. L. Min, M. F. Moffatt, C. Molony, G. Nicholson, E. E. Schadt, K. T. Zondervan, M. F. Feitosa, T. Ferreira, H. Lango Allen, R. J. Weyant, E. Wheeler, A. R. Wood, K. Estrada, M. E. Goddard, G. Lettre, M. Mangino, D. R. Nyholt, S. Purcell, A. V. Smith, P. M. Visscher, J. Yang, S. A. McCarroll, J. Nemesh, B. F. Voight, D. Absher, N. Amin, T. Aspelund, L. Coin, N. L. Glazer, C. Hayward, N. L. Heard-Costa, J. J. Hottenga, A. Johansson, T. Johnson, M. Kaakinen, K. Kapur, S. Ketkar, J. W.

Knowles, P. Kraft, A. T. Kraja, C. Lamina, M. F. Leitzmann, B. McKnight, A. P. Morris, K. K. Ong, J. R. Perry, M. J. Peters, O. Polasek, I. Prokopenko, N. W. Rayner, S. Ripatti, F. Rivadeneira, N. R. Robertson, S. Sanna, U. Sovio, I. Surakka, A. Teumer, S. van Wingerden, V. Vitart, J. H. Zhao, C. Cavalcanti-Proença, P. S. Chines, E. Fisher, J. R. Kulzer, C. Lecoeur, N. Narisu, C. Sandholt, L. J. Scott, K. Silander, K. Stark, M. L. Tammesoo, T. M. Teslovich, N. J. Timpson, R. M. Watanabe, R. Welch, D. I. Chasman, M. N. Cooper, J. O. Jansson, J. Kettunen, R. W. Lawrence, N. Pellikka, M. Perola, L. Vandenput, H. Alavere, P. Almgren, L. D. Atwood, A. J. Bennett, R. Biffar, L. L. Bonnycastle, S. R. Bornstein, T. A. Buchanan, H. Campbell, I. N. Day, M. Dei, M. Dörr, P. Elliott, M. R. Erdos, J. G. Eriksson, N. B. Freimer, M. Fu, S. Gaget, E. J. Geus, A. P. Gjesing, H. Grallert, J. Grässler, C. J. Groves, C. Guiducci, A. L. Hartikainen, N. Hassanali, A. S. Havulinna, K. H. Herzig, A. A. Hicks, J. Hui, W. Igl, P. Jousilahti, A. Jula, E. Kajantie, L. Kinnunen, I. Kolcic, S. Koskinen, P. Kovacs, H. K. Kroemer, V. Krzelj, J. Kuusisto, K. Kvaloy, J. Laitinen, O. Lantieri, G. M. Lathrop, M. L. Lokki, R. N. Luben, B. Ludwig, W. L. McArdle, A. McCarthy, M. A. Morken, M. Nelis, M. J. Neville, G. Paré, A. N. Parker, J. F. Peden, I. Pichler, K. H. Pietiläinen, C. G. Platou, A. Pouta, M. Ridderstråle, N. J. Samani, J. Saramies, J. Sinisalo, J. H. Smit, R. J. Strawbridge, H. M. Stringham, A. J. Swift, M. Teder-Laving, B. Thomson, G. Usala, J. B. van Meurs, G. J. van Ommen, V. Vatin, C. B. Volpato, H. Wallaschofski, G. B. Walters, E. Widen, S. H. Wild, G. Willemsen, D. R. Witte, L. Zgaga, P. Zitting, J. P. Beilby, A. L. James, M. Kähönen, T. Lehtimäki, M. S. Nieminen, C. Ohlsson, L. J. Palmer, O. Raitakari, P. M. Ridker, M. Stumvoll, A. Tönjes, J. Viikari, B. Balkau, Y. Ben-Shlomo, R. N. Bergman, H. Boeing, G. D. Smith, S. Ebrahim, P. Froguel, T. Hansen, C. Hengstenberg, K. Hveem, B. Isomaa, T. Jørgensen, F. Karpe, K. T. Khaw, M. Laakso, D. A. Lawlor, M. Marre, T. Meitinger, A. Metspalu, K. Midthjell, O. Pedersen, V. Salomaa, P. E. Schwarz, T. Tuomi, J. Tuomilehto, T. T. Valle, N. J. Wareham, A. M. Arnold, J. S. Beckmann, S. Bergmann, E. Boerwinkle, D. I. Boomsma, M. J. Caulfield, F. S. Collins, G. Eiriksdottir, V. Gudnason, U. Gyllensten, A. Hamsten, A. T. Hattersley, A. Hofman, F. B. Hu, T. Illig, C. Iribarren, M. R. Jarvelin, W. H. Kao, J. Kaprio, L. J. Launer, P. B. Munroe, B. Oostra, B. W. Penninx, P. P. Pramstaller, B. M. Psaty, T. Quertermous, A. Rissanen, I. Rudan, A. R. Shuldiner, N. Soranzo, T. D. Spector, A. C. Syvanen, M. Uda, A. Uitterlinden, H. Völzke, P. Vollenweider, J. F. Wilson, J. C. Witteman, A. F. Wright, G. R. Abecasis, M. Boehnke, I. B. Borecki, P. Deloukas, T. M. Frayling, L. C. Groop, T. Haritunians, D. J. Hunter, R. C. Kaplan, K. E. North, J. R. O'Connell, L. Peltonen, D. Schlessinger, D. P. Strachan, J. N. Hirschhorn, T. L. Assimes, H. E. Wichmann, U. Thorsteinsdottir, C. M. van Duijn, K. Stefansson, L. A. Cupples, R. J. Loos, I. Barroso, M. I. McCarthy, C. S. Fox, K. L. Mohlke, and C. M. Lindgren. 2010. 'Meta-analysis identifies 13 new loci associated with waist-hip ratio and reveals sexual dimorphism in the genetic basis of fat distribution', *Nat Genet*, 42: 949-60.

Heldt, H. W., H. Jacobs, and M. Klingenberg. 1965. 'ENDOGENOUS ADP OF MITOCHONDRIA, AN EARLY PHOSPHATE ACCEPTOR OF OXIDATIVE PHOSPHORYLATION AS DISCLOSED BY KINETIC STUDIES WITH C14

LABELLED ADP AND ATP AND WITH ATRACTYLOSIDE', *Biochem Biophys Res Commun*, 18: 174-9.

Hershberger, R. E., D. J. Hedges, and A. Morales. 2013. 'Dilated cardiomyopathy: the complexity of a diverse genetic architecture', *Nat Rev Cardiol*, 10: 531-47.

Herzig, S., E. Raemy, S. Montessuit, J. L. Veuthey, N. Zamboni, B. Westermann, E. R. Kunji, and J. C. Martinou. 2012. 'Identification and functional expression of the mitochondrial pyruvate carrier', *Science*, 337: 93-6.

Hindorff, L. A., P. Sethupathy, H. A. Junkins, E. M. Ramos, J. P. Mehta, F. S. Collins, and T. A. Manolio. 2009. 'Potential etiologic and functional implications of genome-wide association loci for human diseases and traits', *Proc Natl Acad Sci U S A*, 106: 9362-7.

Hirabara, S. M., R. Curi, and P. Maechler. 2010. 'Saturated fatty acid-induced insulin resistance is associated with mitochondrial dysfunction in skeletal muscle cells', *J Cell Physiol*, 222: 187-94.

Ho, C. Y., S. M. Day, S. D. Colan, M. W. Russell, J. A. Towbin, M. V. Sherrid, C. E. Canter, J. L. Jefferies, A. M. Murphy, A. L. Cirino, T. P. Abraham, M. Taylor, L. Mestroni, D. A. Bluemke, P. Jarolim, L. Shi, L. A. Sleeper, C. E. Seidman, and E. J. Orav. 2017. 'The Burden of Early Phenotypes and the Influence of Wall Thickness in Hypertrophic Cardiomyopathy Mutation Carriers: Findings From the HCMNet Study', *JAMA Cardiol*, 2: 419-28.

Holness, M. J., and M. C. Sugden. 2003. 'Regulation of pyruvate dehydrogenase complex activity by reversible phosphorylation', *Biochem Soc Trans*, 31: 1143-51.

Hu, H. J., C. Zhang, Z. H. Tang, S. L. Qu, and Z. S. Jiang. 2019. 'Regulating the Warburg effect on metabolic stress and myocardial fibrosis remodeling and atrial intracardiac waveform activity induced by atrial fibrillation', *Biochem Biophys Res Commun*, 516: 653-60.

Hu, Y., A. Comjean, J. Rodiger, Y. Liu, Y. Gao, V. Chung, J. Zirin, N. Perrimon, and S. E. Mohr. 2021. 'FlyRNAi.org-the database of the Drosophila RNAi screening center and transgenic RNAi project: 2021 update', *Nucleic Acids Res*, 49: D908-d15.

Hue, L., and H. Taegtmeyer. 2009. 'The Randle cycle revisited: a new head for an old hat', *Am J Physiol Endocrinol Metab*, 297: E578-91.

Hui, S., J. M. Ghergurovich, R. J. Morscher, C. Jang, X. Teng, W. Lu, L. A. Esparza, T. Reya, Zhan Le, J. Yanxiang Guo, E. White, and J. D. Rabinowitz. 2017. 'Glucose feeds the TCA cycle via circulating lactate', *Nature*, 551: 115-18.

Hütter, J. F., C. Schweickhardt, H. M. Piper, and P. G. Spieckermann. 1984. 'Inhibition of fatty acid oxidation and decrease of oxygen consumption of working rat heart by 4-bromocrotonic acid', *J Mol Cell Cardiol*, 16: 105-8.

Jóhannsson, E., P. K. Lunde, C. Heddle, I. Sjaastad, M. J. Thomas, L. Bergersen, A. P. Halestrap, T. W. Blackstad, O. P. Ottersen, and O. M. Sejersted. 2001. 'Upregulation of the cardiac monocarboxylate transporter MCT1 in a rat model of congestive heart failure', *Circulation*, 104: 729-34.

Karczewski, K. J., L. C. Francioli, G. Tiao, B. B. Cummings, J. Alföldi, Q. Wang, R. L. Collins, K. M. Laricchia, A. Ganna, D. P. Birnbaum, L. D. Gauthier, H. Brand, M. Solomonson, N. A. Watts, D. Rhodes, M. Singer-Berk, E. M. England, E. G. Seaby, J. A. Kosmicki, R. K. Walters, K. Tashman, Y. Farjoun, E. Banks, T.

Poterba, A. Wang, C. Seed, N. Whiffin, J. X. Chong, K. E. Samocha, E. Pierce-Hoffman, Z. Zappala, A. H. O'Donnell-Luria, E. V. Minikel, B. Weisburd, M. Lek, J. S. Ware, C. Vittal, I. M. Armean, L. Bergelson, K. Cibulskis, K. M. Connolly, M. Covarrubias, S. Donnelly, S. Ferriera, S. Gabriel, J. Gentry, N. Gupta, T. Jeandet, D. Kaplan, C. Llanwarne, R. Munshi, S. Novod, N. Petrillo, D. Roazen, V. Ruano-Rubio, A. Saltzman, M. Schleicher, J. Soto, K. Tibbetts, C. Tolonen, G. Wade, M. E. Talkowski, B. M. Neale, M. J. Daly, and D. G. MacArthur. 2020. 'The mutational constraint spectrum quantified from variation in 141,456 humans', *Nature*, 581: 434-43.

Karwi, Q. G., G. M. Uddin, K. L. Ho, and G. D. Lopaschuk. 2018. 'Loss of Metabolic Flexibility in the Failing Heart', *Front Cardiovasc Med*, 5: 68.

Kassab, S., Z. Albalawi, H. Daghistani, and A. Kitmitto. 2021. 'Mitochondrial Arrest on the Microtubule Highway-A Feature of Heart Failure and Diabetic Cardiomyopathy?', *Front Cardiovasc Med*, 8: 689101.

Kato, T., S. Niizuma, Y. Inuzuka, T. Kawashima, J. Okuda, Y. Tamaki, Y. Iwanaga, M. Narazaki, T. Matsuda, T. Soga, T. Kita, T. Kimura, and T. Shioi. 2010. 'Analysis of metabolic remodeling in compensated left ventricular hypertrophy and heart failure', *Circ Heart Fail*, 3: 420-30.

Khan, A. U. H., N. Allende-Vega, D. Gitenay, S. Gerbal-Chaloin, C. Gondeau, D. N. Vo, S. Belkahla, S. Orecchioni, G. Talarico, F. Bertolini, M. Bozic, J. M. Valdivielso, F. Bejjani, I. Jariel, I. C. Lopez-Mejia, L. Fajas, C. H. Lecellier, J. Hernandez, M. Daujat, and M. Villalba. 2017. 'The PDK1 Inhibitor Dichloroacetate Controls Cholesterol Homeostasis Through the ERK5/MEF2 Pathway', *Sci Rep*, 7: 10654.

Khan, Dilshad H., Michael Mullokandov, Yan Wu, Marcela Gronda, Rose Hurren, Xiaoming Wang, Neil MacLean, Danny V. Jeyaraju, G. Wei Xu, Rob C. Laister, Zachary Blatman, Troy Ketela, Mark D. Minden, Atan Gross, and Aaron D. Schimmer. 2017. 'Mitochondrial Carrier Homolog 2 (MTCH2) Regulates the Differentiation of AML Cells By Controlling Pyruvate Entry into the Mitochondria, Nuclear Localization of Pyruvate Dehydrogenase Complex and H3 and H4 Histone Acetylation', *Blood*, 130: 299-99.

Kilpeläinen, T. O., M. den Hoed, K. K. Ong, A. Grøntved, S. Brage, K. Jameson, C. Cooper, K. T. Khaw, U. Ekelund, N. J. Wareham, and R. J. Loos. 2011. 'Obesity-susceptibility loci have a limited influence on birth weight: a meta-analysis of up to 28,219 individuals', *Am J Clin Nutr*, 93: 851-60.

Koch, L. 2020. 'Exploring human genomic diversity with gnomAD', *Nat Rev Genet*, 21: 448.

Kulyté, A., M. Rydén, N. Mejhert, E. Dungner, E. Sjölin, P. Arner, and I. Dahlman. 2011. 'MTCH2 in human white adipose tissue and obesity', *J Clin Endocrinol Metab*, 96: E1661-5.

Labbé, K., S. Mookerjee, M. Le Vasseur, E. Gibbs, C. Lerner, and J. Nunnari. 2021. 'The modified mitochondrial outer membrane carrier MTCH2 links mitochondrial fusion to lipogenesis', *J Cell Biol*, 220.

Lamarca, V., I. Marzo, A. Sanz-Clemente, and J. A. Carrodeguas. 2008. 'Exposure of any of two proapoptotic domains of presenilin 1-associated protein/mitochondrial carrier homolog 1 on the surface of mitochondria is sufficient for induction of apoptosis in a Bax/Bak-independent manner', *Eur J Cell Biol*, 87: 325-34.

Lamarca, V., A. Sanz-Clemente, R. Pérez-Pé, M. J. Martínez-Lorenzo, N. Halaihel, P. Muniesa, and J. A. Carrodeguas. 2007. 'Two isoforms of PSAP/MTCH1 share two proapoptotic domains and multiple internal signals for import into the mitochondrial outer membrane', *Am J Physiol Cell Physiol*, 293: C1347-61.

Landgraf, K., A. Strobach, W. Kiess, and A. Körner. 2016. 'Loss of mtch2 function impairs early development of liver, intestine and visceral adipocytes in zebrafish larvae', *FEBS Lett*, 590: 2852-61.

Lawlor, M. A., A. Mora, P. R. Ashby, M. R. Williams, V. Murray-Tait, L. Malone, A. R. Prescott, J. M. Lucocq, and D. R. Alessi. 2002. 'Essential role of PDK1 in regulating cell size and development in mice', *Embo j*, 21: 3728-38.

Le Guen, M., A. Nicolas-Robin, S. Carreira, M. Raux, P. Leprince, B. Riou, and O. Langeron. 2011. 'Extracorporeal life support following out-of-hospital refractory cardiac arrest', *Crit Care*, 15: R29.

Lee, C. Y., H. J. Wang, J. D. Jhang, and I. C. Cho. 2019. 'Automated drosophila heartbeat counting based on image segmentation technique on optical coherence tomography', *Sci Rep*, 9: 5557.

Lewis, J. F., M. DaCosta, T. Wargowich, and P. Stacpoole. 1998. 'Effects of dichloroacetate in patients with congestive heart failure', *Clin Cardiol*, 21: 888-92.

Li, T., L. Zeng, W. Gao, M. Z. Cui, X. Fu, and X. Xu. 2013. 'PSAP induces a unique Apaf-1 and Smac-dependent mitochondrial apoptotic pathway independent of Bcl-2 family proteins', *Biochim Biophys Acta*, 1832: 453-74.

Lin, N., N. Badie, L. Yu, D. Abraham, H. Cheng, N. Bursac, H. A. Rockman, and M. J. Wolf. 2011. 'A method to measure myocardial calcium handling in adult Drosophila', *Circ Res*, 108: 1306-15.

Liu, M., X. Liu, P. Suo, Y. Gong, B. Qu, X. Peng, W. Xiao, Y. Li, Y. Chen, Z. Zeng, Y. Lu, T. Huang, Y. Zhao, M. Liu, L. Li, Y. Chen, Y. Zhou, G. Liu, J. Yao, S. Chen, and L. Song. 2020. 'The contribution of hereditary cancer-related germline mutations to lung cancer susceptibility', *Transl Lung Cancer Res*, 9: 646-58.

Liu, T., L. Chen, E. Kim, D. Tran, B. S. Phinney, and A. A. Knowlton. 2014. 'Mitochondrial proteome remodeling in ischemic heart failure', *Life Sci*, 101: 27-36.

Locke, A. E., B. Kahali, S. I. Berndt, A. E. Justice, T. H. Pers, F. R. Day, C. Powell, S. Vedantam, M. L. Buchkovich, J. Yang, D. C. Croteau-Chonka, T. Esko, T. Fall, T. Ferreira, S. Gustafsson, Z. Kutalik, J. Luan, R. Mägi, J. C. Randall, T. W. Winkler, A. R. Wood, T. Workalemahu, J. D. Faul, J. A. Smith, J. H. Zhao, W. Zhao, J. Chen, R. Fehrmann, K. Hedman Å, J. Karjalainen, E. M. Schmidt, D. Absher, N. Amin, D. Anderson, M. Beekman, J. L. Bolton, J. L. Bragg-Gresham, S. Buyske, A. Demirkan, G. Deng, G. B. Ehret, B. Feenstra, M. F. Feitosa, K. Fischer, A. Goel, J. Gong, A. U. Jackson, S. Kanoni, M. E. Kleber, K. Kristiansson, U. Lim, V. Lotay, M. Mangino, I. M. Leach, C. Medina-Gomez, S. E. Medland, M. A. Nalls, C. D. Palmer, D. Pasko, S. Pechlivanis, M. J. Peters, I. Prokopenko, D. Shungin, A. Stančáková, R. J. Strawbridge, Y. J. Sung, T. Tanaka, A. Teumer, S. Trompet, S. W. van der Laan, J. van Setten, J. V. Van Vliet-Ostaptchouk, Z. Wang, L. Yengo, W. Zhang, A. Isaacs, E. Albrecht, J. Ärnlöv, G. M. Arscott, A. P. Attwood, S. Bandinelli, A. Barrett, I. N. Bas, C. Bellis, A. J. Bennett, C. Berne, R. Blagieva, M. Blüher, S. Böhringer, L. L. Bonnycastle,

Y. Böttcher, H. A. Boyd, M. Bruinenberg, I. H. Caspersen, Y. I. Chen, R. Clarke, E. W. Daw, A. J. M. de Craen, G. Delgado, M. Dimitriou, A. S. F. Doney, N. Eklund, K. Estrada, E. Eury, L. Folkersen, R. M. Fraser, M. E. Garcia, F. Geller, V. Giedraitis, B. Gigante, A. S. Go, A. Golay, A. H. Goodall, S. D. Gordon, M. Gorski, H. J. Grabe, H. Grallert, T. B. Grammer, J. Gräßler, H. Grönberg, C. J. Groves, G. Gusto, J. Haessler, P. Hall, T. Haller, G. Hallmans, C. A. Hartman, M. Hassinen, C. Hayward, N. L. Heard-Costa, Q. Helmer, C. Hengstenberg, O. Holmen, J. J. Hottenga, A. L. James, J. M. Jeff, Å Johansson, J. Jolley, T. Juliusdottir, L. Kinnunen, W. Koenig, M. Koskenvuo, W. Kratzer, J. Laitinen, C. Lamina, K. Leander, N. R. Lee, P. Lichtner, L. Lind, J. Lindström, K. S. Lo, S. Lobbens, R. Lorbeer, Y. Lu, F. Mach, P. K. E. Magnusson, A. Mahajan, W. L. McArdle, S. McLachlan, C. Menni, S. Merger, E. Mihailov, L. Milani, A. Moayyeri, K. L. Monda, M. A. Morken, A. Mulas, G. Müller, M. Müller-Nurasyid, A. W. Musk, R. Nagaraja, M. M. Nöthen, I. M. Nolte, S. Pilz, N. W. Rayner, F. Renstrom, R. Rettig, J. S. Ried, S. Ripke, N. R. Robertson, L. M. Rose, S. Sanna, H. Scharnagl, S. Scholtens, F. R. Schumacher, W. R. Scott, T. Seufferlein, J. Shi, A. V. Smith, J. Smolonska, A. V. Stanton, V. Steinthorsdottir, K. Stirrups, H. M. Stringham, J. Sundström, M. A. Swertz, A. J. Swift, A. C. Syvänen, S. T. Tan, B. O. Tayo, B. Thorand, G. Thorleifsson, J. P. Tyrer, H. W. Uh, L. Vandenput, F. C. Verhulst, S. H. Vermeulen, N. Verweij, J. M. Vonk, L. L. Waite, H. R. Warren, D. Waterworth, M. N. Weedon, L. R. Wilkens, C. Willenborg, T. Wilsgaard, M. K. Wojczynski, A. Wong, A. F. Wright, Q. Zhang, E. P. Brennan, M. Choi, Z. Dastani, A. W. Drong, P. Eriksson, A. Franco-Cereceda, J. R. Gådin, A. G. Gharavi, M. E. Goddard, R. E. Handsaker, J. Huang, F. Karpe, S. Kathiresan, S. Keildson, K. Kiryluk, M. Kubo, J. Y. Lee, L. Liang, R. P. Lifton, B. Ma, S. A. McCarroll, A. J. McKnight, J. L. Min, M. F. Moffatt, G. W. Montgomery, J. M. Murabito, G. Nicholson, D. R. Nyholt, Y. Okada, J. R. B. Perry, R. Dorajoo, E. Reinmaa, R. M. Salem, N. Sandholm, R. A. Scott, L. Stolk, A. Takahashi, T. Tanaka, F. M. van 't Hooft, A. A. E. Vinkhuyzen, H. J. Westra, W. Zheng, K. T. Zondervan, A. C. Heath, D. Arveiler, S. J. L. Bakker, J. Beilby, R. N. Bergman, J. Blangero, P. Bovet, H. Campbell, M. J. Caulfield, G. Cesana, A. Chakravarti, D. I. Chasman, P. S. Chines, F. S. Collins, D. C. Crawford, L. A. Cupples, D. Cusi, J. Danesh, U. de Faire, H. M. den Ruijter, A. F. Dominiczak, R. Erbel, J. Erdmann, J. G. Eriksson, M. Farrall, S. B. Felix, E. Ferrannini, J. Ferrières, I. Ford, N. G. Forouhi, T. Forrester, O. H. Franco, R. T. Gansevoort, P. V. Gejman, C. Gieger, O. Gottesman, V. Gudnason, U. Gyllensten, A. S. Hall, T. B. Harris, A. T. Hattersley, A. A. Hicks, L. A. Hindorff, A. D. Hingorani, A. Hofman, G. Homuth, G. K. Hovingh, S. E. Humphries, S. C. Hunt, E. Hyppönen, T. Illig, K. B. Jacobs, M. R. Jarvelin, K. H. Jöckel, B. Johansen, P. Jousilahti, J. W. Jukema, A. M. Jula, J. Kaprio, J. J. P. Kastelein, S. M. Keinanen-Kiukaanniemi, L. A. Kiemeney, P. Knekt, J. S. Kooner, C. Kooperberg, P. Kovacs, A. T. Kraja, M. Kumari, J. Kuusisto, T. A. Lakka, C. Langenberg, L. L. Marchand, T. Lehtimäki, V. Lyssenko, S. Männistö, A. Marette, T. C. Matise, C. A. McKenzie, B. McKnight, F. L. Moll, A. D. Morris, A. P. Morris, J. C. Murray, M. Nelis, C. Ohlsson, A. J. Oldehinkel, K. K. Ong, P. A. F. Madden, G. Pasterkamp, J. F. Peden, A. Peters, D. S. Postma, P. P. Pramstaller, J. F. Price, L. Qi, O. T. Raitakari, T. Rankinen,

D. C. Rao, T. K. Rice, P. M. Ridker, J. D. Rioux, M. D. Ritchie, I. Rudan, V. Salomaa, N. J. Samani, J. Saramies, M. A. Sarzynski, H. Schunkert, P. E. H. Schwarz, P. Sever, A. R. Shuldiner, J. Sinisalo, R. P. Stolk, K. Strauch, A. Tönjes, D. A. Trégouët, A. Tremblay, E. Tremoli, J. Virtamo, M. C. Vohl, U. Völker, G. Waeber, G. Willemsen, J. C. Witteman, M. C. Zillikens, L. S. Adair, P. Amouyel, F. W. Asselbergs, T. L. Assimes, M. Bochud, B. O. Boehm, E. Boerwinkle, S. R. Bornstein, E. P. Bottinger, C. Bouchard, S. Cauchi, J. C. Chambers, S. J. Chanock, R. S. Cooper, P. I. W. de Bakker, G. Dedoussis, L. Ferrucci, P. W. Franks, P. Froguel, L. C. Groop, C. A. Haiman, A. Hamsten, J. Hui, D. J. Hunter, K. Hveem, R. C. Kaplan, M. Kivimaki, D. Kuh, M. Laakso, Y. Liu, N. G. Martin, W. März, M. Melbye, A. Metspalu, S. Moebus, P. B. Munroe, I. Njølstad, B. A. Oostra, C. N. A. Palmer, N. L. Pedersen, M. Perola, L. Pérusse, U. Peters, C. Power, T. Quertermous, R. Rauramaa, F. Rivadeneira, T. E. Saaristo, D. Saleheen, N. Sattar, E. E. Schadt, D. Schlessinger, P. E. Slagboom, H. Snieder, T. D. Spector, U. Thorsteinsdottir, M. Stumvoll, J. Tuomilehto, A. G. Uitterlinden, M. Uusitupa, P. van der Harst, M. Walker, H. Wallaschofski, N. J. Wareham, H. Watkins, D. R. Weir, H. E. Wichmann, J. F. Wilson, P. Zanen, I. B. Borecki, P. Deloukas, C. S. Fox, I. M. Heid, J. R. O'Connell, D. P. Strachan, K. Stefansson, C. M. van Duijn, G. R. Abecasis, L. Franke, T. M. Frayling, M. I. McCarthy, P. M. Visscher, A. Scherag, C. J. Willer, M. Boehnke, K. L. Mohlke, C. M. Lindgren, J. S. Beckmann, I. Barroso, K. E. North, E. Ingelsson, J. N. Hirschhorn, R. J. F. Loos, and E. K. Speliotes. 2015. 'Genetic studies of body mass index yield new insights for obesity biology', *Nature*, 518: 197-206.

Lopaschuk, G. D., Q. G. Karwi, R. Tian, A. R. Wende, and E. D. Abel. 2021. 'Cardiac Energy Metabolism in Heart Failure', *Circ Res*, 128: 1487-513.

Lopaschuk, G. D., and J. R. Ussher. 2016. 'Evolving Concepts of Myocardial Energy Metabolism: More Than Just Fats and Carbohydrates', *Circ Res*, 119: 1173-76.

Lopaschuk, G. D., J. R. Ussher, C. D. Folmes, J. S. Jaswal, and W. C. Stanley. 2010. 'Myocardial fatty acid metabolism in health and disease', *Physiol Rev*, 90: 207-58.

Ludwig, D. S. 2020. 'The Ketogenic Diet: Evidence for Optimism but High-Quality Research Needed', *J Nutr*, 150: 1354-59.

Lutter, M., M. Fang, X. Luo, M. Nishijima, X. Xie, and X. Wang. 2000. 'Cardiolipin provides specificity for targeting of tBid to mitochondria', *Nat Cell Biol*, 2: 754-61.

Ma, L., A. Bradu, A. G. Podoleanu, and J. W. Bloor. 2010. 'Arrhythmia caused by a Drosophila tropomyosin mutation is revealed using a novel optical coherence tomography instrument', *PLoS One*, 5: e14348.

Machiela, M. J., and S. J. Chanock. 2015. 'LDlink: a web-based application for exploring population-specific haplotype structure and linking correlated alleles of possible functional variants', *Bioinformatics*, 31: 3555-7.

Manivannan, S. N., S. Darouich, A. Masmoudi, D. Gordon, G. Zender, Z. Han, S. Fitzgerald-Butt, P. White, K. L. McBride, M. Kharrat, and V. Garg. 2020. 'Novel frameshift variant in MYL2 reveals molecular differences between dominant and recessive forms of hypertrophic cardiomyopathy', *PLoS Genet*, 16: e1008639.

Mao, G., J. Tan, W. Gao, Y. Shi, M. Z. Cui, and X. Xu. 2008. 'Both the N-terminal fragment and the protein-protein interaction domain (PDZ domain) are required

for the pro-apoptotic activity of presenilin-associated protein PSAP', *Biochim Biophys Acta*, 1780: 696-708.

Marian, A. J., and E. Braunwald. 2017. 'Hypertrophic Cardiomyopathy: Genetics, Pathogenesis, Clinical Manifestations, Diagnosis, and Therapy', *Circ Res*, 121: 749-70.

Maron, B. J., M. S. Maron, and C. Semsarian. 2012. 'Genetics of hypertrophic cardiomyopathy after 20 years: clinical perspectives', *J Am Coll Cardiol*, 60: 705-15.

Martins, A. R., R. T. Nachbar, R. Gorjao, M. A. Vinolo, W. T. Festuccia, R. H. Lambertucci, M. F. Cury-Boaventura, L. R. Silveira, R. Curi, and S. M. Hirabara. 2012. 'Mechanisms underlying skeletal muscle insulin resistance induced by fatty acids: importance of the mitochondrial function', *Lipids Health Dis*, 11: 30.

Maryanovich, M., Y. Zaltsman, A. Ruggiero, A. Goldman, L. Shachnai, S. L. Zaidman, Z. Porat, K. Golan, T. Lapidot, and A. Gross. 2015. 'An MTCH2 pathway repressing mitochondria metabolism regulates haematopoietic stem cell fate', *Nat Commun*, 6: 7901.

Matsuhashi, T., T. Hishiki, H. Zhou, T. Ono, R. Kaneda, T. Iso, A. Yamaguchi, J. Endo, Y. Katsumata, A. Atsushi, T. Yamamoto, K. Shirakawa, X. Yan, K. Shinmura, M. Suematsu, K. Fukuda, and M. Sano. 2015. 'Activation of pyruvate dehydrogenase by dichloroacetate has the potential to induce epigenetic remodeling in the heart', *J Mol Cell Cardiol*, 82: 116-24.

Mazzeo, R. S., G. A. Brooks, D. A. Schoeller, and T. F. Budinger. 1986. 'Disposal of blood [1-13C]lactate in humans during rest and exercise', *J Appl Physiol (1985)*, 60: 232-41.

McCommis, K. S., A. Kovacs, C. J. Weinheimer, T. M. Shew, T. R. Koves, O. R. Ilkayeva, D. R. Kamm, K. D. Pyles, M. T. King, R. L. Veech, B. J. DeBosch, D. M. Muoio, R. W. Gross, and B. N. Finck. 2020. 'Nutritional modulation of heart failure in mitochondrial pyruvate carrier-deficient mice', *Nat Metab*, 2: 1232-47.

McNally, E. M., D. Y. Barefield, and M. J. Puckelwartz. 2015. 'The genetic landscape of cardiomyopathy and its role in heart failure', *Cell Metab*, 21: 174-82.

McNally, E. M., and L. Mestroni. 2017. 'Dilated Cardiomyopathy: Genetic Determinants and Mechanisms', *Circ Res*, 121: 731-48.

McNally, E. M., M. R. Passos-Bueno, C. G. Bönnemann, M. Vainzof, E. de Sá Moreira, H. G. Lidov, K. B. Othmane, P. H. Denton, J. M. Vance, M. Zatz, and L. M. Kunkel. 1996. 'Mild and severe muscular dystrophy caused by a single gamma-sarcoglycan mutation', *Am J Hum Genet*, 59: 1040-7.

Mei, H., W. Chen, F. Jiang, J. He, S. Srinivasan, E. N. Smith, N. Schork, S. Murray, and G. S. Berenson. 2012. 'Longitudinal replication studies of GWAS risk SNPs influencing body mass index over the course of childhood and adulthood', *PLoS One*, 7: e31470.

Meier, S., W. Neupert, and J. M. Herrmann. 2005. 'Proline residues of transmembrane domains determine the sorting of inner membrane proteins in mitochondria', *J Cell Biol*, 170: 881-8.

Melnikov, S., J. Mailliot, L. Rigger, S. Neuner, B. S. Shin, G. Yusupova, T. E. Dever, R. Micura, and M. Yusupov. 2016. 'Molecular insights into protein synthesis with proline residues', *EMBO Rep*, 17: 1776-84.

Men, J., J. Jerwick, P. Wu, M. Chen, A. Alex, Y. Ma, R. E. Tanzi, A. Li, and C. Zhou. 2016. 'Drosophila Preparation and Longitudinal Imaging of Heart Function In Vivo Using Optical Coherence Microscopy (OCM)', *J Vis Exp*.

Mery, A., O. Taghli-Lamallem, K. A. Clark, M. C. Beckerle, X. Wu, K. Ocorr, and R. Bodmer. 2008. 'The Drosophila muscle LIM protein, Mlp84B, is essential for cardiac function', *J Exp Biol*, 211: 15-23.

Misra, M. K., M. Sarwat, P. Bhakuni, R. Tuteja, and N. Tuteja. 2009. 'Oxidative stress and ischemic myocardial syndromes', *Med Sci Monit*, 15: Ra209-19.

Morgan, A. A., and E. Rubenstein. 2013. 'Proline: the distribution, frequency, positioning, and common functional roles of proline and polyproline sequences in the human proteome', *PLoS One*, 8: e53785.

Nadeau, J. H. 2001. 'Modifier genes in mice and humans', *Nat Rev Genet*, 2: 165-74.

Nagoshi, T., M. Yoshimura, G. M. Rosano, G. D. Lopaschuk, and S. Mochizuki. 2011. 'Optimization of cardiac metabolism in heart failure', *Curr Pharm Des*, 17: 3846-53.

Nasser, S., V. Vialichka, M. Biesiekierska, A. Balcerczyk, and L. Pirola. 2020. 'Effects of ketogenic diet and ketone bodies on the cardiovascular system: Concentration matters', *World J Diabetes*, 11: 584-95.

Neville, K. E., T. L. Bosse, M. Klekos, J. F. Mills, S. E. Weicksel, J. S. Waters, and M. Tipping. 2018. 'A novel ex vivo method for measuring whole brain metabolism in model systems', *J Neurosci Methods*, 296: 32-43.

Ng, M. C., C. H. Tam, W. Y. So, J. S. Ho, A. W. Chan, H. M. Lee, Y. Wang, V. K. Lam, J. C. Chan, and R. C. Ma. 2010. 'Implication of genetic variants near NEGR1, SEC16B, TMEM18, ETV5/DGKG, GNPDA2, LIN7C/BDNF, MTCH2, BCDIN3D/FAIM2, SH2B1, FTO, MC4R, and KCTD15 with obesity and type 2 diabetes in 7705 Chinese', *J Clin Endocrinol Metab*, 95: 2418-25.

Ni, J. Q., M. Markstein, R. Binari, B. Pfeiffer, L. P. Liu, C. Villalta, M. Booker, L. Perkins, and N. Perrimon. 2008. 'Vector and parameters for targeted transgenic RNA interference in Drosophila melanogaster', *Nat Methods*, 5: 49-51.

Nishihara, S. 2007. 'Drosophila development, RNAi, and glycobiology.', *Comprehensive Glycoscience.*, 4: 49-79.

Novak, S. M., A. Joardar, C. C. Gregorio, and D. C. Zarnescu. 2015. 'Regulation of Heart Rate in Drosophila via Fragile X Mental Retardation Protein', *PLoS One*, 10: e0142836.

O'Gara, P. T., R. O. Bonow, B. J. Maron, B. A. Damske, A. Van Lingen, S. L. Bacharach, S. M. Larson, and S. E. Epstein. 1987. 'Myocardial perfusion abnormalities in patients with hypertrophic cardiomyopathy: assessment with thallium-201 emission computed tomography', *Circulation*, 76: 1214-23.

Ocorr, K., T. Akasaka, and R. Bodmer. 2007. 'Age-related cardiac disease model of Drosophila', *Mech Ageing Dev*, 128: 112-6.

Ogunbona, O. B., and S. M. Claypool. 2019. 'Emerging Roles in the Biogenesis of Cytochrome c Oxidase for Members of the Mitochondrial Carrier Family', *Front Cell Dev Biol*, 7: 3.

Palmieri, F. 2013. 'The mitochondrial transporter family SLC25: identification, properties and physiopathology', *Mol Aspects Med*, 34: 465-84.

Perkins, L. A., L. Holderbaum, R. Tao, Y. Hu, R. Sopko, K. McCall, D. Yang-Zhou, I. Flockhart, R. Binari, H. S. Shim, A. Miller, A. Housden, M. Foos, S. Randkelv, C. Kelley, P. Namgyal, C. Villalta, L. P. Liu, X. Jiang, Q. Huan-Huan, X. Wang, A. Fujiyama, A. Toyoda, K. Ayers, A. Blum, B. Czech, R. Neumuller, D. Yan, A. Cavallaro, K. Hibbard, D. Hall, L. Cooley, G. J. Hannon, R. Lehmann, A. Parks, S. E. Mohr, R. Ueda, S. Kondo, J. Q. Ni, and N. Perrimon. 2015. 'The Transgenic RNAi Project at Harvard Medical School: Resources and Validation', *Genetics*, 201: 843-52.

Peters, S. J. 2003. 'Regulation of PDH activity and isoform expression: diet and exercise', *Biochem Soc Trans*, 31: 1274-80.

Petersen, C. E., B. A. Tripoli, T. A. Schoborg, and J. T. Smyth. 2022. 'Analysis of Drosophila cardiac hypertrophy by microcomputerized tomography for genetic dissection of heart growth mechanisms', *Am J Physiol Heart Circ Physiol*, 322: H296-h309.

Pfaff, E., M. Klingenberg, and H. W. Heldt. 1965. 'Unspecific permeation and specific exchange of adenine nucleotides in liver mitochondria', *Biochim Biophys Acta*, 104: 312-5.

Piel, F. B., A. P. Patil, R. E. Howes, O. A. Nyangiri, P. W. Gething, T. N. Williams, D. J. Weatherall, and S. I. Hay. 2010. 'Global distribution of the sickle cell gene and geographical confirmation of the malaria hypothesis', *Nat Commun*, 1: 104.

Pilegaard, H., and P. D. Neufer. 2004. 'Transcriptional regulation of pyruvate dehydrogenase kinase 4 in skeletal muscle during and after exercise', *Proc Nutr Soc*, 63: 221-6.

Piquereau, J., F. Caffin, M. Novotova, C. Lemaire, V. Veksler, A. Garnier, R. Ventura-Clapier, and F. Joubert. 2013. 'Mitochondrial dynamics in the adult cardiomyocytes: which roles for a highly specialized cell?', *Front Physiol*, 4: 102.

Piquereau, J., and R. Ventura-Clapier. 2018. 'Maturation of Cardiac Energy Metabolism During Perinatal Development', *Front Physiol*, 9: 959.

Plecitá-Hlavatá, L., and P. Ježek. 2016. 'Integration of superoxide formation and cristae morphology for mitochondrial redox signaling', *Int J Biochem Cell Biol*, 80: 31-50.

Pottinger, T. D., M. J. Puckelwartz, L. L. Pesce, A. Robinson, S. Kearns, J. A. Pacheco, L. J. Rasmussen-Torvik, M. E. Smith, R. Chisholm, and E. M. McNally. 2020. 'Pathogenic and Uncertain Genetic Variants Have Clinical Cardiac Correlates in Diverse Biobank Participants', *J Am Heart Assoc*, 9: e013808.

Puckelwartz, M. J., L. L. Pesce, L. M. Dellefave-Castillo, M. T. Wheeler, T. D. Pottinger, A. C. Robinson, S. D. Kearns, A. M. Gacita, Z. J. Schoppen, W. Pan, G. Kim, J. E. Wilcox, A. S. Anderson, E. A. Ashley, S. M. Day, T. Cappola, G. W. Dorn, 2nd, and E. M. McNally. 2021. 'Genomic Context Differs Between Human Dilated Cardiomyopathy and Hypertrophic Cardiomyopathy', *J Am Heart Assoc*, 10: e019944.

Rabin-Court, A., M. R. Rodrigues, X. M. Zhang, and R. J. Perry. 2019. 'Obesity-associated, but not obesity-independent, tumors respond to insulin by increasing mitochondrial glucose oxidation', *PLoS One*, 14: e0218126.

Rabinowitz, J. D., and S. Enerbäck. 2020. 'Lactate: the ugly duckling of energy metabolism', *Nat Metab*, 2: 566-71.

Raemy, E., S. Montessuit, S. Pierredon, A. H. van Kampen, F. M. Vaz, and J. C. Martinou. 2016. 'Cardiolipin or MTCH2 can serve as tBID receptors during apoptosis', *Cell Death Differ*, 23: 1165-74.

Rahit, Kmth, and M. Tarailo-Graovac. 2020. 'Genetic Modifiers and Rare Mendelian Disease', *Genes (Basel)*, 11.

Rask-Andersen, M., T. Karlsson, W. E. Ek, and Å Johansson. 2019. 'Genome-wide association study of body fat distribution identifies adiposity loci and sex-specific genetic effects', *Nat Commun*, 10: 339.

Razeghi, P., M. E. Young, J. L. Alcorn, C. S. Moravec, O. H. Frazier, and H. Taegtmeyer. 2001. 'Metabolic gene expression in fetal and failing human heart', *Circulation*, 104: 2923-31.

Reis, T., M. R. Van Gilst, and I. K. Hariharan. 2010. 'A buoyancy-based screen of Drosophila larvae for fat-storage mutants reveals a role for Sir2 in coupling fat storage to nutrient availability', *PLoS Genet*, 6: e1001206.

Renström, F., F. Payne, A. Nordström, E. C. Brito, O. Rolandsson, G. Hallmans, I. Barroso, P. Nordström, and P. W. Franks. 2009. 'Replication and extension of genome-wide association study results for obesity in 4923 adults from northern Sweden', *Hum Mol Genet*, 18: 1489-96.

Ritterhoff, J., and R. Tian. 2017. 'Metabolism in cardiomyopathy: every substrate matters', *Cardiovasc Res*, 113: 411-21.

Robinson, A. J., E. R. Kunji, and A. Gross. 2012. 'Mitochondrial carrier homolog 2 (MTCH2): the recruitment and evolution of a mitochondrial carrier protein to a critical player in apoptosis', *Exp Cell Res*, 318: 1316-23.

Rotstein, B., and A. Paululat. 2016. 'On the Morphology of the Drosophila Heart', *J Cardiovasc Dev Dis*, 3.

Rottiers, V., A. Francisco, M. Platov, Y. Zaltsman, A. Ruggiero, S. S. Lee, A. Gross, and S. Libert. 2017. 'MTCH2 is a conserved regulator of lipid homeostasis', *Obesity (Silver Spring)*, 25: 616-25.

Ruprecht, J. J., and E. R. S. Kunji. 2020. 'The SLC25 Mitochondrial Carrier Family: Structure and Mechanism', *Trends Biochem Sci*, 45: 244-58.

Salas Noain, J., A. Minupuri, A. Kulkarni, and S. Zheng. 2020. 'Significant Impact of the Ketogenic Diet on Low-Density Lipoprotein Cholesterol Levels', *Cureus*, 12: e9418.

Sanchez, W. Y., S. L. McGee, T. Connor, B. Mottram, A. Wilkinson, J. P. Whitehead, S. Vuckovic, and L. Catley. 2013. 'Dichloroacetate inhibits aerobic glycolysis in multiple myeloma cells and increases sensitivity to bortezomib', *Br J Cancer*, 108: 1624-33.

Schreurs, M., F. Kuipers, and F. R. van der Leij. 2010. 'Regulatory enzymes of mitochondrial beta-oxidation as targets for treatment of the metabolic syndrome', *Obes Rev*, 11: 380-8.

Schulze, K. V., N. A. Hanchard, and M. F. Wangler. 2020. 'Biases in arginine codon usage correlate with genetic disease risk', *Genet Med*, 22: 1407-12.

Schumann, G., R. Bonora, F. Ceriotti, P. Clerc-Renaud, C. A. Ferrero, G. Férard, P. F. Franck, F. J. Gella, W. Hoelzel, P. J. Jørgensen, T. Kanno, A. Kessner, R. Klauke, N. Kristiansen, J. M. Lessinger, T. P. Linsinger, H. Misaki, M. Panteghini, J. Pauwels, H. G. Schimmel, A. Vialle, G. Weidemann, and L. Siekmann. 2002.

'IFCC primary reference procedures for the measurement of catalytic activity concentrations of enzymes at 37 degrees C. Part 3. Reference procedure for the measurement of catalytic concentration of lactate dehydrogenase', *Clin Chem Lab Med*, 40: 643-8.

Schurr, A., and S. Passarella. 2022. 'Aerobic Glycolysis: A DeOxymoron of (Neuro)Biology', *Metabolites*, 12.

Sellers, K., M. P. Fox, M. Bousamra, 2nd, S. P. Slone, R. M. Higashi, D. M. Miller, Y. Wang, J. Yan, M. O. Yuneva, R. Deshpande, A. N. Lane, and T. W. Fan. 2015. 'Pyruvate carboxylase is critical for non-small-cell lung cancer proliferation', *J Clin Invest*, 125: 687-98.

Selvaraj, S., D. P. Kelly, and K. B. Margulies. 2020. 'Implications of Altered Ketone Metabolism and Therapeutic Ketosis in Heart Failure', *Circulation*, 141: 1800-12.

Sessions, A. O., G. Kaushik, S. Parker, K. Raedschelders, R. Bodmer, J. E. Van Eyk, and A. J. Engler. 2017. 'Extracellular matrix downregulation in the Drosophila heart preserves contractile function and improves lifespan', *Matrix Biol*, 62: 15-27.

Seymour, A. M., and J. C. Chatham. 1997. 'The effects of hypertrophy and diabetes on cardiac pyruvate dehydrogenase activity', *J Mol Cell Cardiol*, 29: 2771-8.

Shanmughapriya, S., D. Langford, and K. Natarajaseenivasan. 2020. 'Inter and Intracellular mitochondrial trafficking in health and disease', *Ageing Res Rev*, 62: 101128.

Sievers, F., and D. G. Higgins. 2014. 'Clustal omega', *Curr Protoc Bioinformatics*, 48: 3.13.1-16.

Sinnott-Armstrong, N., Y. Tanigawa, D. Amar, N. Mars, C. Benner, M. Aguirre, G. R. Venkataraman, M. Wainberg, H. M. Ollila, T. Kiiskinen, A. S. Havulinna, J. P. Pirruccello, J. Qian, A. Shcherbina, F. Rodriguez, T. L. Assimes, V. Agarwala, R. Tibshirani, T. Hastie, S. Ripatti, J. K. Pritchard, M. J. Daly, and M. A. Rivas. 2021. 'Genetics of 35 blood and urine biomarkers in the UK Biobank', *Nat Genet*, 53: 185-94.

Sousa Fialho, M. D. L., A. H. Abd Jamil, G. A. Stannard, and L. C. Heather. 2019. 'Hypoxia-inducible factor 1 signalling, metabolism and its therapeutic potential in cardiovascular disease', *Biochim Biophys Acta Mol Basis Dis*, 1865: 831-43.

Stanley, W. C., E. W. Gertz, J. A. Wisneski, R. A. Neese, D. L. Morris, and G. A. Brooks. 1986. 'Lactate extraction during net lactate release in legs of humans during exercise', *J Appl Physiol (1985)*, 60: 1116-20.

Sullivan, K. M., K. Scott, C. S. Zuker, and G. M. Rubin. 2000. 'The ryanodine receptor is essential for larval development in Drosophila melanogaster', *Proc Natl Acad Sci U S A*, 97: 5942-7.

Tadamura, E., N. Tamaki, A. Matsumori, Y. Magata, Y. Yonekura, R. Nohara, S. Sasayama, M. Yoshibayashi, T. Kamiya, and J. Konishi. 1996. 'Myocardial metabolic changes in hypertrophic cardiomyopathy', *J Nucl Med*, 37: 572-7.

Taegtmeyer, H., S. Sen, and D. Vela. 2010. 'Return to the fetal gene program: a suggested metabolic link to gene expression in the heart', *Ann N Y Acad Sci*, 1188: 191-8.

Taggart, K., A. Estrada, P. Thompson, F. Lourenco, S. Kirmani, S. Suzuki-Hatano, and C. A. Pacak. 2017. 'PDK4 Deficiency Induces Intrinsic Apoptosis in Response to

Starvation in Fibroblasts from Doberman Pinschers with Dilated Cardiomyopathy', *Biores Open Access*, 6: 182-91.

Talley, J. T., and S. S. Mohiuddin. 2022. 'Biochemistry, Fatty Acid Oxidation.' in, *StatPearls* (StatPearls Publishing

Copyright © 2022, StatPearls Publishing LLC.: Treasure Island (FL)).

Tennessen, J. M., W. E. Barry, J. Cox, and C. S. Thummel. 2014. 'Methods for studying metabolism in Drosophila', *Methods*, 68: 105-15.

Tian, R., W. S. Colucci, Z. Arany, M. M. Bachschmid, S. W. Ballinger, S. Boudina, J. E. Bruce, D. W. Busija, S. Dikalov, G. W. Dorn, II, Z. S. Galis, R. A. Gottlieb, D. P. Kelly, R. N. Kitsis, M. J. Kohr, D. Levy, E. D. Lewandowski, J. M. McClung, D. Mochly-Rosen, K. D. O'Brien, B. O'Rourke, J. Y. Park, P. Ping, M. N. Sack, S. S. Sheu, Y. Shi, S. Shiva, D. C. Wallace, R. G. Weiss, H. J. Vernon, R. Wong, and L. Schwartz Longacre. 2019. 'Unlocking the Secrets of Mitochondria in the Cardiovascular System: Path to a Cure in Heart Failure—A Report from the 2018 National Heart, Lung, and Blood Institute Workshop', *Circulation*, 140: 1205-16.

Tie, J. K., M. Y. Zheng, K. L. Hsiao, L. Perera, D. W. Stafford, and D. L. Straight. 2008. 'Transmembrane domain interactions and residue proline 378 are essential for proper structure, especially disulfide bond formation, in the human vitamin K-dependent gamma-glutamyl carboxylase', *Biochemistry*, 47: 6301-10.

Tovar-Méndez, A., T. A. Hirani, J. A. Miernyk, and D. D. Randall. 2005. 'Analysis of the catalytic mechanism of pyruvate dehydrogenase kinase', *Arch Biochem Biophys*, 434: 159-68.

Tran, D. H., and Z. V. Wang. 2019. 'Glucose Metabolism in Cardiac Hypertrophy and Heart Failure', *J Am Heart Assoc*, 8: e012673.

Trico, D., S. Baldi, S. Frascerra, E. Venturi, P. Marraccini, D. Neglia, and A. Natali. 2016. 'Abnormal Glucose Tolerance Is Associated with a Reduced Myocardial Metabolic Flexibility in Patients with Dilated Cardiomyopathy', *J Diabetes Res*, 2016: 3906425.

Tsutsui, H., S. Kinugawa, and S. Matsushima. 2011. 'Oxidative stress and heart failure', *Am J Physiol Heart Circ Physiol*, 301: H2181-90.

Turcot, V., Y. Lu, H. M. Highland, C. Schurmann, A. E. Justice, R. S. Fine, J. P. Bradfield, T. Esko, A. Giri, M. Graff, X. Guo, A. E. Hendricks, T. Karaderi, A. Lempradl, A. E. Locke, A. Mahajan, E. Marouli, S. Sivapalaratnam, K. L. Young, T. Alfred, M. F. Feitosa, N. G. D. Masca, A. K. Manning, C. Medina-Gomez, P. Mudgal, M. C. Y. Ng, A. P. Reiner, S. Vedantam, S. M. Willems, T. W. Winkler, G. Abecasis, K. K. Aben, D. S. Alam, S. E. Alharthi, M. Allison, P. Amouyel, F. W. Asselbergs, P. L. Auer, B. Balkau, L. E. Bang, I. Barroso, L. Bastarache, M. Benn, S. Bergmann, L. F. Bielak, M. Blüher, M. Boehnke, H. Boeing, E. Boerwinkle, C. A. Böger, J. Bork-Jensen, M. L. Bots, E. P. Bottinger, D. W. Bowden, I. Brandslund, G. Breen, M. H. Brilliant, L. Broer, M. Brumat, A. A. Burt, A. S. Butterworth, P. T. Campbell, S. Cappellani, D. J. Carey, E. Catamo, M. J. Caulfield, J. C. Chambers, D. I. Chasman, Y. I. Chen, R. Chowdhury, C. Christensen, A. Y. Chu, M. Cocca, F. S. Collins, J. P. Cook, J. Corley, J. Corominas Galbany, A. J. Cox, D. S. Crosslin, G. Cuellar-Partida, A. D'Eustacchio, J. Danesh, G. Davies, P. I. W. Bakker, M. C. H. Groot, R. Mutsert, I. J. Deary, G. Dedoussis, E. W. Demerath, M. Heijer, A. I. Hollander, H. M.

Ruijter, J. G. Dennis, J. C. Denny, E. Di Angelantonio, F. Drenos, M. Du, M. P. Dubé, A. M. Dunning, D. F. Easton, T. L. Edwards, D. Ellinghaus, P. T. Ellinor, P. Elliott, E. Evangelou, A. E. Farmaki, I. S. Farooqi, J. D. Faul, S. Fauser, S. Feng, E. Ferrannini, J. Ferrieres, J. C. Florez, I. Ford, M. Fornage, O. H. Franco, A. Franke, P. W. Franks, N. Friedrich, R. Frikke-Schmidt, T. E. Galesloot, W. Gan, I. Gandin, P. Gasparini, J. Gibson, V. Giedraitis, A. P. Gjesing, P. Gordon-Larsen, M. Gorski, H. J. Grabe, S. F. A. Grant, N. Grarup, H. L. Griffiths, M. L. Grove, V. Gudnason, S. Gustafsson, J. Haessler, H. Hakonarson, A. R. Hammerschlag, T. Hansen, K. M. Harris, T. B. Harris, A. T. Hattersley, C. T. Have, C. Hayward, L. He, N. L. Heard-Costa, A. C. Heath, I. M. Heid, Ø Helgeland, J. Hernesniemi, A. W. Hewitt, O. L. Holmen, G. K. Hovingh, J. M. M. Howson, Y. Hu, P. L. Huang, J. E. Huffman, M. A. Ikram, E. Ingelsson, A. U. Jackson, J. H. Jansson, G. P. Jarvik, G. B. Jensen, Y. Jia, S. Johansson, M. E. Jørgensen, T. Jørgensen, J. W. Jukema, B. Kahali, R. S. Kahn, M. Kähönen, P. R. Kamstrup, S. Kanoni, J. Kaprio, M. Karaleftheri, S. L. R. Kardia, F. Karpe, S. Kathiresan, F. Kee, L. A. Kiemeney, E. Kim, H. Kitajima, P. Komulainen, J. S. Kooner, C. Kooperberg, T. Korhonen, P. Kovacs, H. Kuivaniemi, Z. Kutalik, K. Kuulasmaa, J. Kuusisto, M. Laakso, T. A. Lakka, D. Lamparter, E. M. Lange, L. A. Lange, C. Langenberg, E. B. Larson, N. R. Lee, T. Lehtimäki, C. E. Lewis, H. Li, J. Li, R. Li-Gao, H. Lin, K. H. Lin, L. A. Lin, X. Lin, L. Lind, J. Lindström, A. Linneberg, C. T. Liu, D. J. Liu, Y. Liu, K. S. Lo, A. Lophatananon, A. J. Lotery, A. Loukola, J. Luan, S. A. Lubitz, L. P. Lyytikäinen, S. Männistö, G. Marenne, A. L. Mazul, M. I. McCarthy, R. McKean-Cowdin, S. E. Medland, K. Meidtner, L. Milani, V. Mistry, P. Mitchell, K. L. Mohlke, L. Moilanen, M. Moitry, G. W. Montgomery, D. O. Mook-Kanamori, C. Moore, T. A. Mori, A. D. Morris, A. P. Morris, M. Müller-Nurasyid, P. B. Munroe, M. A. Nalls, N. Narisu, C. P. Nelson, M. Neville, S. F. Nielsen, K. Nikus, P. R. Njølstad, B. G. Nordestgaard, D. R. Nyholt, J. R. O'Connel, M. L. O'Donoghue, L. M. Olde Loohuis, R. A. Ophoff, K. R. Owen, C. J. Packard, S. Padmanabhan, C. N. A. Palmer, N. D. Palmer, G. Pasterkamp, A. P. Patel, A. Pattie, O. Pedersen, P. L. Peissig, G. M. Peloso, C. E. Pennell, M. Perola, J. A. Perry, J. R. B. Perry, T. H. Pers, T. N. Person, A. Peters, E. R. B. Petersen, P. A. Peyser, A. Pirie, O. Polasek, T. J. Polderman, H. Puolijoki, O. T. Raitakari, A. Rasheed, R. Rauramaa, D. F. Reilly, F. Renström, M. Rheinberger, P. M. Ridker, J. D. Rioux, M. A. Rivas, D. J. Roberts, N. R. Robertson, A. Robino, O. Rolandsson, I. Rudan, K. S. Ruth, D. Saleheen, V. Salomaa, N. J. Samani, Y. Sapkota, N. Sattar, R. E. Schoen, P. J. Schreiner, M. B. Schulze, R. A. Scott, M. P. Segura-Lepe, S. H. Shah, W. H. Sheu, X. Sim, A. J. Slater, K. S. Small, A. V. Smith, L. Southam, T. D. Spector, E. K. Speliotes, J. M. Starr, K. Stefansson, V. Steinthorsdottir, K. E. Stirrups, K. Strauch, H. M. Stringham, M. Stumvoll, L. Sun, P. Surendran, A. J. Swift, H. Tada, K. E. Tansey, J. C. Tardif, K. D. Taylor, A. Teumer, D. J. Thompson, G. Thorleifsson, U. Thorsteinsdottir, B. H. Thuesen, A. Tönjes, G. Tromp, S. Trompet, E. Tsafantakis, J. Tuomilehto, A. Tybjaerg-Hansen, J. P. Tyrer, R. Uher, A. G. Uitterlinden, M. Uusitupa, S. W. Laan, C. M. Duijn, N. Leeuwen, J. van Setten, M. Vanhala, A. Varbo, T. V. Varga, R. Varma, D. R. Velez Edwards, S. H. Vermeulen, G. Veronesi, H. Vestergaard, V. Vitart, T. F. Vogt, U. Völker, D. Vuckovic, L. E. Wagenknecht, M. Walker, L. Wallentin, F.

Wang, C. A. Wang, S. Wang, Y. Wang, E. B. Ware, N. J. Wareham, H. R. Warren, D. M. Waterworth, J. Wessel, H. D. White, C. J. Willer, J. G. Wilson, D. R. Witte, A. R. Wood, Y. Wu, H. Yaghootkar, J. Yao, P. Yao, L. M. Yerges-Armstrong, R. Young, E. Zeggini, X. Zhan, W. Zhang, J. H. Zhao, W. Zhao, W. Zhao, W. Zhou, K. T. Zondervan, J. I. Rotter, J. A. Pospisilik, F. Rivadeneira, I. B. Borecki, P. Deloukas, T. M. Frayling, G. Lettre, K. E. North, C. M. Lindgren, J. N. Hirschhorn, and R. J. F. Loos. 2018. 'Protein-altering variants associated with body mass index implicate pathways that control energy intake and expenditure in obesity', *Nat Genet*, 50: 26-41.

Vakrou, S., and M. R. Abraham. 2014. 'Hypertrophic cardiomyopathy: a heart in need of an energy bar?', *Front Physiol*, 5: 309.

Vanderperre, B., K. Cermakova, J. Escoffier, M. Kaba, T. Bender, S. Nef, and J. C. Martinou. 2016. 'MPC1-like Is a Placental Mammal-specific Mitochondrial Pyruvate Carrier Subunit Expressed in Postmeiotic Male Germ Cells', *J Biol Chem*, 291: 16448-61.

Vanhollebeke, B., P. Truc, P. Poelvoorde, A. Pays, P. P. Joshi, R. Katti, J. G. Jannin, and E. Pays. 2006. 'Human Trypanosoma evansi infection linked to a lack of apolipoprotein L-I', *N Engl J Med*, 355: 2752-6.

Ventura-Clapier, R., A. Garnier, V. Veksler, and F. Joubert. 2011. 'Bioenergetics of the failing heart', *Biochim Biophys Acta*, 1813: 1360-72.

Verdonschot, J. A. J., E. L. Robinson, K. N. James, M. W. Mohamed, G. R. F. Claes, K. Casas, E. K. Vanhoutte, M. R. Hazebroek, G. Kringlen, M. M. Pasierb, A. van den Wijngaard, J. F. C. Glatz, S. R. B. Heymans, I. P. C. Krapels, S. Nahas, H. G. Brunner, and R. Szklarczyk. 2020. 'Mutations in PDLIM5 are rare in dilated cardiomyopathy but are emerging as potential disease modifiers', *Mol Genet Genomic Med*, 8: e1049.

Viswanathan, M. C., A. C. Blice-Baum, T. K. Sang, and A. Cammarato. 2016. 'Cardiac-Restricted Expression of VCP/TER94 RNAi or Disease Alleles Perturbs Drosophila Heart Structure and Impairs Function', *J Cardiovasc Dev Dis*, 3.

Viswanathan, M. C., G. Kaushik, A. J. Engler, W. Lehman, and A. Cammarato. 2014. 'A Drosophila melanogaster model of diastolic dysfunction and cardiomyopathy based on impaired troponin-T function', *Circ Res*, 114: e6-17.

Vogler, G., and K. Ocorr. 2009. 'Visualizing the beating heart in Drosophila', *J Vis Exp*.

Wang, J., H. Mei, W. Chen, Y. Jiang, W. Sun, F. Li, Q. Fu, and F. Jiang. 2012. 'Study of eight GWAS-identified common variants for association with obesity-related indices in Chinese children at puberty', *Int J Obes (Lond)*, 36: 542-7.

Wang, Y., and N. Tjandra. 2013. 'Structural insights of tBid, the caspase-8-activated Bid, and its BH3 domain', *J Biol Chem*, 288: 35840-51.

Warburg, Otto. 1956. 'On the origin of cancer cells', *Science*, 123: 309-14.

Warburg, Otto Heinrich. 1926. 'Uber den stoffwechsel der tumoren'.

Willer, C. J., E. K. Speliotes, R. J. Loos, S. Li, C. M. Lindgren, I. M. Heid, S. I. Berndt, A. L. Elliott, A. U. Jackson, C. Lamina, G. Lettre, N. Lim, H. N. Lyon, S. A. McCarroll, K. Papadakis, L. Qi, J. C. Randall, R. M. Roccasecca, S. Sanna, P. Scheet, M. N. Weedon, E. Wheeler, J. H. Zhao, L. C. Jacobs, I. Prokopenko, N. Soranzo, T. Tanaka, N. J. Timpson, P. Almgren, A. Bennett, R. N. Bergman, S. A. Bingham, L. L. Bonnycastle, M. Brown, N. P. Burtt, P. Chines, L. Coin, F. S.

Collins, J. M. Connell, C. Cooper, G. D. Smith, E. M. Dennison, P. Deodhar, P. Elliott, M. R. Erdos, K. Estrada, D. M. Evans, L. Gianniny, C. Gieger, C. J. Gillson, C. Guiducci, R. Hackett, D. Hadley, A. S. Hall, A. S. Havulinna, J. Hebebrand, A. Hofman, B. Isomaa, K. B. Jacobs, T. Johnson, P. Jousilahti, Z. Jovanovic, K. T. Khaw, P. Kraft, M. Kuokkanen, J. Kuusisto, J. Laitinen, E. G. Lakatta, J. Luan, R. N. Luben, M. Mangino, W. L. McArdle, T. Meitinger, A. Mulas, P. B. Munroe, N. Narisu, A. R. Ness, K. Northstone, S. O'Rahilly, C. Purmann, M. G. Rees, M. Ridderstråle, S. M. Ring, F. Rivadeneira, A. Ruokonen, M. S. Sandhu, J. Saramies, L. J. Scott, A. Scuteri, K. Silander, M. A. Sims, K. Song, J. Stephens, S. Stevens, H. M. Stringham, Y. C. Tung, T. T. Valle, C. M. Van Duijn, K. S. Vimaleswaran, P. Vollenweider, G. Waeber, C. Wallace, R. M. Watanabe, D. M. Waterworth, N. Watkins, J. C. Witteman, E. Zeggini, G. Zhai, M. C. Zillikens, D. Altshuler, M. J. Caulfield, S. J. Chanock, I. S. Farooqi, L. Ferrucci, J. M. Guralnik, A. T. Hattersley, F. B. Hu, M. R. Jarvelin, M. Laakso, V. Mooser, K. K. Ong, W. H. Ouwehand, V. Salomaa, N. J. Samani, T. D. Spector, T. Tuomi, J. Tuomilehto, M. Uda, A. G. Uitterlinden, N. J. Wareham, P. Deloukas, T. M. Frayling, L. C. Groop, R. B. Hayes, D. J. Hunter, K. L. Mohlke, L. Peltonen, D. Schlessinger, D. P. Strachan, H. E. Wichmann, M. I. McCarthy, M. Boehnke, I. Barroso, G. R. Abecasis, and J. N. Hirschhorn. 2009. 'Six new loci associated with body mass index highlight a neuronal influence on body weight regulation', *Nat Genet*, 41: 25-34.

Wisneski, J. A., E. W. Gertz, R. A. Neese, L. D. Gruenke, and J. C. Craig. 1985. 'Dual carbon-labeled isotope experiments using D-[6-14C] glucose and L-[1,2,3-13C3] lactate: a new approach for investigating human myocardial metabolism during ischemia', *J Am Coll Cardiol*, 5: 1138-46.

Wolf, M. J. 2012. 'Modeling dilated cardiomyopathies in Drosophila', *Trends Cardiovasc Med*, 22: 55-61.

Wolf, M. J., H. Amrein, J. A. Izatt, M. A. Choma, M. C. Reedy, and H. A. Rockman. 2006. 'Drosophila as a model for the identification of genes causing adult human heart disease', *Proc Natl Acad Sci U S A*, 103: 1394-9.

Xie, H. B., A. Cammarato, N. S. Rajasekaran, H. Zhang, J. A. Suggs, H. C. Lin, S. I. Bernstein, I. J. Benjamin, and K. G. Golic. 2013. 'The NADPH metabolic network regulates human αB-crystallin cardiomyopathy and reductive stress in Drosophila melanogaster', *PLoS Genet*, 9: e1003544.

Xu, X., Y. C. Shi, W. Gao, G. Mao, G. Zhao, S. Agrawal, G. M. Chisolm, D. Sui, and M. Z. Cui. 2002. 'The novel presenilin-1-associated protein is a proapoptotic mitochondrial protein', *J Biol Chem*, 277: 48913-22.

Youle, R. J., and A. M. van der Bliek. 2012. 'Mitochondrial fission, fusion, and stress', *Science*, 337: 1062-5.

Yu, L., J. Daniels, A. E. Glaser, and M. J. Wolf. 2013. 'Raf-mediated cardiac hypertrophy in adult Drosophila', *Dis Model Mech*, 6: 964-76.

Yu, L., J. P. Daniels, H. Wu, and M. J. Wolf. 2015. 'Cardiac hypertrophy induced by active Raf depends on Yorkie-mediated transcription', *Sci Signal*, 8: ra13.

Zaltsman, Y., L. Shachnai, N. Yivgi-Ohana, M. Schwarz, M. Maryanovich, R. H. Houtkooper, F. M. Vaz, F. De Leonardis, G. Fiermonte, F. Palmieri, B. Gillissen, P. T. Daniel, E. Jimenez, S. Walsh, C. M. Koehler, S. S. Roy, L. Walter, G.

Hajnóczky, and A. Gross. 2010. 'MTCH2/MIMP is a major facilitator of tBID recruitment to mitochondria', *Nat Cell Biol*, 12: 553-62.

Zandi, P., and E. Schnug. 2022. 'Reactive Oxygen Species, Antioxidant Responses and Implications from a Microbial Modulation Perspective', *Biology (Basel)*, 11.

Zarndt, R., S. M. Walls, K. Ocorr, and R. Bodmer. 2017. 'Reduced Cardiac Calcineurin Expression Mimics Long-Term Hypoxia-Induced Heart Defects in Drosophila', *Circ Cardiovasc Genet*, 10.

Zhang, J., W. S. Ahn, P. A. Gameiro, M. A. Keibler, Z. Zhang, and G. Stephanopoulos. 2014. '13C isotope-assisted methods for quantifying glutamine metabolism in cancer cells', *Methods Enzymol*, 542: 369-89.

Zhang, S., M. W. Hulver, R. P. McMillan, M. A. Cline, and E. R. Gilbert. 2014. 'The pivotal role of pyruvate dehydrogenase kinases in metabolic flexibility', *Nutr Metab (Lond)*, 11: 10.

Zhang, Y., P. V. Taufalele, J. D. Cochran, I. Robillard-Frayne, J. M. Marx, J. Soto, A. J. Rauckhorst, F. Tayyari, A. D. Pewa, L. R. Gray, L. M. Teesch, P. Puchalska, T. R. Funari, R. McGlauflin, K. Zimmerman, W. J. Kutschke, T. Cassier, S. Hitchcock, K. Lin, K. M. Kato, J. L. Stueve, L. Haff, R. M. Weiss, J. E. Cox, J. Rutter, E. B. Taylor, P. A. Crawford, E. D. Lewandowski, C. Des Rosiers, and E. D. Abel. 2020. 'Mitochondrial pyruvate carriers are required for myocardial stress adaptation', *Nat Metab*, 2: 1248-64.

Zhao, G., N. H. Jeoung, S. C. Burgess, K. A. Rosaaen-Stowe, T. Inagaki, S. Latif, J. M. Shelton, J. McAnally, R. Bassel-Duby, R. A. Harris, J. A. Richardson, and S. A. Kliewer. 2008. 'Overexpression of pyruvate dehydrogenase kinase 4 in heart perturbs metabolism and exacerbates calcineurin-induced cardiomyopathy', *Am J Physiol Heart Circ Physiol*, 294: H936-43.

Zhu, Y., J. Wu, and S. Y. Yuan. 2013. 'MCT1 and MCT4 expression during myocardial ischemic-reperfusion injury in the isolated rat heart', *Cell Physiol Biochem*, 32: 663-74.

Zlotogora, J., G. P. Patrinos, and V. Meiner. 2018. 'Ashkenazi Jewish genomic variants: integrating data from the Israeli National Genetic Database and gnomAD', *Genet Med*, 20: 867-71.

Zymliński, R., J. Biegus, M. Sokolski, P. Siwołowski, S. Nawrocka-Millward, J. Todd, E. A. Jankowska, W. Banasiak, G. Cotter, J. G. Cleland, and P. Ponikowski. 2018. 'Increased blood lactate is prevalent and identifies poor prognosis in patients with acute heart failure without overt peripheral hypoperfusion', *Eur J Heart Fail*, 20: 1011-18.

APPENDIX

When analyzing whole genome short read sequences (WGS), there was poor alignment for specific regions of *MTCH2*, which mapped to specific exons of the gene (**Figure A1**). Specifically reads spanning these exons also did not match the *MTCH2* reference sequence. To evaluate this, I conducted PCR on genomic DNA using with primers designed to intronic regions flanking these exons. The PCR products were subjected to Sanger sequencing and aligned using the National Center for Biotechnology Information Basic Local Alignment Search Tool (NCBI BLAST) tool. This analysis showed revealed segments of the *MTCH2* gene mapped to alternative genomic loci in what appears to be atypical pseudogenes, at least one of which is located on chromosome 22. These atypical pseudogenes did not represent the typical processed cDNA pseudogene but rather contained exons with some flanking region at more than one site in the genome. Other sequences were determined to be nonreference unique insertion sequences. Atypical pseudogene sequences were observed containing sequences similar to exons 1, 3, 10, 11, 12, and 13 which confounded the analysis for genomic variation in *MTCH2,* which is located on chromosome 11. In order to more accurately identify true variants in the canonical *MTCH2* gene located on chromosome 11, we excluded variants that were appearing within these nonreference reads (**Figure A2**). These findings were consistent with the observations in gnomAD that some of these variants did not pass filtration in the gnomAD database. Variants that may appear from sequencing in *MTCH2* exons 1, 3, 11, 12, and 13 should be viewed with caution in that they may not be located in *MTCH2*, but instead in nonreference sequences elsewhere in the genome.

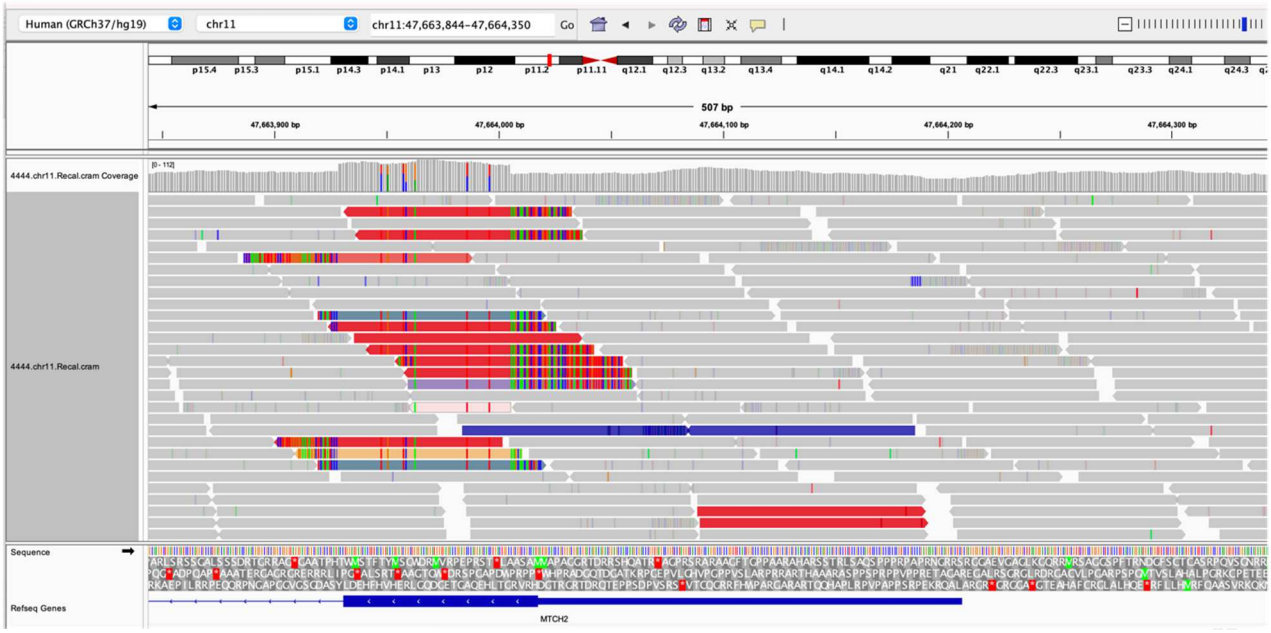

***MTCH2* Exon 1**

***MTCH2* Exon 12**

Figure A1. Short read sequencing of *MTCH2* shows nonreference reads in exons containing excess variation. WGS of multiple exons in *MTCH2* had nonreference reads which not align well to the canonical MTCH2 gene on chromosome 11. These reads mapped to unique nonreference flanking sequence and atypical pseudogene sequences.

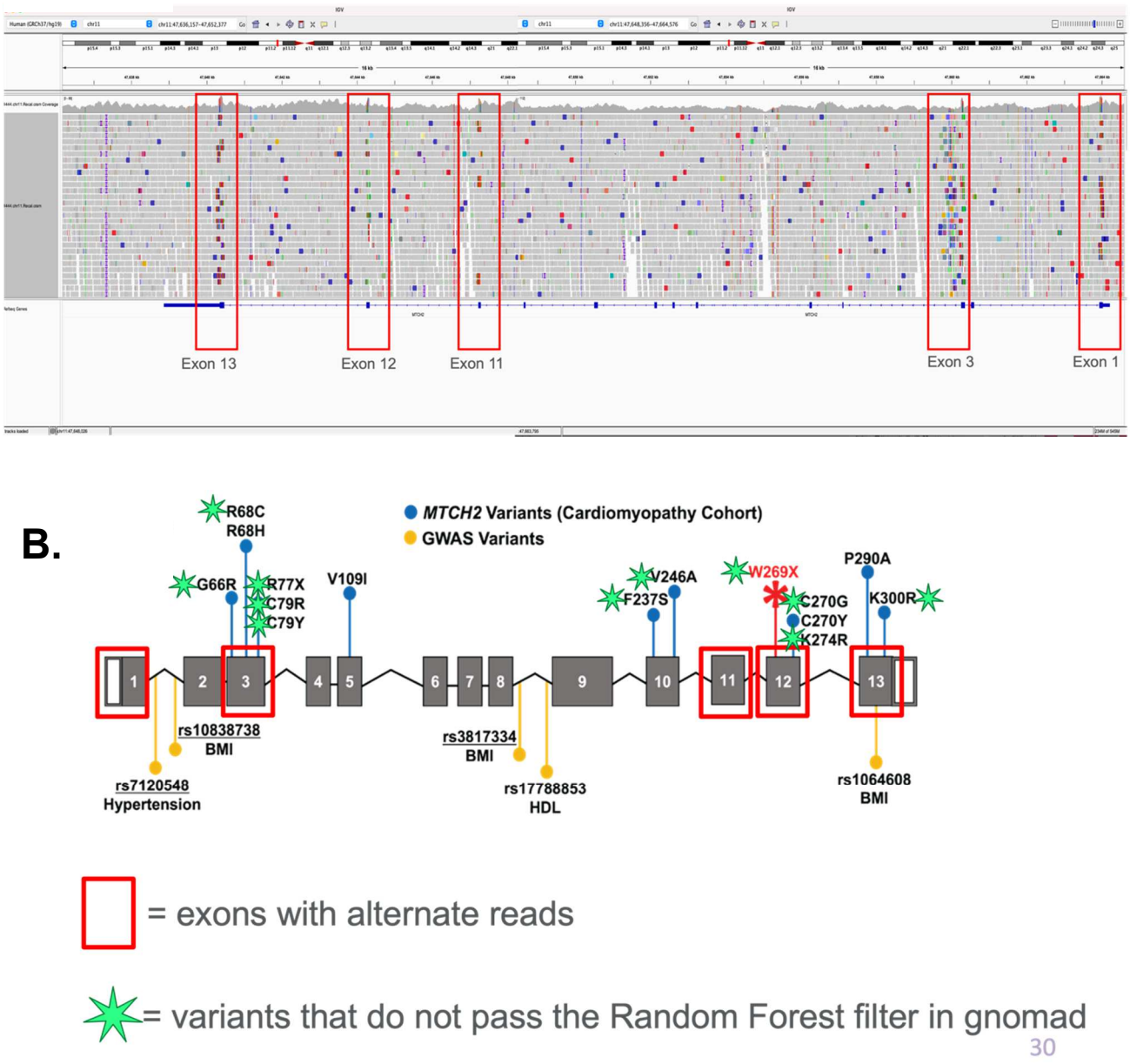

Figure A2. Exons in *MTCH2* with excess variation. A. Red boxes highlight the exons in *MTCH2* which show nonreference reads. There is evidence for alternative copies of these exons in the genome that represent atypical pseudogene sequences. **B.** Exon map of *MTCH2.* Blue pins represent variants in specific exons in the *MTCH2* gene which were identified initially as having excess variation in the cardiomyopathy cohort. Yellow pins represent GWAS variants in *MTCH2* that correlate with metabolic phenotypes. Red boxes are highlighting exons in which sequencing reads of these regions did not map to the reference genome and instead mapped to nonreference unique insertion sequences (atypical pseudogene sequences). Green stars represent variants that also did not pass the Random Forest filter in gnomAD. Many of the variants that did not pass the Random Forest filter are located in exons that had sequencing reads that aligned to unique nonreference insertions and atypical pseudogene sequences.